Microporous and Mesoporous Materials 125 (2009) 126–134

Contents lists available at ScienceDirect

Microporous and Mesoporous Materials

journal homepage: www.elsevier.com/locate/micromeso

A molecular dynamics investigation of a variety of influences of temperature on diffusion in zeolites

R. Krishna *, J.M. van Baten

Van 't Hoff Institute for Molecular Sciences, University of Amsterdam, Nieuwe Achtergracht 166, 1018 WV Amsterdam, The Netherlands

ARTICLE INFO

Article history:
Received 23 October 2008
Received in revised form 31 December 2008
Accepted 15 January 2009
Available online 24 January 2009

Keywords:
Maxwell–Stefan diffusivity
Self diffusivity
Molecular dynamics
Zeolites
Activation energy
Loading dependence
Correlations

ABSTRACT

Molecular dynamics (MD) simulations were performed to determine both the Maxwell–Stefan diffusivity, $Đ_i$, and the self-diffusivity, $D_{i,self}$, of a variety of molecules (Ne, Ar, Kr, CH_4, C_2H_4, CO_2, O_2, and N_2) in five different zeolites (LTA, DDR, CHA, FAU, MFI) for a range of temperatures, T, and molecular loadings, q_i. The simulation results show that for cage-type zeolites with narrow windows (LTA, CHA, and DDR) with guest molecules such as CH_4 and Kr, that are tightly constrained at the window regions, the $Đ_i - q_i$ dependence varies significantly with T. Furthermore, the activation energy changes with the loading q_i. The model of Reed and Ehrlich (D.A. Reed, G. Ehrlich, Surf. Sci. 102 (1981) 588) provides a convenient description of the combined influence of q_i and T on $Đ_i$. For other guest–host combinations that were investigated the $Đ_i - q_i$ dependence was found to depend relatively weakly on T. The strength of correlations, quantified by $(Đ_i/D_{i,self} - 1)$ is found to be practically T-independent for all guest–host combinations examined. Generally speaking, for a specified loading q_i, the activation energy for $Đ_i - T$ and $D_{i,self} - T$ variations are different; the difference is about 10% when the strength of correlations is large.

1. Introduction

Due to their regular nanometer sized pore structures, zeolites are widely used as catalysts and adsorbents that rely on either molecular sieving principles or subtle configurational effects for achieving high selectivities in separation and reaction applications [1–8]. For the design of catalytic and separation processes employing zeolites it is necessary to have accurate information on the Fick diffusivity D_i of guest molecules, defined for one-component diffusion by [9–11]

$$N_i = -\rho D_i \frac{dq_i}{dx}. \tag{1}$$

In Eq. (1), N_i is the molecular flux, q_i is molecular loading expressed in molecules per unit cell or per cage. The Fick diffusivity D_i is obtained by experimentally monitoring transient intra-crystalline uptake or response to pulse injection in chromatographic columns. For interpretation in terms of theoretical models, and for prediction of mixture diffusion characteristics, it is preferable to use the alternative Maxwell–Stefan (M–S) approach [12–14] in which the chemical potential gradient $d\mu_i/dx$ is used as the driving force and the M–S diffusivity $Đ_i$ is defined by

$$N_i = -\rho q_i Đ_i \frac{1}{RT}\frac{d\mu_i}{dx}. \tag{2}$$

The Fick and M–S diffusivities are inter-related,

$$D_i = Đ_i \Gamma_i, \tag{3}$$

where Γ_i is the thermodynamic correction factor,

$$\Gamma_i \equiv \frac{d\ln f_i}{d\ln q_i}. \tag{4}$$

The thermodynamic factor Γ_i can be determined from knowledge of the adsorption isotherm that relates the molecular loading q_i to the bulk gas fugacity f_i.

The M–S diffusivity $Đ_i$ can be determined directly from molecular dynamics (MD) simulations by analyzing the mean square displacement of an *ensemble* of molecules for each of the coordinate directions from

$$Đ_i = \frac{1}{2}\lim_{\Delta t\to\infty}\frac{1}{n_i}\frac{1}{\Delta t}\left\langle\left(\sum_{l=1}^{n_i}(\mathbf{r}_{l,i}(t+\Delta t)-\mathbf{r}_{l,i}(t))\right)^2\right\rangle. \tag{5}$$

MD simulations also yield the self-diffusivities, $D_{i,self}$, by analyzing the mean square displacement of *individual* molecules i,

$$D_{i,self} = \frac{1}{2n_i}\lim_{\Delta t\to\infty}\frac{1}{\Delta t}\left\langle\left(\sum_{l=1}^{n_i}(\mathbf{r}_{l,i}(t+\Delta t)-\mathbf{r}_{l,i}(t))^2\right)\right\rangle. \tag{6}$$

As alternatives to Einstein expressions (5) and (6), the diffusivities can also be determined using the velocity auto-correlations and the Green–Kubo formula [15] or from non-equilibrium MD simulations [16]. The $D_{i,self}$ can also be obtained from NMR and

* Corresponding author. Tel.: +31 20 257007; fax: +31 20 5255604.
E-mail address: r.krishna@uva.nl (R. Krishna).

1387-1811/$ - see front matter © 2009 Elsevier Inc. All rights reserved.
doi:10.1016/j.micromeso.2009.01.015

Nomenclature

D_i	Fick diffusivity of species i, $m^2\ s^{-1}$
$D_{i,self}$	self-diffusivity, $m^2\ s^{-1}$
$Đ_i$	Maxwell–Stefan diffusivity of species i, $m_2\ s^{-1}$
$Đ_i(0)$	zero-loading M–S diffusivity of species i, $m_2\ s^{-1}$
$Đ_{ii}$	self-exchange diffusivity, $m_2\ s^{-1}$
$E_{diff,i}$	activation energy for diffusion i, J mol^{-1}
f_i	fugacity of species i, Pa
N_i	molecular flux of species i, molecules, $m^{-2}\ s^{-1}$
n_i	number of molecules of species i in simulation box, dimensionless
q_i	loading of species i, mol kg^{-1} or molecules per unit cell or molecules per cage
$q_{i,sat}$	saturation loading of species i, mol kg^{-1} or molecules per unit cell or molecules per cage
R	gas constant, 8.314 J $mol^{-1}\ K^{-1}$
T	absolute temperature, K
x	spatial distance, m
z	coordination number, dimensionless

Greek letters

β_i	Reed–Ehrlich parameter, dimensionless
δE_i	reduction in energy barrier for diffusion, J mol^{-1}
ε_i	Reed–Ehrlich parameter, dimensionless
ϕ_i	Reed–Ehrlich parameter, dimensionless
θ_i	fractional occupancy of component i, dimensionless
μ_i	molar chemical potential, J mol^{-1}
ρ	density of zeolite, number of unit cells per m^3

Subscripts

sat	referring to saturation conditions
i	referring to component i

QENS experiments. In general, the $D_{i,self}$ is lower than $Đ_i$ due to *correlation* effects. In the M–S formulation the correlation effects are quantified by defining the *self-exchange* coefficient, $Đ_{ii}$. The *strength* of the correlations can be quantified by the dimensionless parameter [13],

$$\frac{\theta_i Đ_i}{Đ_{ii}} = \frac{Đ_i}{D_{i,self}} - 1, \tag{7}$$

where θ_i is the fractional occupancy:

$$\theta_i = \frac{q_i}{q_{i,sat}}. \tag{8}$$

The higher the value of $\theta_i Đ_i / Đ_{ii}$, the stronger is the correlation.

Both experimental data and MD simulations show that the diffusivities ($Đ_i$,$D_{i,self}$), and correlations ($Đ_{ii}$) are strong functions of the molecular loading q_i [14,17]. Often, diffusivity data available at a certain temperature needs to be extrapolated to a different temperature. Nagumo et al. [18,19], for example suggest a methodology for performing simulations at high T, with attendant high diffusivities, and extrapolating these results to low T, where the diffusivities are too low to determine accurately using MD. Three questions that arise are as follows:

(1) Does the loading dependence of the diffusivities ($Đ_i - q_i$, or $D_{i,self} - q_i$) vary with T?
(2) Can we expect the strength of correlation effects, calculated from Eq. (7), to be T-independent?
(3) Is the activation energy for self-diffusivity the same as that for the M–S diffusivity?

To obtain answers to the three questions posed above we performed MD simulations to determine both the M–S diffusivity, $Đ_i$, and the self-diffusivity, $D_{i,self}$, of a variety of molecules (Ne, Ar, Kr, CH_4, C_2H_4, CO_2, O_2, and N_2) in five different zeolites (LTA, DDR, CHA, FAU, and MFI) for a range of temperatures, T, and molecular loadings, q_i. The choice of the five zeolites was dictated by the importance of the structures in practice. The zeolite frameworks were considered to be rigid in all the simulations. Additionally, Monte Carlo simulations in the grand canonical (GC) ensemble were performed to determine the adsorption isotherms; these are required to determine the saturation capacity, $q_{i,sat}$, required for modeling of the loading dependence of $Đ_i$ using the model of Reed and Ehrlich [20–22]. Two kinds of MD simulation campaigns were run; for a fixed temperature the loading was varied up to saturation limit, and also for a fixed loading, the temperatures were varied. The entire data base of simulation results is available in the Supplementary material accompanying this publication; this material includes details of the GCMC and MD simulation methodologies, description of the force fields used, validation of force fields used by comparison with experimental data on adsorption isotherms of a variety of molecules in DDR, simulation data (pure component isotherms; $D_{i,self}$; $Đ_i$; $q_{i,sat}$; $Đ_{ii}$), along with snapshots showing the location of molecules in the zeolite structures. A selection of the simulation results is presented below with the objective of drawing a range of generic conclusions.

2. Influence of T on loading dependence of the M–S diffusivity

Generally speaking the loading dependence of $Đ_i$ is strongest for zeolite structures, such as LTA, DDR, and CHA that consist of cages separated by narrow windows [14], and it may be anticipated that the $Đ_i - q_i$ dependence in such structures would be more sensitive to variations in T. Let us begin by considering diffusion of CH_4 in LTA, that consists of cages separated by windows of 4.1 Å size. The MD simulations results for the M–S diffusivities, $Đ_i$ are shown in Fig. 1 as a function of q_i at different T in the range 800–1800 K. The chosen temperature range was motivated by the desire to allow comparison with the earlier study of Nagumo et al. [18]; in this

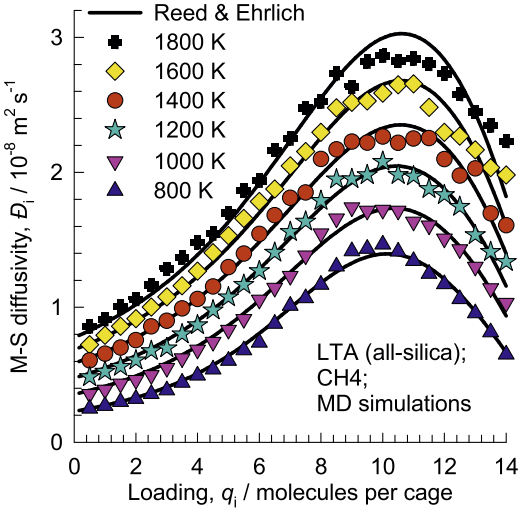

Fig. 1. MD simulations results for M–S diffusivities, $Đ_i$, of CH_4 in all-silica LTA zeolite at T = 800, 1000, 1200, 1400, 1600, and 1800 K, as a function of the molecular loading q_i.

connection it must be remarked that LTA is only stable up to 1200 K [23]. Diffusion in LTA is isotropic and the reported diffusivities are the average of those in the three coordinate directions.

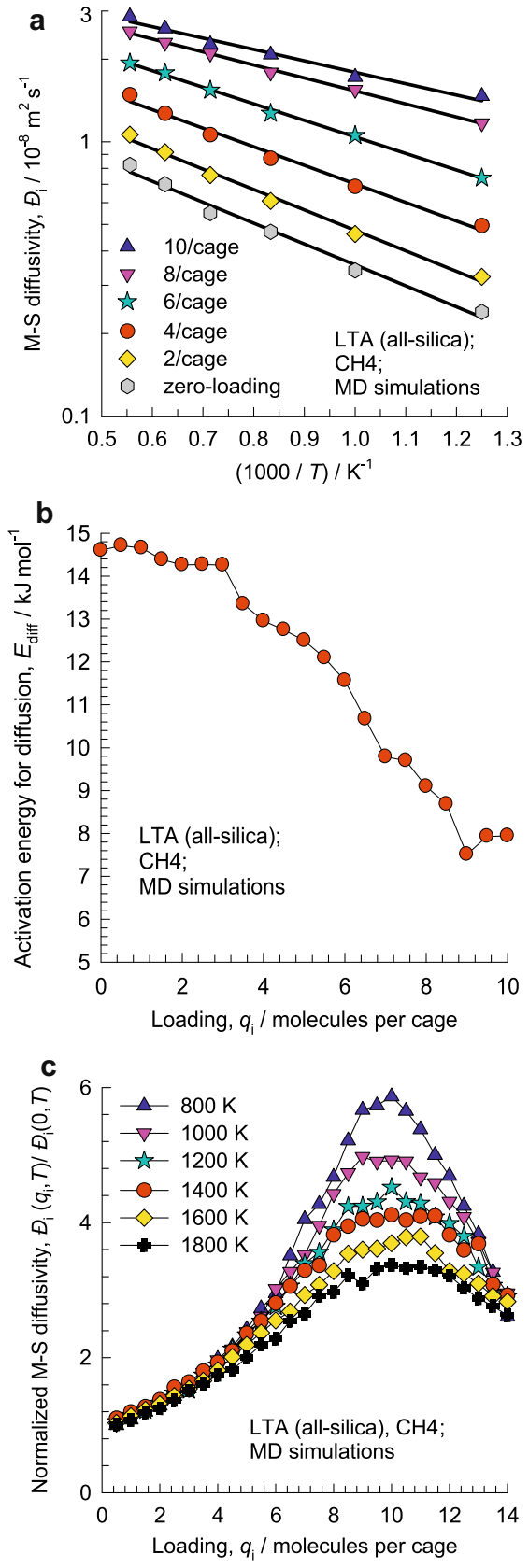

Fig. 2. (a) Arrhenius plots at various loadings in LTA. (b) Activation energy as a function of q_i. (c) Normalized M–S diffusivity as a function of q_i for various T.

From the data presented in Fig. 1, Arrhenius plots can be constructed for each loading; see Fig. 2a. The activation energy appears to be dependent on the loading within the cages. The $E_{i,diff}$, determined for each loading from the Arrhenius plots, are shown in Fig. 2b. The value of $E_{i,diff}$ varies from 14.6 at $q_i = 0$ to about 8 at $q_i = 10$. From the results in Fig. 2b we can conclude that extrapolation of diffusivity data in the manner suggested by Nagumo et al. [18,19] is only justified provided the loadings are the same between the two temperature levels. The $Đ_i(q_i,T)$ data, normalized with respect to the zero-loading diffusivities, are plotted in Fig. 2c; this figure shows that the $Đ_i - q_i$ variation changes with T, and is significantly sharper at lower T. We now examine the fundamental reasons for this.

At any given T, the most convenient and practical physical model to quantify the $Đ_i - q_i$ relation is that developed by Reed and Ehrlich for surface diffusion of adsorbed molecules [20]. In the Reed and Ehrlich model, as applied earlier for zeolites [21,22], the intermolecular interactions *within* a cage is assumed to influence the hopping frequencies of molecules *between* cages, by a factor

$$\phi_i = \exp\left(\frac{\delta E_i}{RT}\right), \tag{9}$$

where δE_i represents the *reduction* in the inter-cage hopping of molecules across the narrow windows [24,25]. The Reed and Ehrlich model leads to the following expression for the M–S diffusivity as a function of the fractional occupancy, $\theta_i = q_i/q_{i,sat}$,

$$Đ_i(\theta_i, T) = Đ(0,T)\frac{(1+\varepsilon_i)^{z-1}}{(1+\varepsilon_i/\phi_i)^z}, \tag{10}$$

where z is the coordination number, representing the maximum number of nearest neighbors within a cage. From an engineering point of view the precise choice of the value of z is not crucial, as the *combination* of z and ϕ_i prescribes the loading dependence. For LTA, a choice of $z = 5$ is made, based on earlier work [13,14]. The other parameters are defined as follows (see Krishna et al. [21,26] for more detailed discussions and derivations)

$$\varepsilon_i = \frac{(\beta_i - 1 + 2\theta_i)\phi_i}{2(1-\theta_i)}; \quad \beta_i = \sqrt{1 - 4\theta_i(1-\theta_i)(1-1/\phi_i)}. \tag{11}$$

In the limiting case when there is no reduction in the energy barrier for diffusion, $\delta E_i = 0$, we get $\phi_i = 1$, $\beta_i = 1$, and $\varepsilon_i = \theta_i/(1-\theta_i)$ and the M–S diffusivity $Đ_i$ decreases linearly with the vacancy $(1-\theta_i)$. When the reduction in the free energy barrier is large enough, $\phi_i \gg 1$, there is a significant increase in $Đ_i$ with increasing q_i. As the saturation capacity, $q_{i,sat}$, is approached, there is an inevitable decline in $Đ_i$ and therefore $\phi_i \gg 1$ leads to a maximum in the $Đ_i - q_i$.

The MD simulated M–S diffusivities, extrapolated to $q_i = 0$, can be fitted as follows:

$$Đ(0,T) = 2.06 \times 10^{-8} \exp\left(-\frac{E_{i,diff}}{RT}\right), \tag{12}$$

where $E_{i,diff} = 14.6$ kJ mol^{-1} is the activation energy for diffusion in the limit of zero-loading. Fitting the data set for each T, we obtain the δE_i and ϕ_i values as shown in Fig. 3a and b. With these fitted ϕ_i values the continuous solid lines in Fig. 1a are obtained. We note that the parameter ϕ_i, that determines the loading dependence of $Đ_i$ shows significant variation with T for $1200 < T < 800$ K; for $T > 1400$ K the ϕ_i is practically T-independent. From Fig. 3a it can be seen that the free energy barrier δE_i is T- dependent. In previous work [13,14,26] we had fitted the loading dependence at a fixed temperature with the functional form $\phi_i = a\exp(b\theta_i)$. The entire data set could be fitted in the form

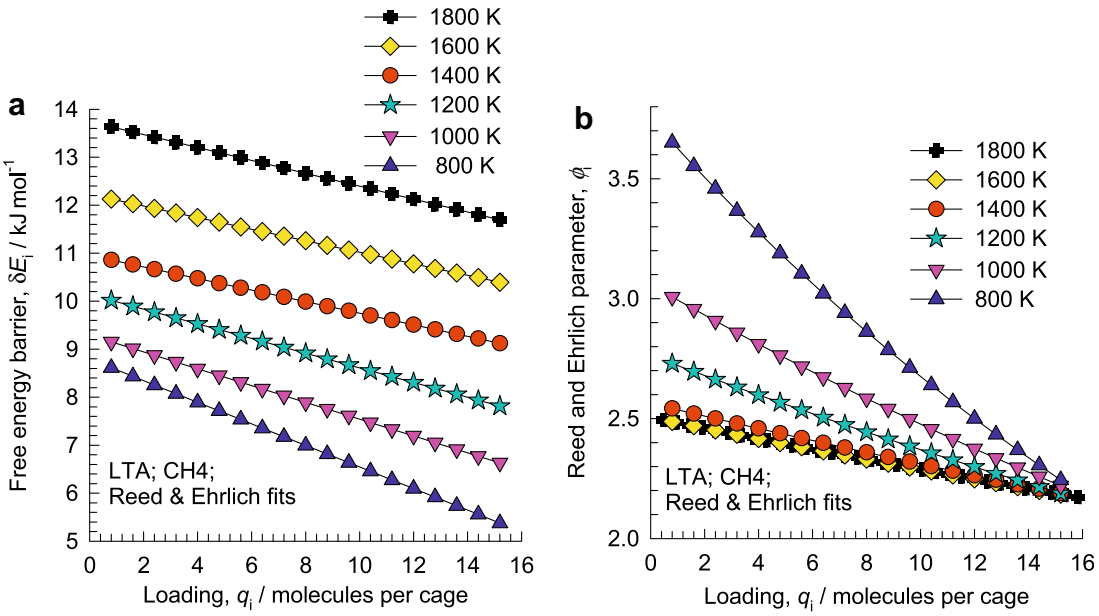

Fig. 3. (a) Free-energy barrier, and (b) ϕ_i for diffusion of CH_4 in LTA as a function of q_i for various temperatures.

$$\phi_i = \exp\left(\frac{a_0 + a_1 T}{RT}\right)\exp(b\theta_i), \tag{13}$$

with $a_0 = 1530$ J mol^{-1}, and $a_1 = 7.3$ J mol^{-1} K^{-1}, and $b = -0.25$.

Results similar to CH_4/LTA are obtained for CH_4/DDR, Kr/DDR, and CH_4/CHA; for all these guest–host combinations the degree of confinement, defined as the diameter of the molecule divided by the size of the window opening, is close to unity. Example Arrhenius plots for the M–S diffusivities at two different loadings are shown in Fig. 4a and b. As for LTA, the activation energy is lower at the higher loading for CH_4 diffusion in both DDR and CHA.

For molecules such as Ne, Ar, CO_2, and N_2, that are less strongly constrained at the window regions of DDR, the free energy barrier for hopping of molecules across the narrow windows of DDR are significantly lower. As a consequence, the influence of T on the loading dependence is either negligibly small or weak at best; see data on the normalized M–S diffusivity in Fig. 5. For all these four molecules the Reed and Ehrlich model, as described above, provides a good description of the loading dependence (details can be found in the Supplementary material). Analogous results are obtained for Ar/CHA, and O_2/DDR. In this connection it worth mentioning the MD simulation of Schüring et al. [27] for ethane in LTA; they found that entropic effects lead to an anomalous T dependence in the 150–300 K range. Our simulation results do not show any anomaly.

The experimental data of van den Bergh et al. [6,28] for permeation of CH_4, CO_2, and N_2 across a DDR membrane can be modeled using the T-dependent variant of the Reed and Ehrlich approach presented above; details are provided in the Supplementary material. For CH_4 permeation the best fits with experimental data on permeation fluxes is obtained with $\phi_i = \exp((3000 + 4T)/RT)\exp(0.4\theta_i)$. With this fitted ϕ_i the normalized M–S diffusivities

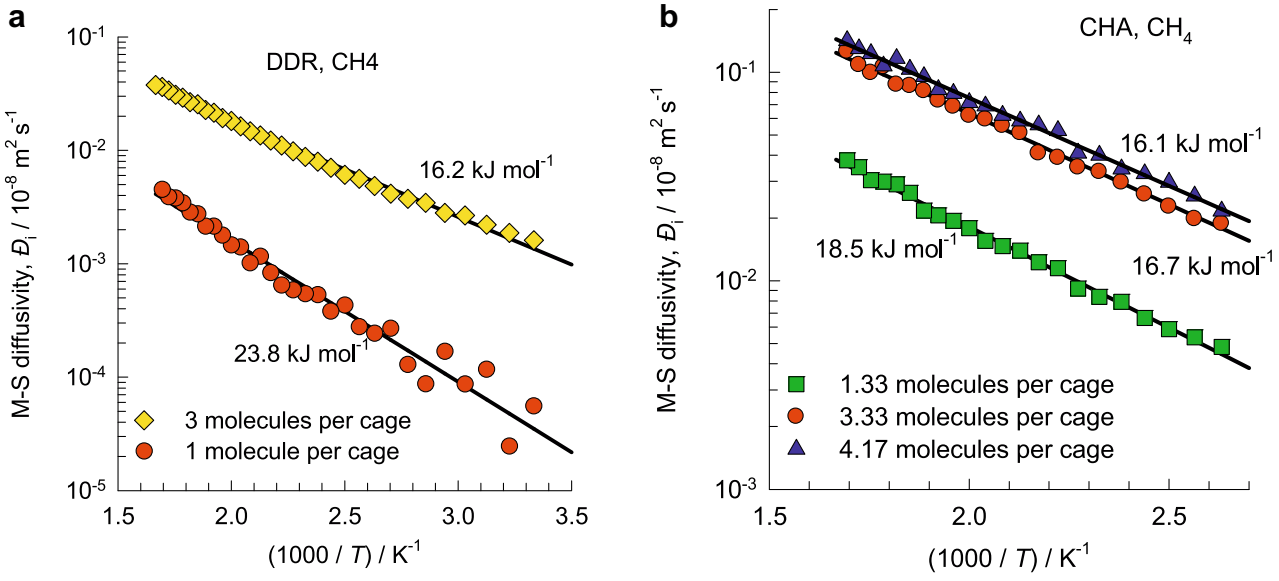

Fig. 4. Arrhenius plots for the M–S diffusivity of (a) CH_4/DDR and (b) CH_4/CHA at different loadings per cage.

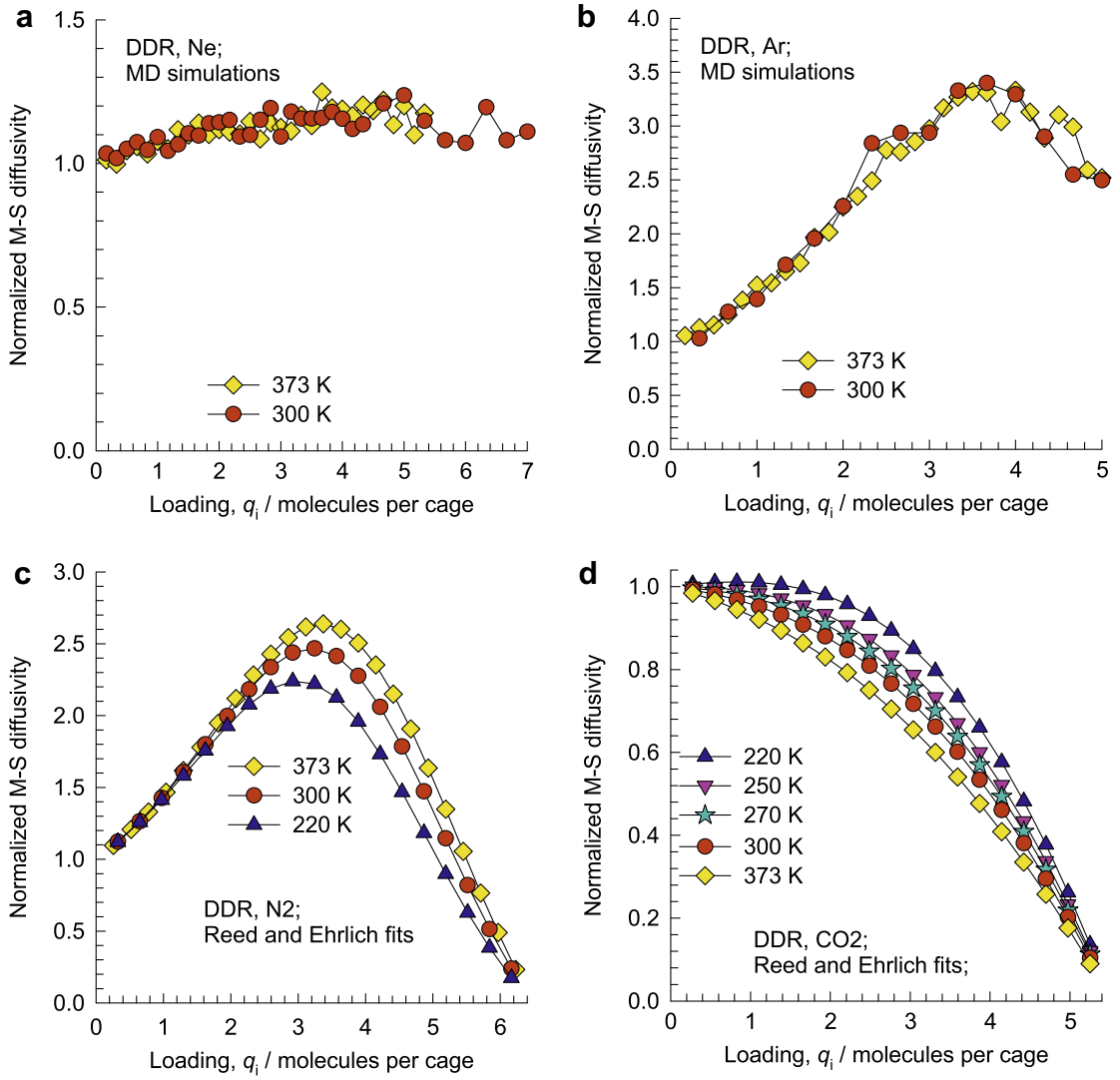

Fig. 5. Normalized M–S diffusivity for (a) Ne, (b) Ar, (c) CO_2, and (d) N_2 in DDR for a variety of temperatures as a function of the molecular loading q_i.

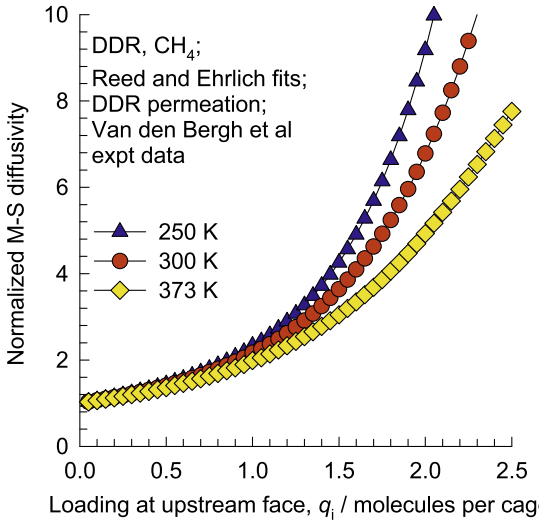

Fig. 6. Normalized Maxwell–Stefan diffusivities of CH_4 as a function of the cage loading at the upstream face of DDR membrane, for T = 250 K, 300 K, and 373 K. The calculations are the best fits to match the experimental DDR membrane permeation data of van den Bergh et al. [6,28]; details are available in the Supplementary material.

can be calculated as a function of the loading for T = 250 K, 300 K, and 373 K; see Fig. 6. We note that the loading dependence is steeper at lower T, than at higher T, in line with the MD simulation results. For CO_2 and N_2 permeation, on the other hand, the experimental data could be fitted with the parameter ϕ_i that is T-independent, broadly in line with MD simulation results.

As evidenced in published MD simulations [13,14,26], in other zeolite structures such as 1D channels (AFI, TON, MTW, MOR), intersecting channels (MFI, ISV, BEA), cages with large windows (FAU), the loading dependence is qualitatively different than for LTA, CHA, ERI and DDR; the $Đ_i$ generally decreases with increasing q_i. The influence of T on the $Đ_i - q_i$ dependence is also usually of less importance. This is illustrated in Fig. 7 by data on the normalized M–S diffusivity for CH_4/FAU, CH_4/MFI, and C_2H_4/MFI at different T. We note that the loading dependences for these guest–host combinations are practically independent of T.

3. Influence of T on the strength of correlations

At any given value of q_i, $D_{i,self}$ is lower than $Đ_i$, because of correlation effects [13,14]. Fig. 8 shows a plot of the parameter quantifying correlation effects, $(Đ_i/D_{i,self} - 1)$, versus the loading q_i at a variety of T for six different guest–host combinations: CH_4/LTA, Ar/DDR, Ne/DDR, CH_4/FAU, CH_4/MFI, and C_2H_4/MFI. In all cases

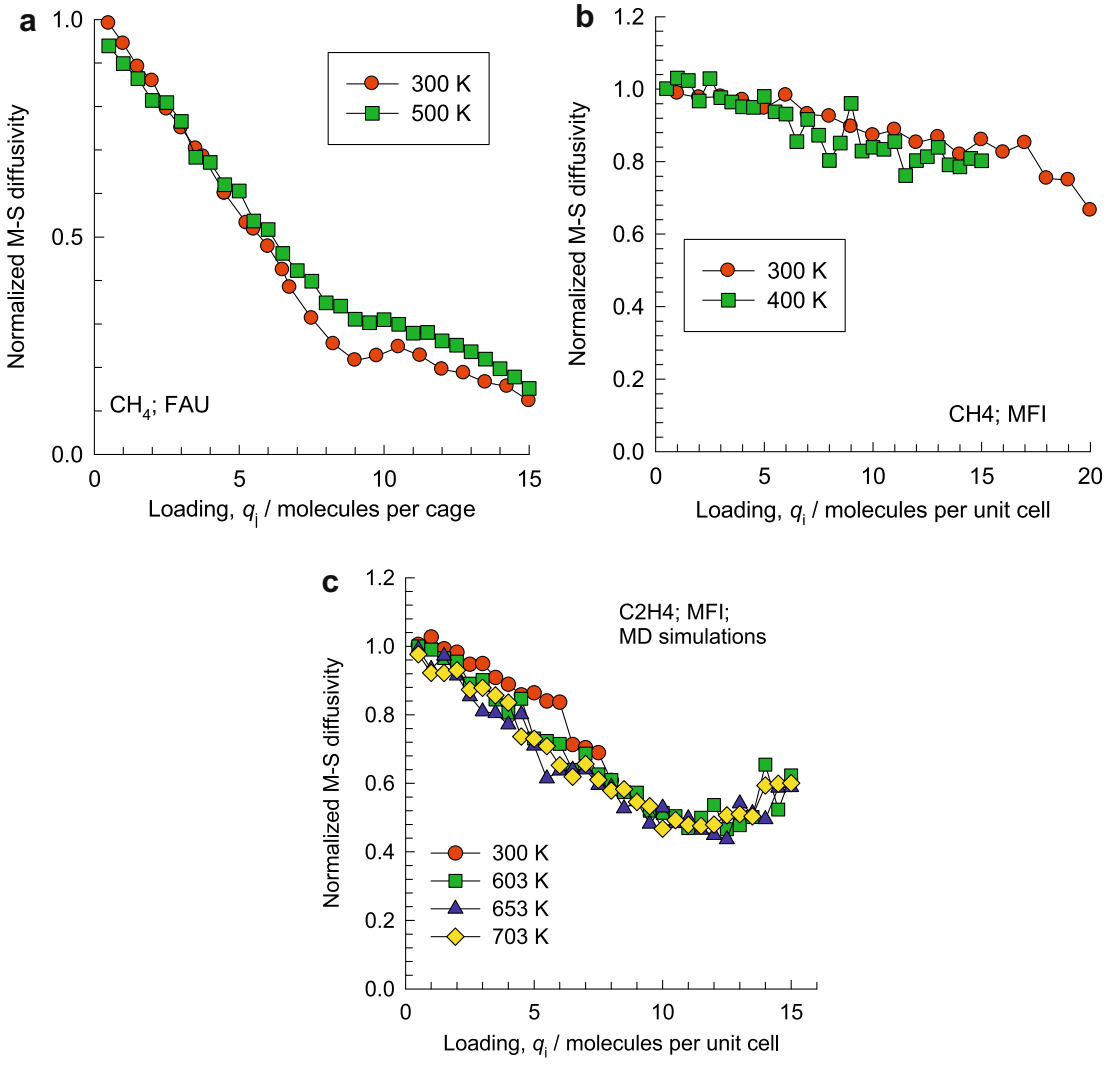

Fig. 7. Normalized M–S diffusivity for (a) CH_4/FAU, (b) CH_4/MFI, and (c) C_2H_4/MFI as a function of the molecular loading q_i for a variety of temperatures.

we note that $(Đ_i/D_{i,self} - 1)$ versus q_i is practically T-independent; this is a convenient result.

If $Đ_i/D_{i,self}$ is T-independent, the inescapable conclusion is that the activation energy for $D_{i,self}$ cannot be identical to that for $Đ_i$, unless correlation effects are negligibly small. To illustrate this let us consider three guest–host combinations: CH_4/LTA, Ar/DDR, and Ne/DDR at loadings q_i = 8, 3, and 3 molecules per cage, respectively. At these loadings the values of $(Đ_i/D_{i,self} - 1)$ for each case is smaller than 0.5 (cf. Fig. 8a, b, and c), signifying relatively weak correlations. The activation energies for $Đ_i$, and $D_{i,self}$ are equal to each other for all three combinations; see Fig. 9a, b, and c. Consider now the guest–host combinations CH_4/FAU, CH_4/MFI, and C_2H_4/MFI at loadings q_i = 80, 10, and 8 molecules per unit cell. In these cases $(Đ_i/D_{i,self} - 1) > 1.5$ (cf. Fig. 8d, e, and f), signifying relatively strong correlations. The activation energies for $Đ_i$ and $D_{i,self}$ differ by about 10% for all three combinations; see Fig. 9d, e, and f. For practical engineering design purposes the 10% differences could perhaps be ignored, but for consistent modeling purposes, the differences should be accounted for.

4. Conclusions

MD simulations for diffusion of a variety of guest molecules in five different zeolites LTA, FAU, MFI, CHA, and DDR have provided the following answers to the three questions posed in the Section 1.

(1) The loading dependence of the diffusivities ($Đ_i - q_i$, and $D_{i,self} - q_i$), in general, varies significantly with T for diffusion of cage-type zeolites such as LTA, CHA and DDR in which the guest molecules such as CH_4 and Kr that are tightly constrained at the window regions. In such cases the activation energy for diffusion changes with loading q_i. For diffusion of lightly constrained molecules such as CO_2, N_2, O_2, Ar, and Ne in DDR, or in CHA, the influence of T on the loading dependence is negligibly small or weak; this is also the case for CH_4/MFI, C_2H_4/MFI and CH_4/FAU. The model of Reed and Ehrlich [14,20,26] provides a good description of the combined influence of q_i and T on $Đ_i$.

(2) The strength of correlations, quantified by $(Đ_i/D_{i,self} - 1)$ is found to be practically T-independent for all guest–host combinations investigated.

(3) The activation energy for $D_{i,self}$, in general, differs than that for $Đ_i$. The difference is negligibly small if the correlation effects are small. Conversely, when correlation effects are significant the activation energy for $D_{i,self}$ can be approximately 10% different than that for $Đ_i$.

The current study has been restricted to cation-free zeolites, and the influence of the presence of cations on the loading dependence needs further investigation.

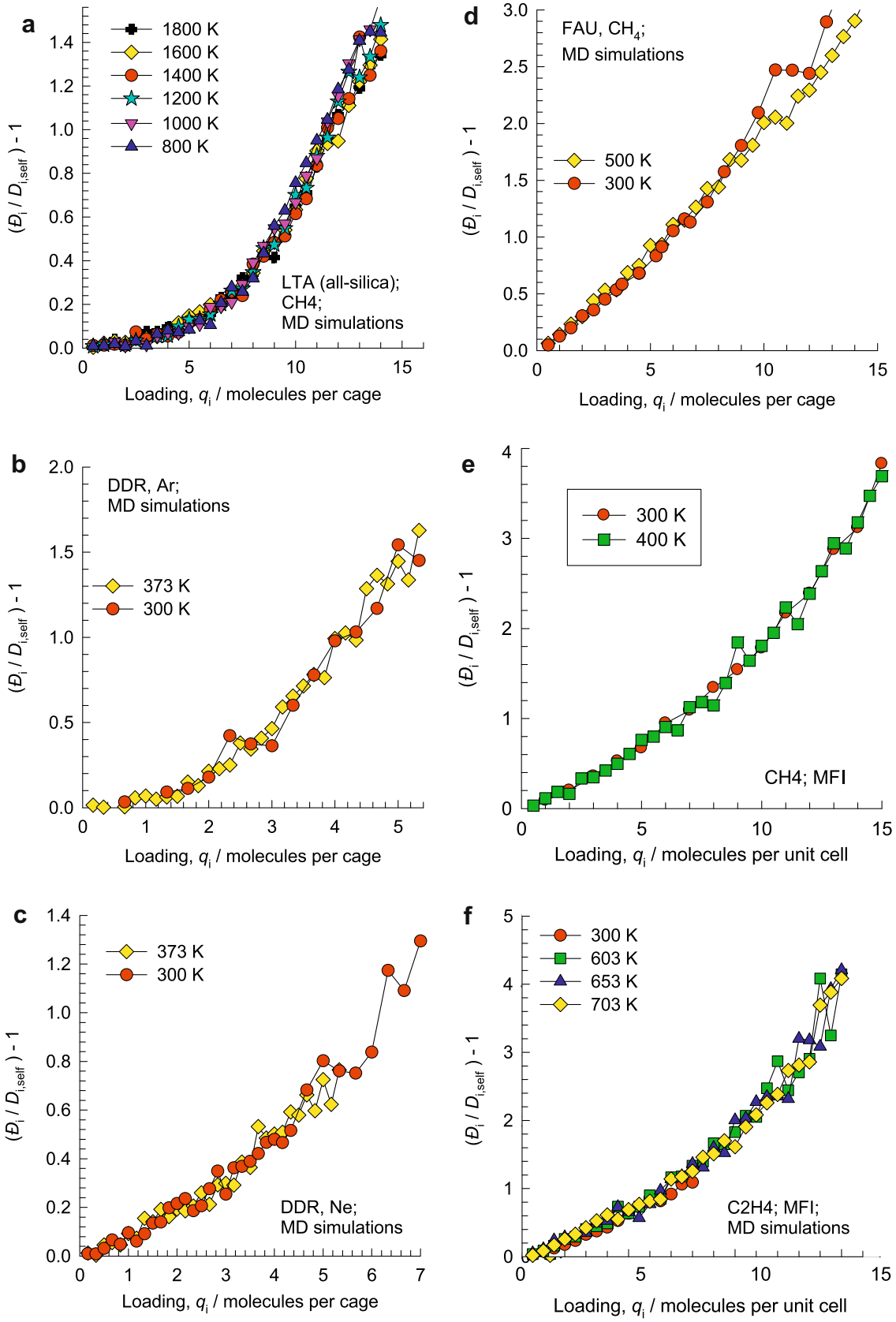

Fig. 8. The correlation parameter $(Đ_i/D_{i,self} - 1)$ for (a) CH_4/LTA, (b) Ar/DDR, (c) Ne/DDR, (d) CH_4/FAU, (e) CH_4/MFI, and (f) C_2H_4/MFI as function of loading q_i for various temperatures.

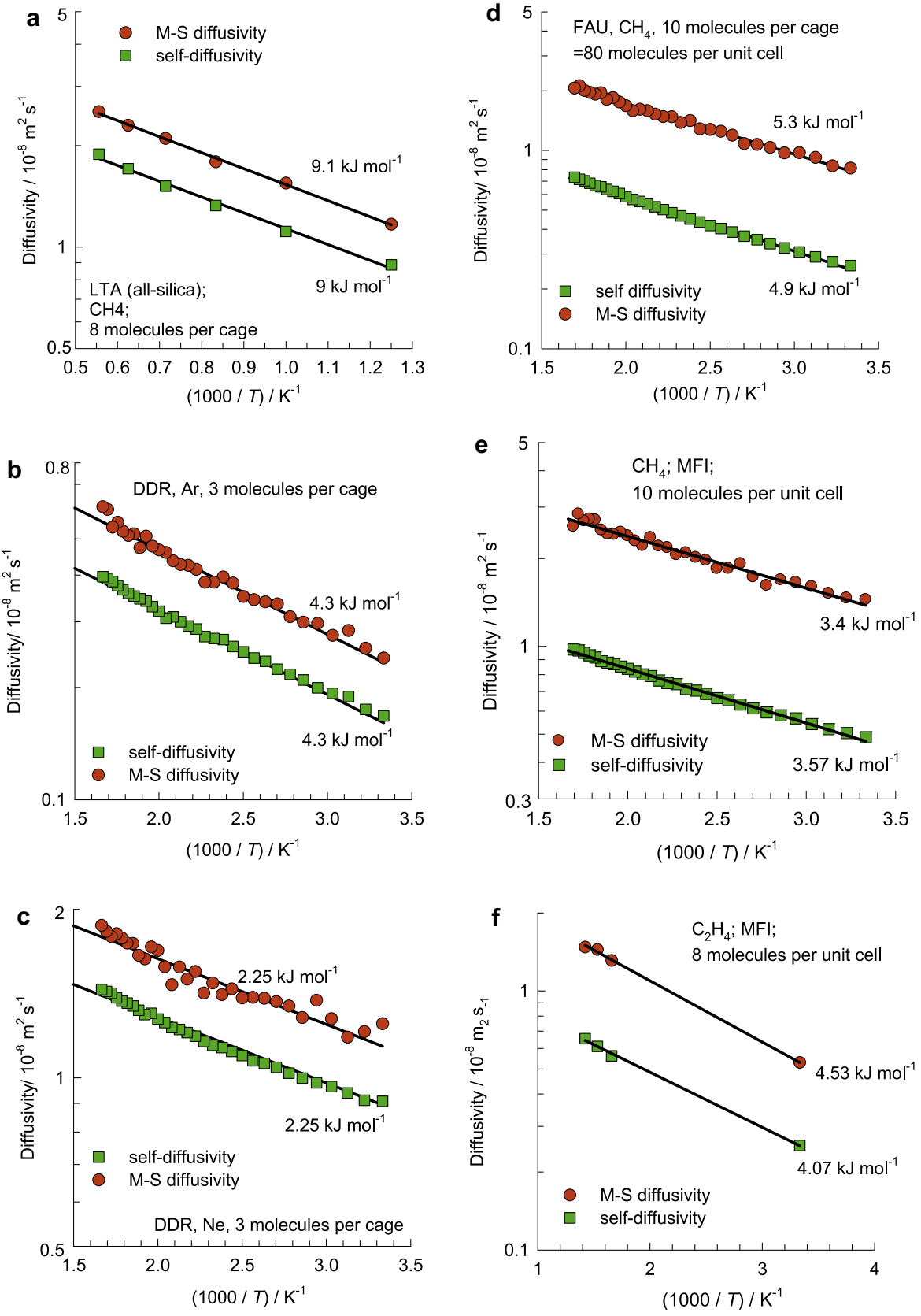

Fig. 9. Comparison of Arrhenius plots for $D_{i,self}$ and $Đ_i$ at a fixed loading for (a) CH_4/LTA, (b) Ar/DDR, (c) Ne/DDR, (d) CH_4/FAU, (e) CH_4/MFI, and (f) C_2H_4/MFI.

Acknowledgments

RK acknowledges the grant of a TOP subsidy from the Netherlands Foundation for Fundamental Research (NWO-CW) for intensification of reactors.

Appendix A. Supplementary data

Supplementary data associated with this article can be found, in the online version, at doi:10.1016/j.micromeso.2009.01.015.

References

[1] J. Kärger, D.M. Ruthven, Diffusion in Zeolites and Other Microporous Solids, John Wiley, New York, 1992.
[2] J. Caro, M. Noack, Microporous Mesoporous Mat. 115 (2008) 215.
[3] B. Smit, T.L.M. Maesen, Chem. Rev. 108 (2008) 4125.
[4] N. Hansen, R. Krishna, J.M. van Baten, A.T. Bell, F.J. Keil, J. Phys. Chem. C 113 (2009) 235.
[5] S. Li, J.L. Falconer, R.D. Noble, R. Krishna, J. Phys. Chem. C 111 (2007) 5075.
[6] J. van den Bergh, W. Zhu, J. Gascon, J.A. Moulijn, F. Kapteijn, J. Membrane Sci. 316 (2008) 35.
[7] S. Himeno, T. Tomita, K. Suzuki, K. Nakayama, S. Yoshida, Ind. Eng. Chem. Res. 46 (2007) 6989.
[8] M. Schenk, S.L. Vidal, T.J.H. Vlugt, B. Smit, R. Krishna, Langmuir 17 (2001) 1558.
[9] D.M. Ruthven, Principles of Adsorption and Adsorption Processes, John Wiley, New York, 1984.
[10] J. Kärger, S. Vasenkov, S.M. Auerbach, Diffusion in zeolites, in: S.M. Auerbach, K.A. Carrado, P.K. Dutta (Eds.), Handbook of Zeolite Science and Technology, Marcel Dekker, New York, 2003 (Chapter 10).
[11] G.R. Gavalas, Ind. Eng. Chem. Res. 47 (2008) 5797.
[12] A.I. Skoulidas, D.S. Sholl, R. Krishna, Langmuir 19 (2003) 7977.
[13] R. Krishna, J.M. van Baten, Chem. Eng. Sci. 63 (2008) 3120.
[14] R. Krishna, J.M. van Baten, Microporous Mesoporous Mater. 109 (2008) 91.
[15] A.T. Bell, E.J. Maginn, D.N. Theodorou, Molecular simulation of adsorption and diffusion in zeolites, in: G. Ertl, H. Knözinger, J. Weitkamp (Eds.), Handbook of Heterogeneous Catalysis, VCH, Weinheim, 1997.
[16] S. Chempath, R. Krishna, R.Q. Snurr, J. Phys. Chem. B 108 (2004) 13481.
[17] H. Jobic, D.N. Theodorou, Microporous Mesoporous Mater. 102 (2006) 21.
[18] R. Nagumo, H. Takaba, S. Nakao, J. Phys. Chem. C 112 (2008) 2805.
[19] R. Nagumo, H. Takaba, S. Nakao, Chem. Phys. Lett. 458 (2008) 281.
[20] D.A. Reed, G. Ehrlich, Surf. Sci. 102 (1981) 588.
[21] R. Krishna, D. Paschek, R. Baur, Microporous Mesoporous Mater. 76 (2004) 233.
[22] G.K. Papadopoulos, H. Jobic, D.N. Theodorou, J. Phys. Chem. B 108 (2004) 12748.
[23] P. Demontis, G.B. Suffritti, S. Yashonath, J. Phys. Chem. C 112 (2008) 17030.
[24] E. Beerdsen, D. Dubbeldam, B. Smit, Phys. Rev. Lett. 95 (2005) 164505.
[25] E. Beerdsen, D. Dubbeldam, B. Smit, Phys. Rev. Lett. 96 (2006) 044501.
[26] R. Krishna, J.M. van Baten, J. Phys. Chem. B 109 (2005) 6386.
[27] A. Schüring, S.M. Auerbach, S. Fritzsche, R. Haberlandt, J. Chem. Phys. 116 (2002) 10890.
[28] J. van den Bergh, W. Zhu, J.C. Groen, F. Kapteijn, J.A. Moulijn, K. Yajima, K. Nakayama, T. Tomita, S. Yoshida, Stud. Surf. Sci. Catal. 170 (2007) 1021.

-Supplementary material to accompany:

A molecular dynamics investigation of a variety of influences of temperature on diffusion in zeolites

R. Krishna*, J.M. van Baten

Van 't Hoff Institute for Molecular Sciences, University of Amsterdam, Nieuwe Achtergracht 166,

1018 WV Amsterdam, The Netherlands

GCMC simulation methodology

Adsorption equilibria of a variety of molecules (CO_2, CH_4, C_2H_4, N_2, Ar, Ne, Kr, and O_2) in LTA, CHA, FAU, MFI, and DDR zeolites were computed using Monte Carlo (MC) simulations in the grand canonical (GC) ensemble. The crystallographic data are available elsewhere.[1] The window sizes of these cage-type zeolites are listed in Table 1. The zeolite lattices are rigid during simulations, with static atomic charges that are assigned by choosing q_{Si} = +2.05 and q_O = -1.025, following the works of Jaramillo and Auerbach [2] and Calero et al.[3]. CH_4 molecules are described with a united atom model, in which each molecule is treated as a single interaction center.[4] The interaction between adsorbed molecules is described with Coulombic and Lennard-Jones terms. The Coulombic interactions in the system are calculated by Ewald summation for periodic systems[5]. The parameters for CH_4 are taken from Dubbeldam et al[6] and Calero et al.[3]. CO_2 molecules are taken linear and rigid with bond length C–O of 1.16Å according to the 3LJ3CB.EPM2 model developed by Harris and Young [7]. We use the 2LJ3CB.MSKM model for N_2 dumbbell molecules with a rigid interatomic bond of 1.098Å[8, 9]. The partial charges of N_2 and CO_2 are distributed around each molecule to reproduce experimental quadrupole moment. The interactions between adsorbed molecules and the zeolite are dominated by dispersive forces between the pseudo-atoms and the oxygen atoms of the zeolite [10, 11] and the interactions of silicon and aluminium are considered through an effective potential with only the oxygen atoms. The Lennard-Jones parameters for CH_4-zeolite interactions are taken from Dubbeldam et al.[6]. The Lennard-Jones parameters for CO_2-zeolite and N_2-zeolite interactions are essentially those of Makrodimitris et al.[9]; see also García-Pérez et al.[12]. The force fields for Ne and Ar are taken from the paper by Skoulidas and Sholl[13]. The force field for Kr is from Talu and Myers [14]. The force field for O_2 is taken from the work of Mellot and Lignieres[15]. The force field for ethene is taken form the work of Ban et al. [16].

Table 2 summarizes the information on the force fields. Figure 1 presents cartoons showing the approximate molecular dimensions of Ne, Ar, Kr, N_2, O_2, CO_2, CH_4. and C_2H_4. The molecular diameters are estimated on the basis of the Lennard-Jones size parameters σ for molecule-molecule interactions. The molecular lengths are estimated on the basis of the bond lengths.

The Lennard-Jones potentials are shifted and cut at 12 Å. The number of unit cells in the simulation box was chosen such that the minimum length in each of the coordinate directions was larger than 24 Å. Periodic boundary conditions were employed. Further GCMC simulation details are available in earlier publications[3, 6, 17].

The GCMC simulations were performed using the BIGMAC code developed by T.J.H. Vlugt[18] as basis. The code was modified to handle rigid molecular structures and charges. S. Calero is gratefully acknowledged for her technical inputs in this regard. Detailed validation of the force fields used for CH_4, CO_2, and N_2 is available elsewhere[6, 12]. Additional verification of the force fields used is provided by comparison of the simulated adsorption isotherms for a variety of gases in DDR zeolite with recent experimental data of Van den Bergh et al. [19, 20] and Himeno et al. [21, 22].

1. MD simulation methodology

Diffusion is simulated using Newton's equations of motion until the system properties, on average, no longer change in time. The Verlet algorithm is used for time integration. A time step of 1 fs was used in all simulations. For each simulation, *initializing* GCMC moves are used to place the molecules in the domain, minimizing the energy. Next, follows an *equilibration* stage. These are essentially the same as the production cycles, only the statistics are not yet taken into account. This removes any initial large disturbances in the system do not affect statistics. After a fixed number of initialization and equilibrium steps, the MD simulation *production* cycles start. For every cycle, the statistics for determining the mean square displacements (MSDs) are updated. The MSDs are determined for time intervals ranging from 2 fs to 1 ns. In order to do this, an order-*N* algorithm, as detailed in Chapter 4 of Frenkel and Smit[5] is implemented. The Nosé-Hoover thermostat is applied to all the diffusing particles.

The DLPOLY code[23] was used along with the force field implementation as described in the previous section. DL_POLY is a molecular dynamics simulation package written by W. Smith, T.R. Forester and I.T. Todorov and has been obtained from CCLRCs Daresbury Laboratory via the website.[23]

MD simulations were carried out to determine the diffusivities of both pure components and binary mixtures for a variety of molecular loadings. All simulations were carried out on clusters of PCs equipped with Intel Xeon processors running at 3.4 GHz on the Linux operating system. Each MD simulation, for a specified loading, was run for 120 h, determined to be long enough to obtain reliable statistics for determination of the diffusivities. Several independent MD simulations were run and the results averaged.

The self-diffusivities, $D_{\mathrm{i,self}}$, were computed by analyzing the mean square displacement of each species i for each of the coordinate directions:

$$D_{i,self} = \frac{1}{2n_i} \lim_{\Delta t \to \infty} \frac{1}{\Delta t} \left\langle \left(\sum_{l=1}^{n_i} \left(\mathbf{r}_{l,i}(t + \Delta t) - \mathbf{r}_{l,i}(t) \right)^2 \right) \right\rangle \qquad (1)$$

In this expression n_{i} represents the number of molecules of species i respectively, and $\mathbf{r}_{\mathrm{l,i}}(t)$ is the position of molecule l of species i at any time t. The expression (1) also defines the self-diffusivity in a n-component mixture.

For single component diffusion, the Maxwell-Stefan diffusivity was determined for each of the coordinate directions from

$$Đ_i = \frac{1}{2} \lim_{\Delta t \to \infty} \frac{1}{n_i} \frac{1}{\Delta t} \left\langle \left(\sum_{l=1}^{n_i} \left(\mathbf{r}_{l,i}(t + \Delta t) - \mathbf{r}_{l,i}(t) \right) \right)^2 \right\rangle \qquad (2)$$

For DDR the reported diffusivities are the averages in x- and y- directions $Đ = \left(Đ_x + Đ_y \right)/2$. For MFI, CHA and LTA the average values calculated according to $Đ = \left(Đ_x + Đ_y + Đ_z \right)/3$ are presented. In all cases reported here, the MSD values were linear in t for $t > 10$ ps (used in data regression analysis to determine the diffusivities) and we found no evidence of single file diffusion characteristics.

For CH_4/DDR the molecules are tightly constrained at the window regions; the self- and M-S diffusivities are close to each other. In this case only, the reported in the manuscript as M-S diffusivities $Đ_i$ are, in actual fact, the self-diffusivities, $D_{i,self}$ that are more accurately determinable.

The self-exchange coefficient $Đ_{ii}$ were calculated from

$$Đ_{ii} = \frac{\theta_i}{\frac{1}{D_{i,self}} - \frac{1}{Đ_i}} \tag{3}$$

where θ_i is the fractional occupancy:

$$\theta_i = \frac{q_i}{q_{i,sat}} \tag{4}$$

Two kinds of MD campaigns were carried out. Firstly, for a fixed temperature the loading was varied up to saturation limit. Secondly, for a fixed loading, the temperatures were varied.

2. MD animations

Animations of MD simulations for diffusion of a variety of molecules in DDR, CHA, MFI, FAU, and LTA are available on our web site [24].

3. Simulation results for CH_4 in LTA

LTA consists of cages separated by windows of 4.1 Å size; see the framework structure and pore landscape in Figure 2. Figure 3 presents the GCMC simulations of the pure component isotherms for CH_4 in LTA at temperatures T = 800 K, 1000 K, 1200 K, 1400 K, 1600 K, and 1800 K. From this data the saturation capacity $q_{i,sat}$ is determined as 16 molecules per cage. Also shown are the data for $\left(Đ_i / D_{i,self} - 1\right)$ at various T. Figure 4 shows the data on $D_{i,self}$ and $Đ_i$ for CH_4 in LTA at different temperatures T. Also shown in Figure 4 are the diffusivity data normalized with respect to the zero-loading diffusivities. Figure 5 presents the Arrhenius plots and activation energies for diffusion of CH_4 in LTA.

4. Simulation results for CH_4 in CHA

CHA consists of cages separated by windows of 3.8 Å size; see the framework structure and pore landscape in Figure 6.

Figure 7 presents data on $D_{\mathrm{i,self}}$, $Đ_{\mathrm{i}}$, and $\left(Đ_i / D_{i,self} - 1\right)$ data for CH_4 in CHA at different temperatures T, along with Arrhenius plots.

Figure 8 presents data on $D_{\mathrm{i,self}}$, $Đ_{\mathrm{i}}$, and $\left(Đ_i / D_{i,self} - 1\right)$ data for Ar in CHA at different temperatures T, along with Arrhenius plots.

5. Simulation results for CH_4 in FAU

FAU consists of cages separated by 12-ring windows of 7.4 Å size; see the framework structure and pore landscape in Figure 9

Figure 10 shows $D_{\mathrm{i,self}}$, $Đ_{\mathrm{i}}$, and $\left(Đ_i / D_{i,self} - 1\right)$ data for CH_4 in FAU at different temperatures T, along with Arrhenius plots

6. Simulation results for CH_4 and C_2H_4 in MFI

MFI consists of two 10 T-ring intersecting channels of 5.1 – 5.5 Å and 5.3 – 5.6 Å sizes; the pore structure and landscape are shown in Figure 11.

Figure 12 Data on $D_{\mathrm{i,self}}$, $Đ_{\mathrm{i}}$, and $\left(Đ_i / D_{i,self} - 1\right)$ data for CH_4 in MFI at different temperatures T, along with Arrhenius plots

Figure 13 shows the GCMC simulations of the pure component isotherm for C_2H_4 in MFI at 300 K, along with snapshot showing the location of molecules. Figure 14 presents data on $D_{\mathrm{i,self}}$ and $Đ_{\mathrm{i}}$ for C_2H_4 in MFI at temperatures T = 300 K, 603 K, 653 K, and 703 K. Figure 15 presents the Arrhenius

plots for the T-dependence of $D_{i,self}$ and $Đ_i$. Also shown in Figure 15 are $\left(Đ_i / D_{i,self} - 1\right)$ data for diffusion of C_2H_4 in MFI T = 300 K, 603 K, 653 K, and 703 K..

7. Simulation data for DDR, and force field validation

DDR zeolite consists of cages separated by narrow elliptical shaped windows of 3.6 – 4.4 Å size. See the pore structure and landscapes in Figure 16. Comparisons of the experimental data of Van den Bergh et al. [19, 20] and Himeno et al. [21, 22] with GCMC simulations for CH_4, CO_2, N_2, O_2, Ar, and Kr in DDR are given in Figures 17, 18, 19, 20, 21, and 22. These data give an indication of the validity of the force fields used in this study. We also carried out GCMC simulations for pure component isotherms for Ne, for which Van den Bergh et al. [20] were not able to determine the isotherms.

For re-analysis and re-interpretation of the data of Van den Bergh et al. [19, 20] for permeation across a DDR membrane, to be presented below, we need to fit the isotherms. All the GCMC simulated isotherms were fitted with the 3-site Langmuir model

$$q_i = \frac{q_{i,sat,A} b_{i,A} f_i}{1 + b_{i,A} f_i} + \frac{q_{i,at,B} b_{i,B} f_i}{1 + b_{i,B} f_i} + \frac{q_{i,at,C} b_{i,C} f_i}{1 + b_{i,C} f_i} \qquad (5)$$

It was found impossible to fit any of the component isotherms with either a 2-site or single site Langmuir model. The 3-site Langmuir fits are "empirical" and the individual sites cannot be identified with specific locations within DDR. In eq. (5) q_i is the molar loading expressed in mol kg^{-1}, $q_{i,sat,A}$ is the saturation loading of site A, and f_i is the fugacity of the bulk gas phase. The values of the fitted T-dependent parameters b_i and $q_{i,sat}$ are specified in Table 3. Note that the data were fitted with loading in the units of mol kg^{-1}. In the main text of the paper, the data have been presented in the units of molecules per cage. A loading of 1 molecule per cage corresponds with 0.832 mol kg^{-1}. The total number of GCMC data points (at varying fugacity and temperature) used in the data fits were: CH_4 = 378; CO_2 = 320; N_2 = 321; O_2 = 168; Ar = 194; Kr = 192; Ne = 95.

The MD simulation results for $Đ_i$, and $\left(Đ_i / D_{i,self} - 1\right)$ of CO_2, N_2, CH_4, Ar, O_2, Kr, and Ne are presented in Figures 23, 24, 25, 26, 27, 28, and 29. Also presented in these figures are the fitted values of the Reed and Ehrlich parameter ϕ_i.

8. Re-analysis of Van den Bergh [19, 20] unary permeation data

Van den Bergh et al. [19, 20] have published data for unary permeation of CH_4, CO_2, and N_2 across a DDR membrane for a set of temperatures and pressures. We begin by developing a model to describe their unary permeation data. For this purpose we use the approach developed in our earlier publication [25]. A brief summary of the approach is given below.

The Reed-Ehrlich model is used to describe the M-S diffusivity as a function of the fractional occupancy, θ_i and temperature, T:

$$Đ_i(T) = Đ_i(0)\exp(-\frac{E_{diff,i}}{RT})\frac{(1+\varepsilon_i)^{z-1}}{(1+\varepsilon_i/\phi_i)^z} \tag{6}$$

where z is the coordination number, representing the maximum number of nearest neighbors within a cage. The parameter $E_{diff,i}$ is the activation energy for diffusion of species i. The value of z is chosen to be 5, as this represents the maximum number of molecules within a cage. The choice of this z parameter is not crucial because the key parameter ϕ_i is to be fitted empirically in any event. The other parameters are defined as

$$\varepsilon_i = \frac{(\beta_i - 1 + 2\theta_i)\phi_i}{2(1-\theta_i)}; \quad \beta_i = \sqrt{1 - 4\,\theta_i(1-\theta_i)(1-1/\phi_i)} \tag{7}$$

Using the Reed-Ehrlich loading dependence, and a 3-site Langmuir fit for the pure component isotherms we define a modified driving force MDF_i

$$MDF_i \equiv \int_{f_{i,down}}^{f_{i,up}} \frac{(1+\varepsilon_i)^{z-1}}{(1+\varepsilon_i/\phi_i)^z}\frac{q_i}{f_i}df_i = \int_{f_{i,down}}^{f_{i,up}} \frac{(1+\varepsilon_i)^{z-1}}{(1+\varepsilon_i/\phi_i)^z}\left(\frac{q_{i,sat,A}b_{iA}}{1+b_{iA}f_i} + \frac{q_{i,sat,B}b_{iB}}{1+b_{iB}f_i} + \frac{q_{i,sat,C}b_{iC}}{1+b_{iC}f_i}\right)df_i \tag{8}$$

The unary permeation flux at any given T is

$$N_i(T) = \frac{\rho Đ_i(0)}{\delta} \exp(-\frac{E_{diff,i}}{RT}) MDF_i \qquad (9)$$

It is to be noted that eq (9) assumes each permeation experiment is carried out under isothermal conditions and there is no temperature gradient across the membrane. From the unary permeation data, $\rho Đ_i(0)/\delta$, $E_{\text{diff,i}}$ and ϕ_i can be backed out by fitting to the measured permeation fluxes. For the reasons discussed in the main text of this paper, the ϕ_i was fitted in the form

$$\phi_i = \exp(\frac{a_0 + a_1 T}{RT}) \exp(b\theta_i) \qquad (10)$$

The backed-out data are summarized in Table 4. Figure 30 shows the unary permeation data of Van den Bergh et al. [19, 20], along with the calculations following eq (9). The unary permeation data for CH_4, CO_2, and N_2 includes the sets published in both papers [19, 20].

Figure 31. shows the fitted Reed-Ehrlich parameter ϕ_i for CO_2, N_2, and CH_4 as a function of the cage loading, for T = 250 K, 300 K, and 373 K. The experimental data for CO_2 permeation covers a range of upstream loadings up to a maximum of about 4.2 molecules per cage. The experimental data for N_2 permeation covers a range of upstream loadings up to a maximum of about 1 molecules per cage. The experimental data for CH_4 permeation covers a range of upstream loadings up to a maximum of about 2.3 molecules per cage. Figure 32 presents the normalized Maxwell-Stefan diffusivities of CO_2, N_2, and CH_4 as a function of the cage loading, for T = 250 K, 300 K, and 373 K.

9. Notation

b_i	Langmuir constant, Pa^{-1}
$D_{i,self}$	self-diffusivity, $m^2\ s^{-1}$
$Đ_i$	Maxwell-Stefan diffusivity of species *i*, $m^2\ s^{-1}$
$Đ_i(0)$	zero-loading M-S diffusivity of species *i*, $m^2\ s^{-1}$
$Đ_{ii}$	self-exchange diffusivity, $m^2\ s^{-1}$
$E_{diff,i}$	activation energy for diffusion *i*, J mol^{-1}
f_i	fugacity of species *i*, Pa
MDF_i	modified driving force for transport across membrane, mol kg^{-1}
N_i	molar flux of species *i*, mol $m^{-2}\ s^{-1}$
n_i	number of molecules of species *i* in simulation box, dimensionless
q_i	loading of species *i*, mol kg^{-1} or molecules per unit cell or molecules per cage
$q_{i,sat}$	saturation loading of species *i*, mol kg^{-1} or molecules per unit cell or molecules per cage
$\mathbf{r}_{l,i}(t)$	position of molecule *l* of species *i* at any time *t*, m
R	gas constant, 8.314 J $mol^{-1}\ K^{-1}$
t	time, s
T	absolute temperature, K
x	spatial distance, m
z	coordination number, dimensionless

Greek letters

β_i	Reed-Ehrlich parameter, dimensionless
Γ_i	thermodynamic factor, dimensionless
δ	thickness of zeolite membrane, m
θ_i	fractional occupancy of component *i*, dimensionless
μ_i	molar chemical potential, J mol^{-1}
ρ	framework density of zeolite, kg m^{-3} or unit cells m^{-3} or cages m^{-3}

Subscripts

sat	referring to saturation conditions
i,j	components in mixture

10. References

[1] C. Baerlocher, L.B. McCusker, Database of Zeolite Structures, International Zeolite Association, http://www.iza-structure.org/databases/, 26 June 2001.

[2] E. Jaramillo, S.M. Auerbach, New force field for Na cations in faujasite-type zeolites, J. Phys. Chem. B 103 (1999) 9589-9594.

[3] S. Calero, D. Dubbeldam, R. Krishna, B. Smit, T.J.H. Vlugt, J.F.M. Denayer, J.A. Martens, T.L.M. Maesen, Understanding the role of sodium during adsorption. A force field for alkanes in sodium exchanged faujasites, J. Am. Chem. Soc. 126 (2004) 11377-11386.

[4] J.P. Ryckaert, A. Bellemans, Molecular dynamics of liquid alkanes, Faraday Discuss. Chem. Soc. 66 (1978) 95-106.

[5] D. Frenkel, B. Smit, Understanding molecular simulations: from algorithms to applications, Academic Press, 2nd Edition, San Diego, 2002.

[6] D. Dubbeldam, S. Calero, T.J.H. Vlugt, R. Krishna, T.L.M. Maesen, B. Smit, United Atom Forcefield for Alkanes in Nanoporous Materials, J. Phys. Chem. B 108 (2004) 12301-12313.

[7] J.G. Harris, K.H. Yung, Carbon Dioxide's Liquid-Vapor Coexistence Curve And Critical Properties as Predicted by a Simple Molecular Model, J. Phys. Chem. 99 (1995) 12021-12024.

[8] C.S. Murthy, K. Singer, M.L. Klein, I.R. McDonald, Pairwise additive effective potentials for nitrogen, Mol. Phys. 41 (1980) 1387-1399.

[9] K. Makrodimitris, G.K. Papadopoulos, D.N. Theodorou, Prediction of permeation properties of CO_2 and N_2 through silicalite via molecular simulations, J. Phys. Chem. B 105 (2001) 777-788.

[10] A.G. Bezus, A.V. Kiselev, A.A. Lopatkin, P.Q. Du, Molecular statistical calculation of the thermodynamic adsorption characteristics of zeolites using the atom-atom approximation. Part 1. Adsorption of methane by zeolite sodium-X, J.Chem.Soc., Faraday Trans. II 74 (1978) 367-379.

[11] A.V. Kiselev, A.A. Lopatkin, A.A. Shul'ga, Molecular statistical calculation of gas adsorption by silicalite, Zeolites 5 (1985) 261-267.

[12] E. García-Pérez, J.B. Parra, C.O. Ania, A. García-Sánchez, J.M. Van Baten, R. Krishna, D. Dubbeldam, S. Calero, A computational study of CO_2, N_2 and CH_4 adsorption in zeolites, Adsorption 13 (2007) 469-476.

[13] A.I. Skoulidas, D.S. Sholl, Transport diffusivities of CH_4, CF_4, He, Ne, Ar, Xe, and SF_6 in silicalite from atomistic simulations, J. Phys. Chem. B 106 (2002) 5058-5067.

[14] O. Talu, A.L. Myers, Reference potentials for adsorption of helium, argon, methane and krypton in high-silica zeolites, Colloids Surf., A 187-188 (2001) 83-93.

[15] C. Mellot, J. Lignieres, Monte Carlo SImulations of N_2 and O_2 adsorption in silicalites and CaLSX zeolites, Mol. Simulation 18 (1997) 349-365.

[16] S. Ban, A. van Laak, P.E. de Jongh, J.P.J.M. van der Eerden, T.J.H. Vlugt, Adsorption Selectivity of Benzene and Propene Mixtures for Various Zeolites, J. Phys. Chem. C 111 (2007) 17241-17248.

[17] T.J.H. Vlugt, R. Krishna, B. Smit, Molecular simulations of adsorption isotherms for linear and branched alkanes and their mixtures in silicalite, J. Phys. Chem. B 103 (1999) 1102-1118.

[18] T.J.H. Vlugt, BIGMAC, University of Amsterdam, http://molsim.chem.uva.nl/bigmac/, 1 November 2000.

[19] J. van den Bergh, W. Zhu, J.C. Groen, F. Kapteijn, J.A. Moulijn, K. Yajima, K. Nakayama, T. Tomita, S. Yoshida, Natural Gas Purification with a DDR Zeolite Membrane; Permeation Modelling with Maxwell-Stefan Equations, Stud. Surf. Sci. Catal. 170 (2007) 1021-1027.

[20] J. van den Bergh, W. Zhu, J. Gascon, J.A. Moulijn, F. Kapteijn, Separation and Permeation Characteristics of a DD3R Zeolite Membrane, J. Membr. Sci. 316 (2008) 35-45.

[21] S. Himeno, T. Tomita, K. Suzuki, S. Yoshida, Characterization and selectivity for methane and carbon dioxide adsorption on the all-silica DD3R zeolite, Microporous Mesoporous Mater. 98 (2007) 62-69.
[22] S. Himeno, T. Tomita, K. Suzuki, K. Nakayama, S. Yoshida, Synthesis and Permeation Properties of a DDR-type zeolite membrane for Separation of CO_2/CH_4 Gaseous Mixtures, Ind. Eng. Chem. Res. 46 (2007) 6989-6997.
[23] W. Smith, T.R. Forester, I.T. Todorov, The DL_POLY Molecular Simulation Package, Warrington, England, http://www.cse.clrc.ac.uk/msi/software/DL_POLY/index.shtml, March 2006.
[24] J.M. van Baten, R. Krishna, MD animations of diffusion in nanoporous materials, University of Amsterdam, Amsterdam, http://www.science.uva.nl/research/cr/animateMD/, 4 November 2008.
[25] R. Krishna, J.M. van Baten, E. García-Pérez, S. Calero, Incorporating the loading dependence of the Maxwell-Stefan diffusivity in the modeling of CH_4 and CO_2 permeation across zeolite membranes, Ind. Eng. Chem. Res. 46 (2007) 2974-2986.

Table 1. Characteristic sizes of channels or windows for zeolite structures

Zeolite	**Channel or window size/ Å**
FAU	12-ring window of 7.4 Å size
MFI	10 T-ring intersecting channels of 5.1 – 5.6 Å size
LTA	8 T-ring window of 4.1 Å size
CHA	8 T-ring window of 3.8 Å size
DDR	8 T-ring window of 3.6 Å- 4.4 Å size

Table 2. Summary of force field used in GCMC and MD simulations

The interaction between adsorbates was calculated using Lennard-Jones potentials and electrostatic interactions using an Ewald summation method. For adsorbate-adsorbate interactions, Lorentz-Berthelot mixing rules were applied for σ and ε/k_B. Leonard-Jones interaction with the zeolite was only taken σ and ε/k_B and epsilon for the adsorbates and for the interaction with the adsorbates and with the zeolites. The charges are also shown for the pseudo atoms.

(pseudo-) atom	Atom-atom σ / Å	Atom-atom ε/k_B / K	Atom - O in zeolite σ / Å	Atom - O in zeolite ε/k_B / K	charge
CH_4	3.72	158.5	3.47	115	0
C (CO_2)	2.757	28.129	2.7815	50.2	0.6512
O (CO_2)	3.033	80.507	2.9195	84.93	-0.3256
N (N_2)	3.32	36.4	3.06	58.25	-0.40484
O (O_2)	3.0896	44.5	2.97	67.8	-0.112
Ar	3.42	124.07	3.17	95.61	0
Ne	2.789	35.7	2.798	56.87	0
Kr	3.636	166.4	3.45	109.6	0

The molecule geometries were fixed. The bond angle for CO_2 is 180°. For N_2, a point charge is located in the middle between the two atoms, that is twice the magnitude of the charges on N, and opposite in sign, so that the total molecule charge is zero. Similarly, for O_2, a point charge is located in the middle between the two atoms, that is twice the magnitude of the charges on O, and opposite in sign, so that the total molecule charge is zero. The following table shows the bond lengths that were used:

bond	bond length / Å
N-N (N_2)	1.098
O-O (O_2)	1.2
C-O (CO_2)	1.16

The zeolite atoms are considered immobile. The following table shows the charges used for the zeolite atoms:

atom	charge
$O_{Zeolite}$	-1.025
$Si_{Zeolite}$	2.05

Table 3. Temperature dependent 3-site Langmuir parameters for DDR

$$q = \frac{q_{sat,A} b_A f}{1 + b_A f} + \frac{q_{sat,B} b_B f}{1 + b_B f} + \frac{q_{sat,C} b_C f}{1 + b_C f}$$

For CO_2: $b_A = 7.8 \times 10^{-11} \exp(\frac{3400}{T})$; $q_{sat,A} = 3.0$ mol/kg;

$b_B = 2 \times 10^{-13} \exp(\frac{3800}{T})$; $q_{sat,B} = 1.0$ mol/kg; $b_C = 1.9 \times 10^{-14} \exp(\frac{3450}{T})$; $q_{sat,C} = 0.6$ mol/kg

For CH_4: $b_A = 2.39 \times 10^{-9} \exp(\frac{2200}{T})$; $q_{sat,A} = 1.6$ mol/kg;

$b_B = 1.24 \times 10^{-11} \exp(\frac{2200}{T})$; $q_{sat,B} = 1.6$ mol/kg; $b_C = 1.27 \times 10^{-12} \exp(\frac{1000}{T})$; $q_{sat,C} = 1.0$ mol/kg

For N_2: $b_A = 1.57 \times 10^{-9} \exp(\frac{1650}{T})$; $q_{sat,A} = 1.8$ mol/kg;

$b_B = 4.5 \times 10^{-11} \exp(\frac{1650}{T})$; $q_{sat,B} = 1.8$ mol/kg; $b_C = 3 \times 10^{-13} \exp(\frac{1650}{T})$; $q_{sat,C} = 1.8$ mol/kg

For Ar: $b_A = 2.336 \times 10^{-9} \exp(\frac{1460}{T})$; $q_{sat,A} = 2.1$ mol/kg;

$b_B = 4.55 \times 10^{-9} \exp(\frac{620}{T})$; $q_{sat,B} = 1.3$ mol/kg; $b_C = 5.738 \times 10^{-13} \exp(\frac{2200}{T})$; $q_{sat,C} = 2$ mol/kg

For Kr: $b_A = 2.18\times10^{-9}\ \exp(\frac{2100}{T})$; $q_{sat,A} = 1.6$ mol/kg;

$b_B = 1.3\times10^{-11}\ \exp(\frac{2270}{T})$; $q_{sat,B} = 1.6$ mol/kg; $b_C = 5.6\times10^{-12}\ \exp(\frac{1000}{T})$; $q_{sat,C} = 1.0$ mol/kg

For O_2: $b_A = 2.223\times10^{-9}\ \exp(\frac{1600}{T})$; $q_{sat,A} = 1.8$ mol/kg;

$b_B = 1.79\times10^{-10}\ \exp(\frac{1600}{T})$; $q_{sat,B} = 1.8$ mol/kg; $b_C = 5.16\times10^{-13}\ \exp(\frac{2200}{T})$; $q_{sat,C} = 1.8$ mol/kg

For Ne: $b_A = 4.088\times10^{-9}\ \exp(\frac{500}{T})$; $q_{sat,A} = 5$ mol/kg;

$b_B = 1.374\times10^{-10}\ \exp(\frac{500}{T})$; $q_{sat,B} = 5$ mol/kg; $b_C = 1.545\times10^{-12}\ \exp(\frac{500}{T})$; $q_{sat,C} = 5$ mol/kg

Table 4. Unary permeation parameters for DDR membrane backed out from the data of Van den Bergh et al. [19, 20]. In all cases we take the coordination number in the Reed and Ehrlich model, $z = 5$.

Molecule	$\rho Đ_i(0)/\delta$ 10^{-3} kg m^{-2} s^{-1}	ϕ_1
CO_2	$933\exp(-13600/RT)$	$1.49\exp(0.4\theta_i)$
CH_4	$43\exp(-19100/RT)$	$\exp((3000+4T)/RT)\exp(0.4\theta_i)$
N_2	$123\exp(-8076/RT)$	$1.7\exp(0.6\theta_i)$

11. Captions for Figures

Figure 1. Cartoon showing the approximate molecular dimensions of Ne, Ar, Kr, N_2, O_2, CO_2, CH_4. and C_2H_4. The molecular diameters are estimated on the basis of the Lennard-Jones size parameters σ for molecule-molecule interactions. The molecular lengths are estimated on the basis of the bond lengths.

Figure 2. LTA structure and pore landscape.

Figure 3. Pure component isotherms for CH_4 in LTA at different temperatures T. Also shown are the data for $\left(Đ_i / D_{i,self} - 1\right)$ at various T.

Figure 4. Data on $D_{i,self}$ and $Đ_i$ for CH_4 in LTA at different temperatures T.

Figure 5. Arrhenius plots and activation energies for diffusion of CH_4 in LTA.

Figure 6. CHA structure and pore landscape.

Figure 7. $D_{i,self}$, $Đ_i$, and $\left(Đ_i / D_{i,self} - 1\right)$ data for CH_4 in CHA at different temperatures T, along with Arrhenius plots

Figure 8. $D_{\mathrm{i,self}}$, $Đ_{\mathrm{i}}$, and $\left(Đ_i / D_{i,self} - 1\right)$ data for Ar in CHA at different temperatures T, along with Arrhenius plots.

Figure 9. FAU structure and pore landscape.

Figure 10. $D_{\mathrm{i,self}}$, $Đ_{\mathrm{i}}$, and $\left(Đ_i / D_{i,self} - 1\right)$ data for CH_4 in FAU at different temperatures T, along with Arrhenius plots

Figure 11. MFI structure and pore landscape.

Figure 12. $D_{\mathrm{i,self}}$, $Đ_{\mathrm{i}}$, and $\left(Đ_i / D_{i,self} - 1\right)$ data for CH_4 in MFI at different temperatures T, along with Arrhenius plots

Figure 13. Pure component isotherm for C_2H_4 in MFI at 300 K, along with snapshot showing the location of molecules.

Figure 14. Data on $D_{\mathrm{i,self}}$ and $Đ_{\mathrm{i}}$ for C_2H_4 in MFI at different temperatures T.

Figure 15. Arrhenius plots and $\left(Đ_i / D_{i,self} - 1\right)$ data for diffusion of C_2H_4 in MFI.

Figure 16. DDR structure and pore landscape.

Figure 17. Comparison of GCMC simulations for pure component isotherms for CH_4 in DDR at various *T* with experimental data of Van den Bergh et al.[19, 20] and Himeno et al.[21, 22].

Figure 18. Comparison of GCMC simulations for pure component isotherms for CO_2 in DDR at various *T* with experimental data of Van den Bergh et al. [19, 20] and Himeno et al. [21, 22].

Figure 19. Comparison of GCMC simulations for pure component isotherms for N_2 in DDR at various *T* with experimental data of Van den Bergh et al. [19, 20] and Himeno et al. [22].

Figure 20. Comparison of GCMC simulations for pure component isotherms for O_2 in DDR at various *T* with experimental data of van den Bergh et al.[20].

Figure 21. Comparison of GCMC simulations for pure component isotherms for Ar in DDR at various *T* with experimental data of van den Bergh et al.[20].

Figure 22. Comparison of GCMC simulations for pure component isotherms for Kr in DDR at various *T* with experimental data of van den Bergh et al.[20].

Figure 23. MD simulation data for $Đ_i$, and $\left(Đ_i / D_{i,self} - 1\right)$ for CO_2 in DDR at T = 220 K, 250 K, 270 K, 300 K, and 373 K. The Reed and Ehrlich fits of ϕ_i are also plotted.

Figure 24. MD simulation data for $Đ_i$, and $\left(Đ_i / D_{i,self} - 1\right)$ for N_2 in DDR at T = 220 K, 300 K, and 373 K. The Reed and Ehrlich fits of ϕ_i are also plotted.

Figure 25. MD simulation data for $Đ_i \approx D_{i,self}$ for CH_4 in DDR at T = 300 K, 373 K, 400 K, 500 K, and 600 K. Also shown are the Arrhenius plots for loadings of 1 and 3 molecules per cage.

Figure 26. MD simulation data for $Đ_i$, and $\left(Đ_i / D_{i,self} - 1\right)$ for Ar in DDR at T = 300 K, and 373 K. The Reed and Ehrlich fits of ϕ_i are also plotted.

Figure 27. MD simulation data for $Đ_i$, and $\left(Đ_i / D_{i,self} - 1\right)$ for O_2 in DDR at T = 300 K, and 373 K. The Reed and Ehrlich fits of ϕ_i are also plotted.

Figure 28. MD simulation data for $Đ_i \approx D_{i,self}$ for Kr in DDR at T = 300 K, and 373 K.

Figure 29. MD simulation data for $Đ_i$, and $\left(Đ_i / D_{i,self} - 1\right)$ for Ne in DDR at T = 300 K, and 373 K. The Reed and Ehrlich fits of ϕ_i are also plotted

Figure 30. Unary permeation fluxes of CO_2, N_2, and CH_4 across a DDR membrane at specified upstream pressures and varying T. The experimental data of Van den Bergh et al. [19, 20] are denoted by filled symbols. The continuous solid lines represent the model calculations using eq. (9). Further data inputs are as given in Table 3 and Table 4.

Figure 31. Fitted Reed-Ehrlich parameter ϕ_i for CO_2, N_2, and CH_4 as a function of the cage loading, for T = 250 K, 300 K, and 373 K.

Figure 32. Normalized Maxwell-Stefan diffusivities of CO_2, N_2, and CH_4 as a function of the cage loading, for T = 250 K, 300 K, and 373 K. The presented calculations are based on fitted parameters to the Reed and Ehrlich model.

Figure 1

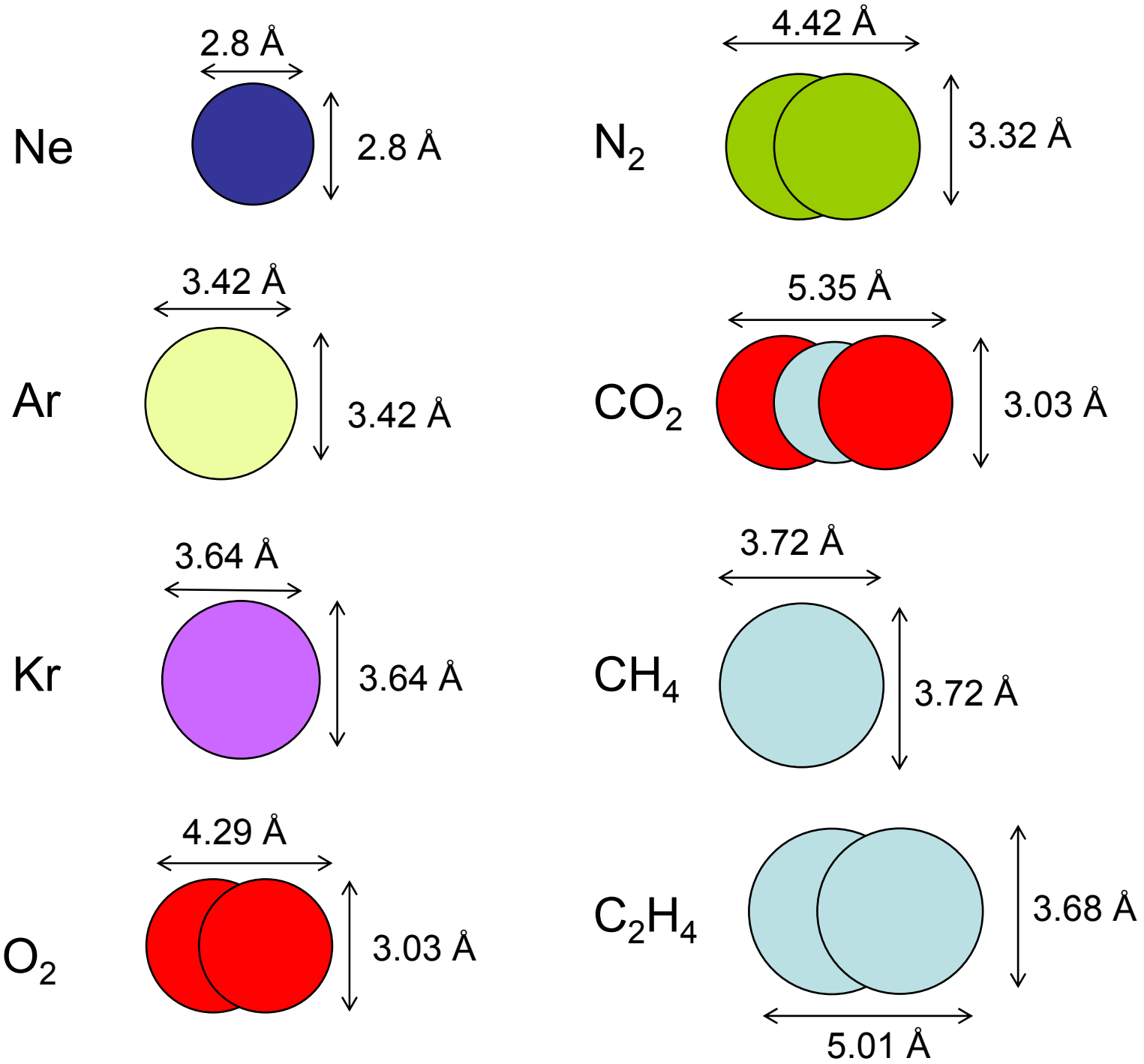
Ne
2.8 Å
2.8 Å
N2
4.42 Å
3.32 Å
Ar
3.42 Å
3.42 Å
CO2
5.35 Å
3.03 Å
Kr
3.64 Å
3.64 Å
CH4
3.72 Å
3.72 Å
O2
4.29 Å
3.03 Å
C2H4
3.68 Å
5.01 Å

LTA (all silica)

Figure 2

8-ring window of LTA

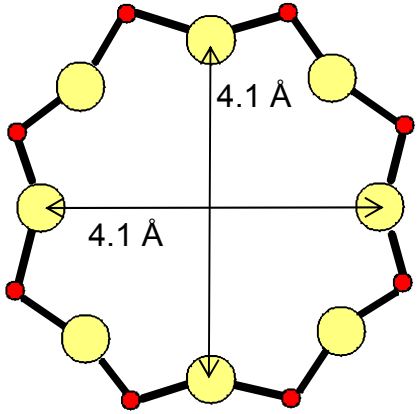

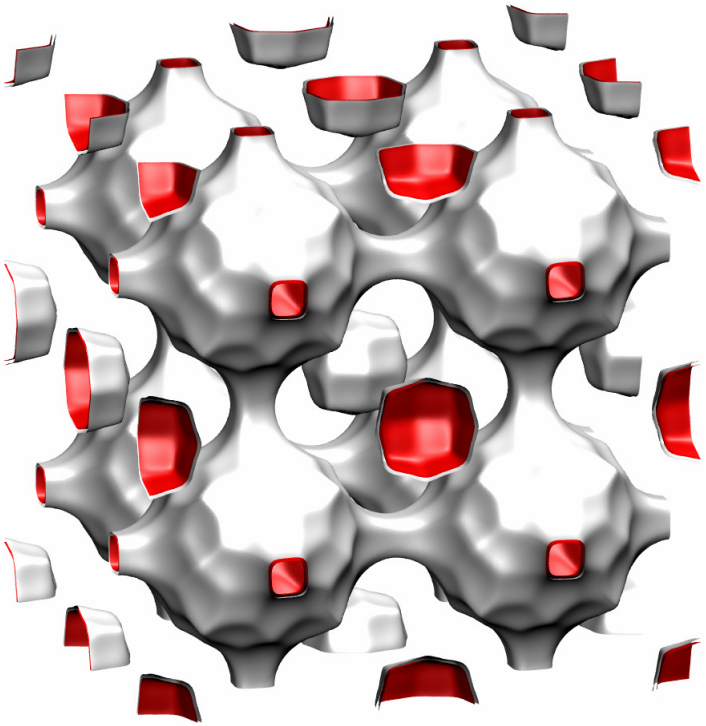

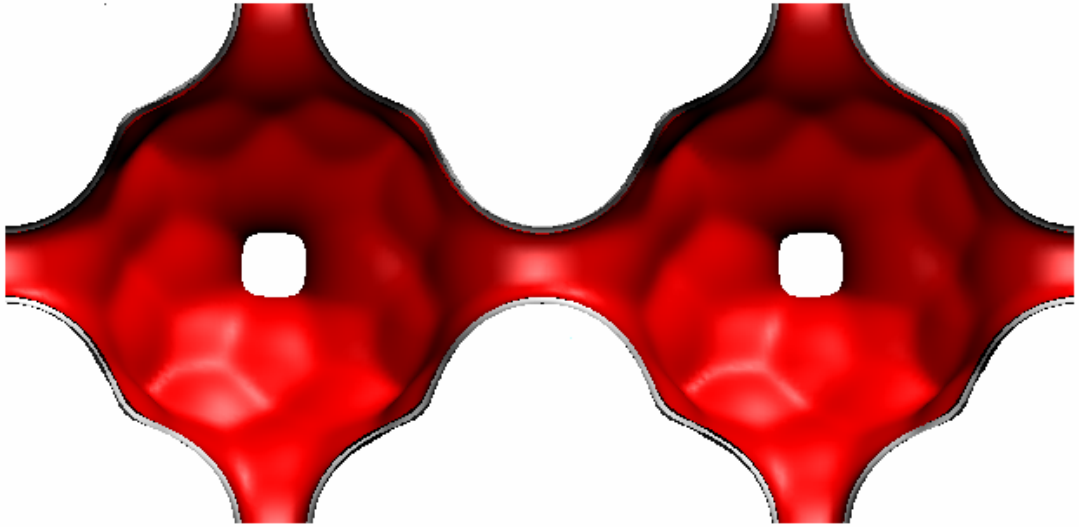

Pure component isotherms

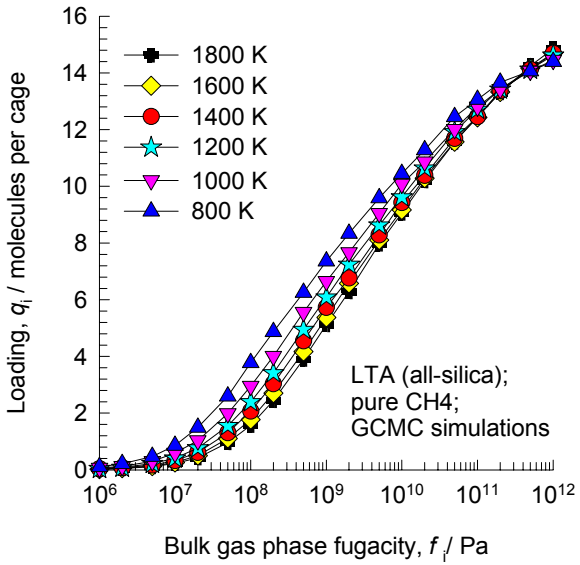

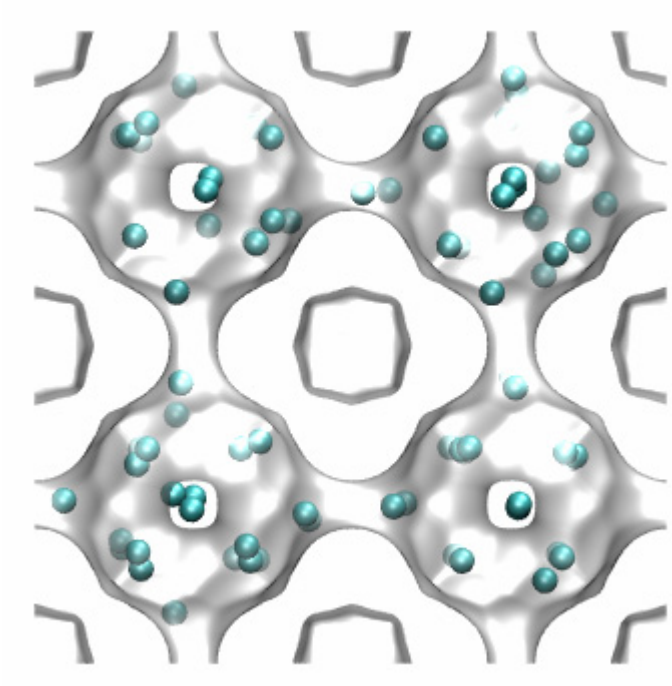

Figure 3

Correlations

For Reed & Ehrlich fits we take
$q_{i,sat}$ = 16 molecules per cage for all T.

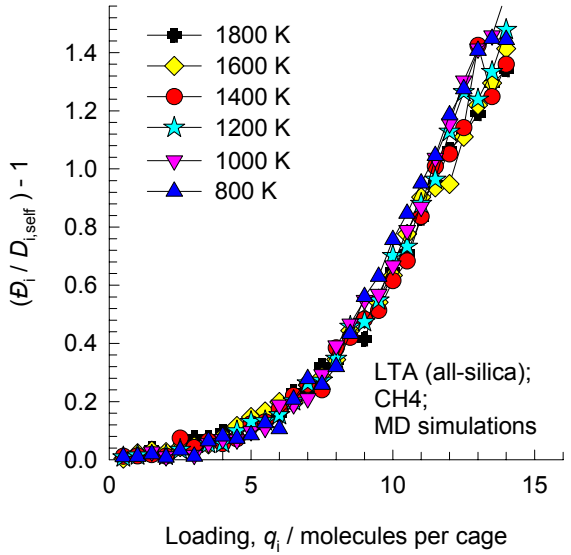

Figure 4

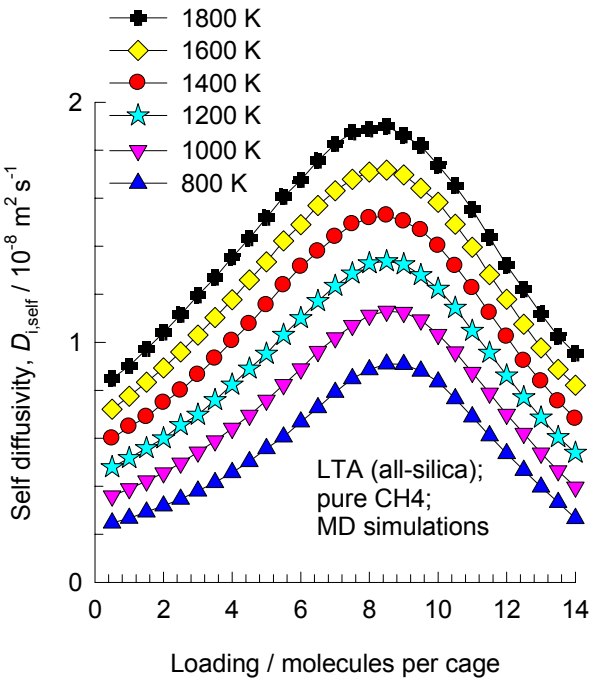

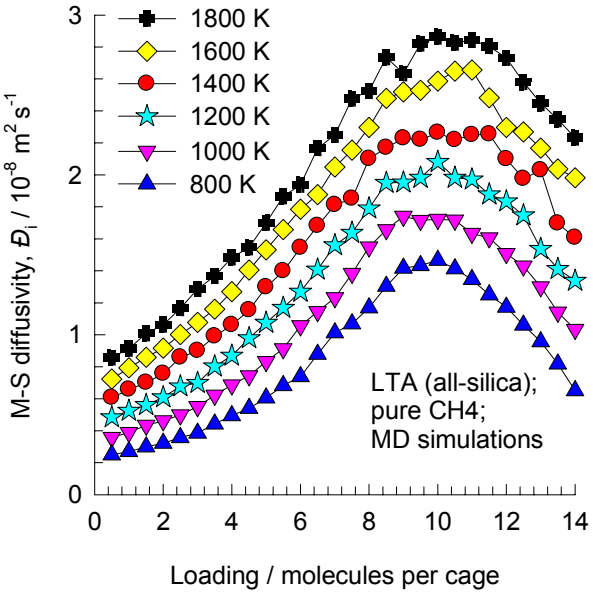

Self-diffusivities

Maxwell-Stefan diffusivities

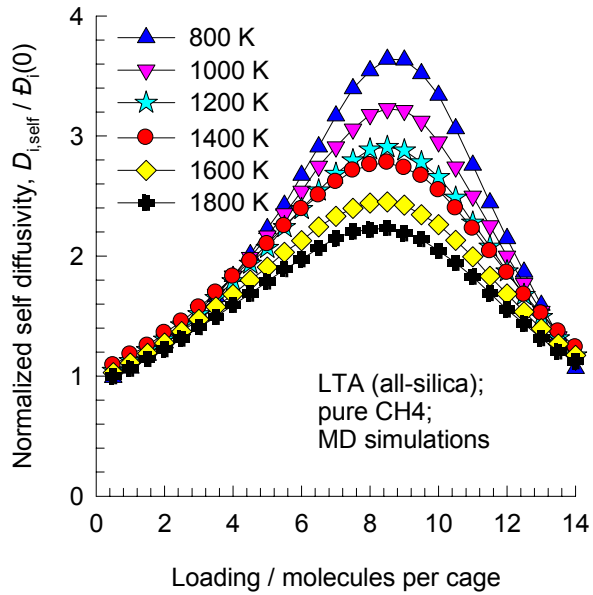

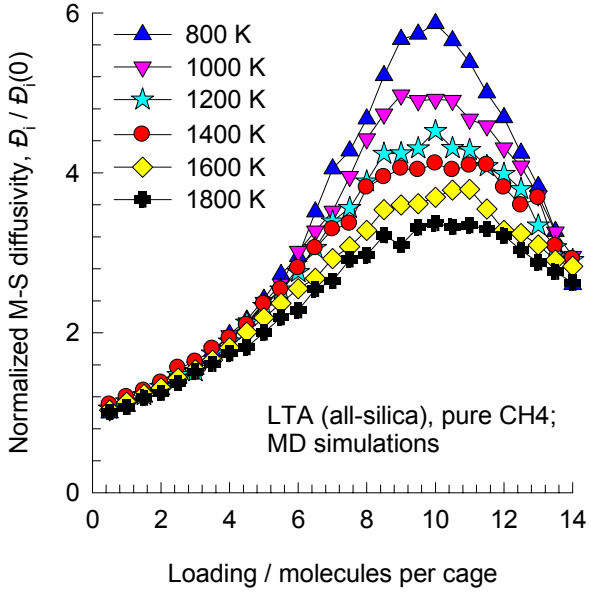

Figure 5

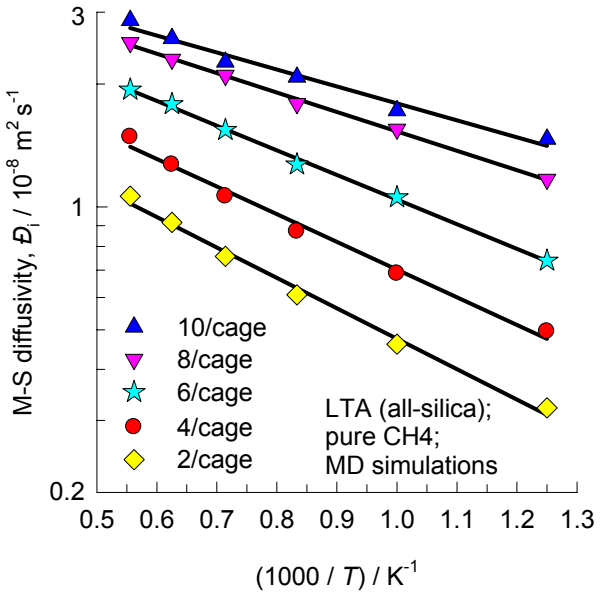

Arrhenius plot

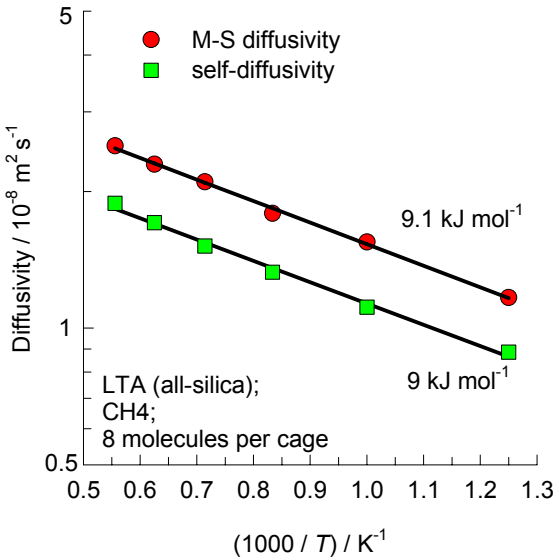

Activation energies

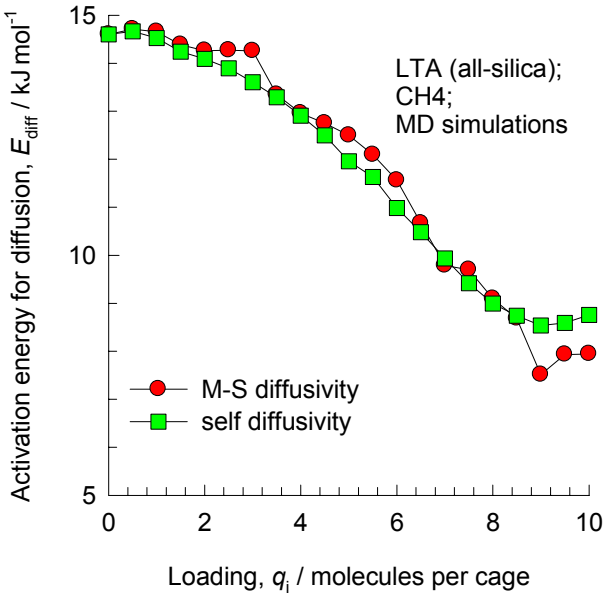

CHA (all silica)

Figure 6

8-ring window of CHA

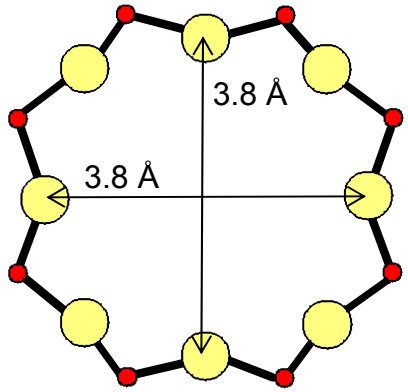

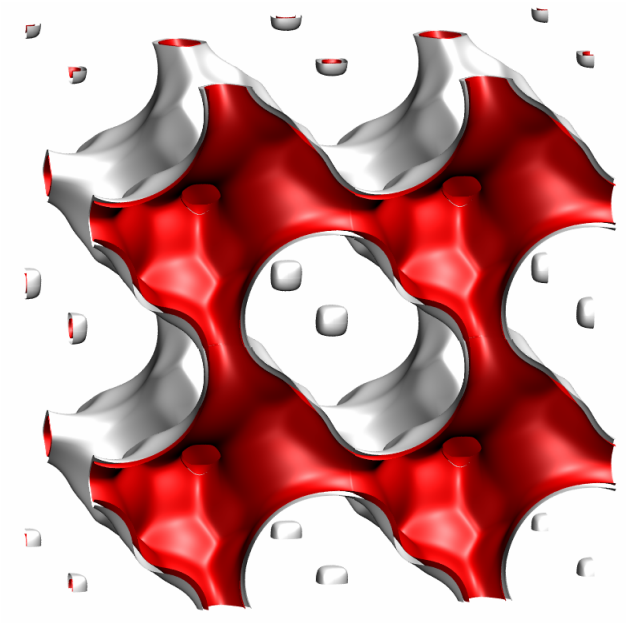

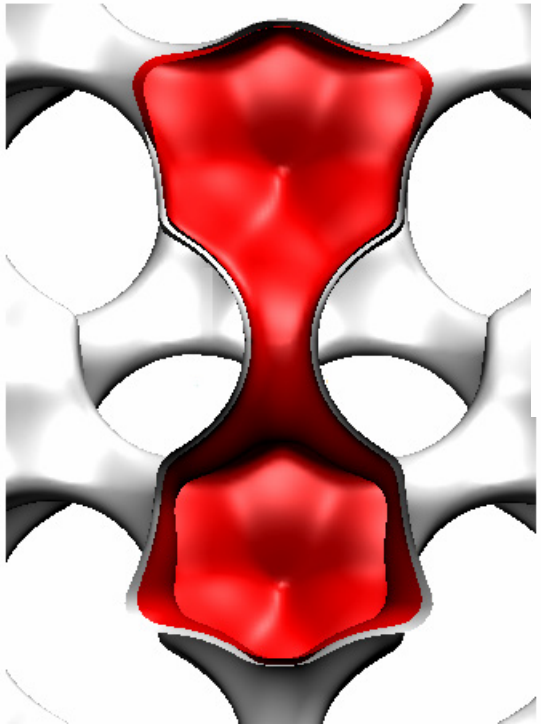

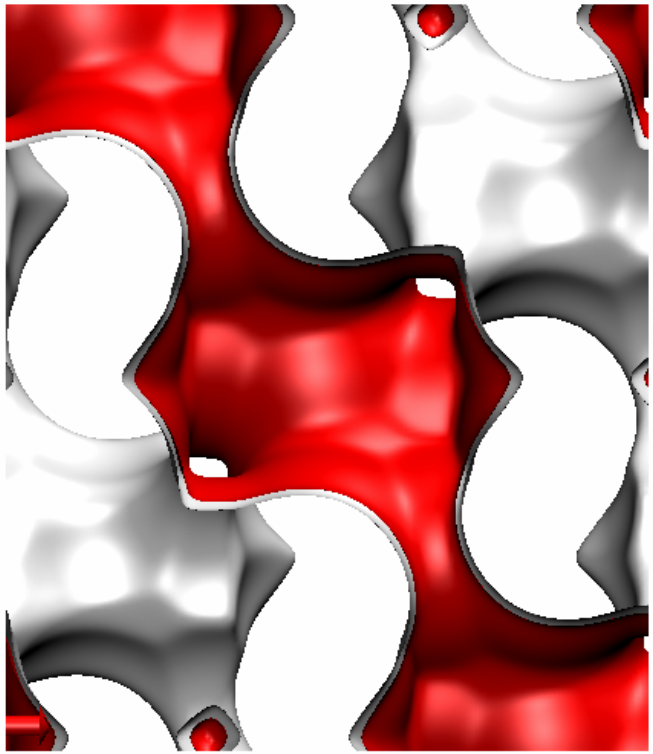

Figure 7

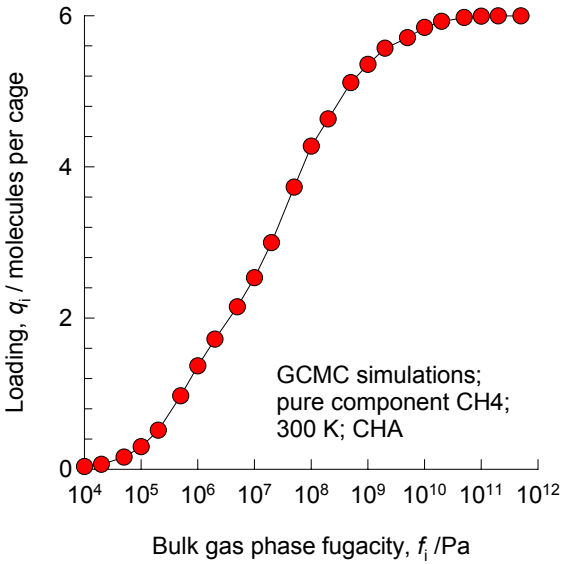

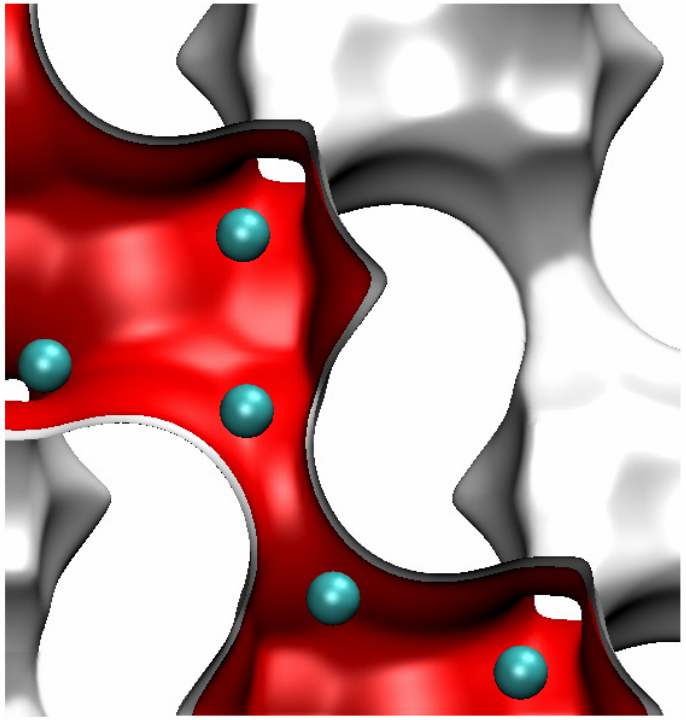

CHA, CH_4

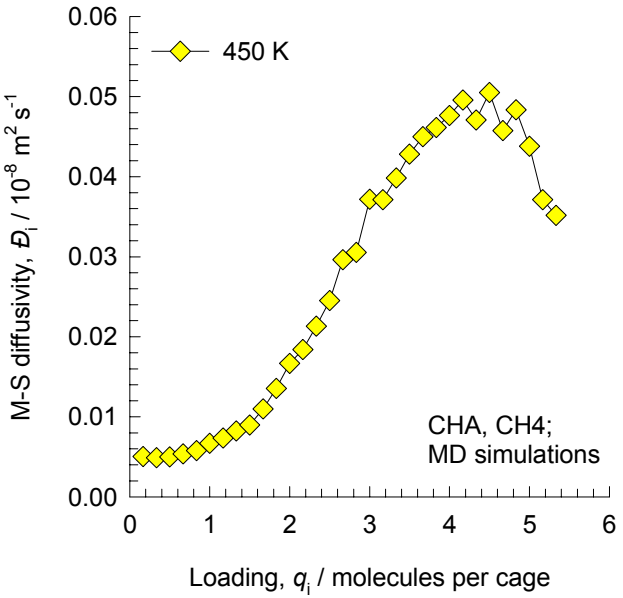

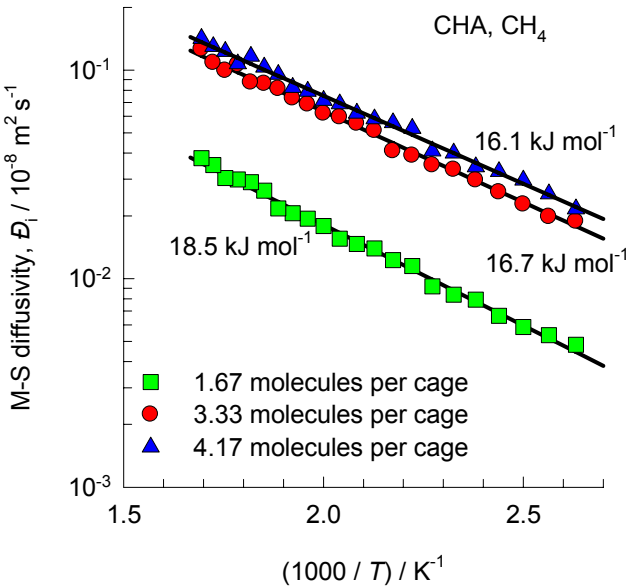

Figure 8

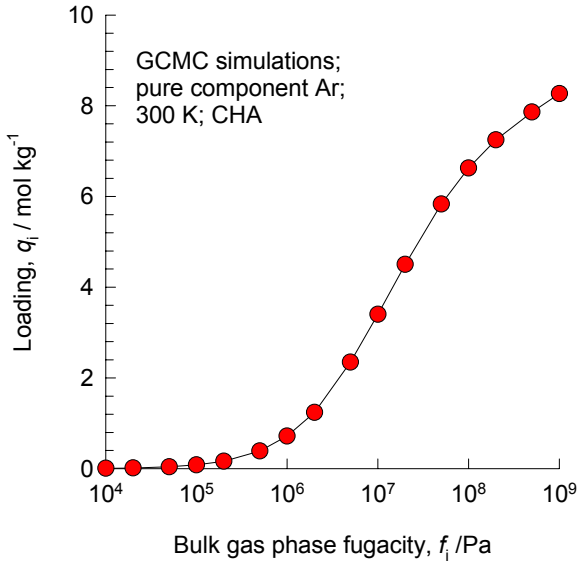

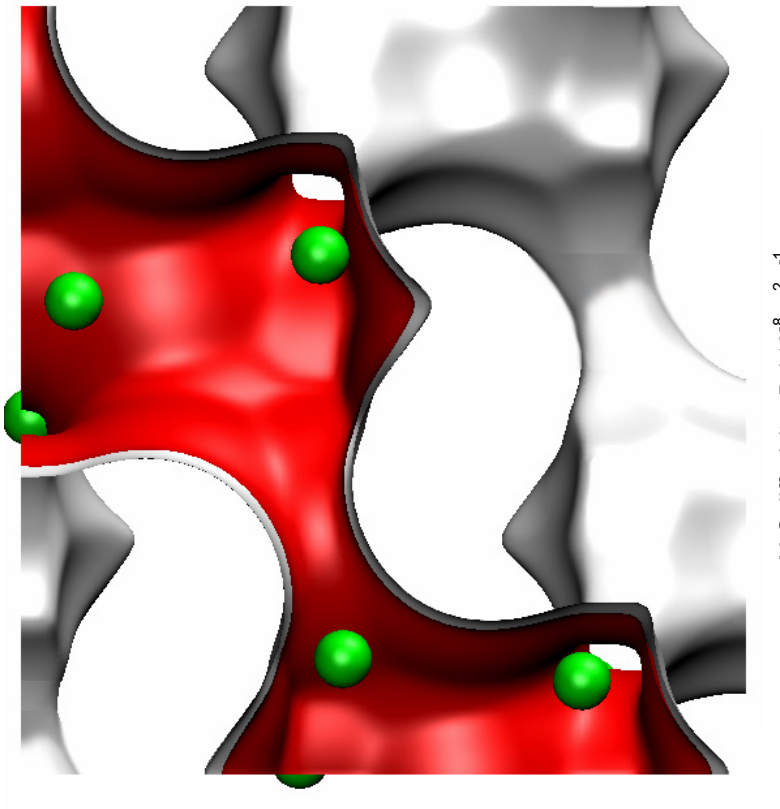

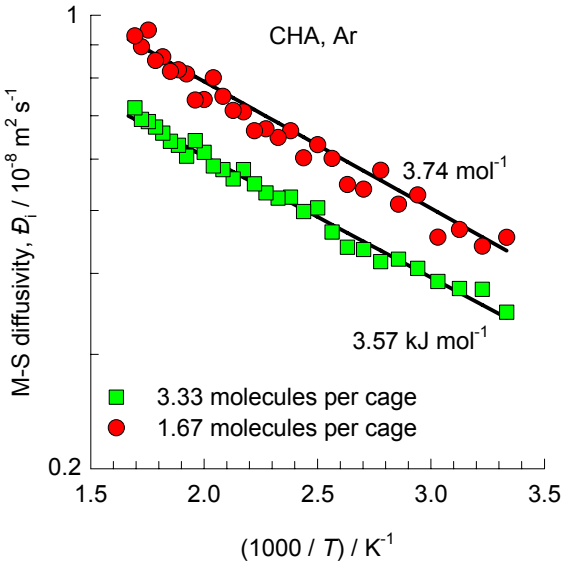

CHA, Ar

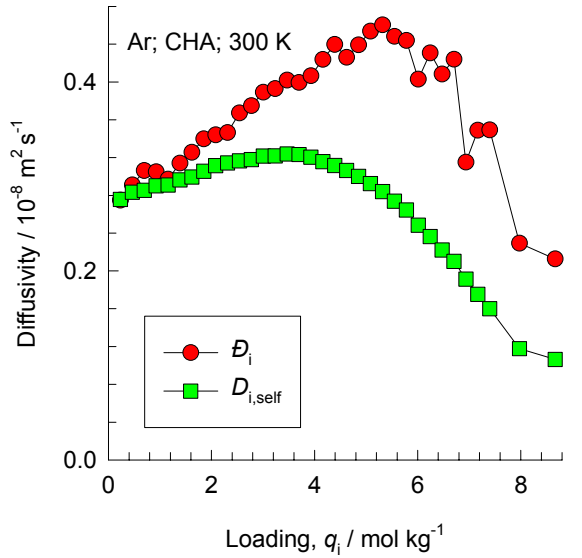

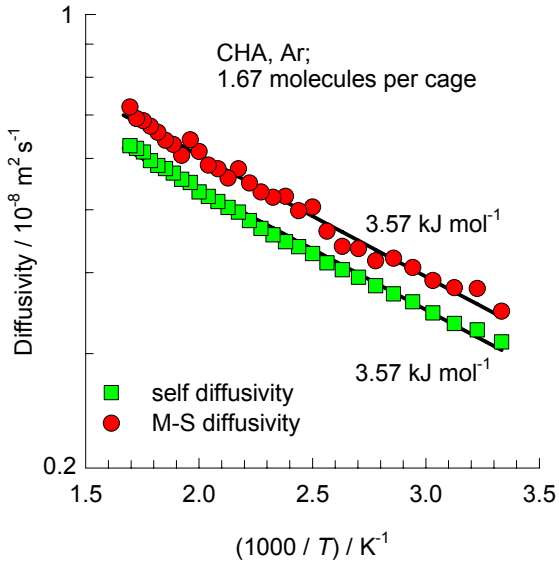

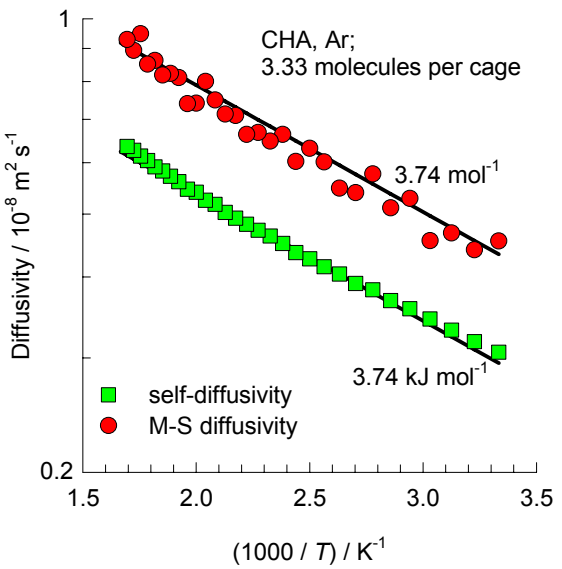

FAU (all silica)

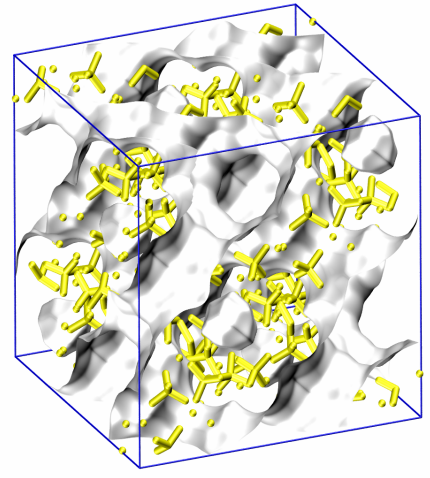

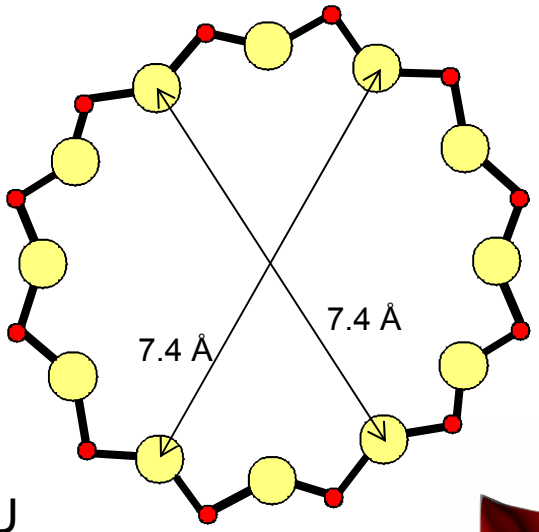

12-ring
window of FAU

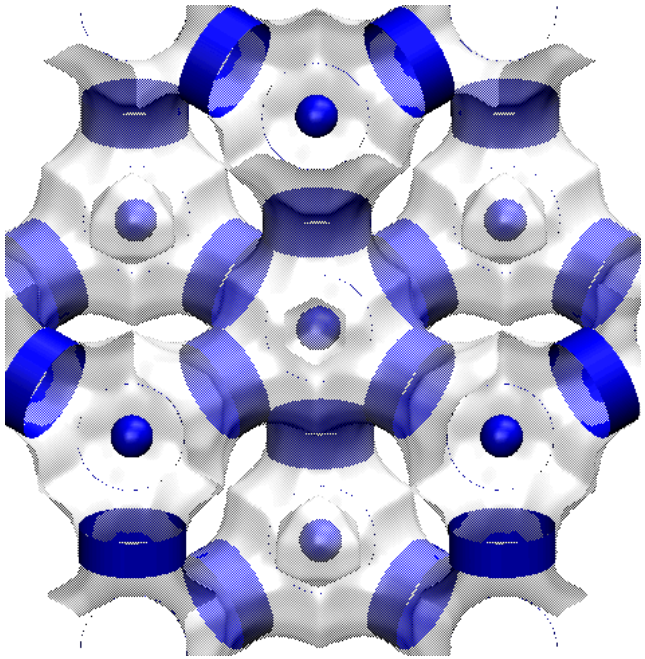

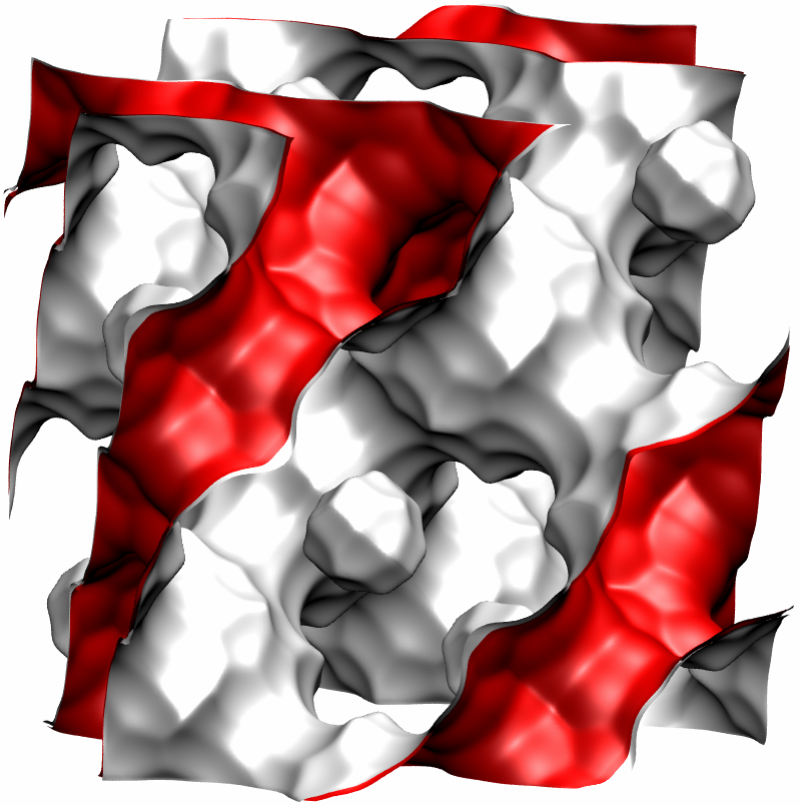

FAU, CH4

Figure 10

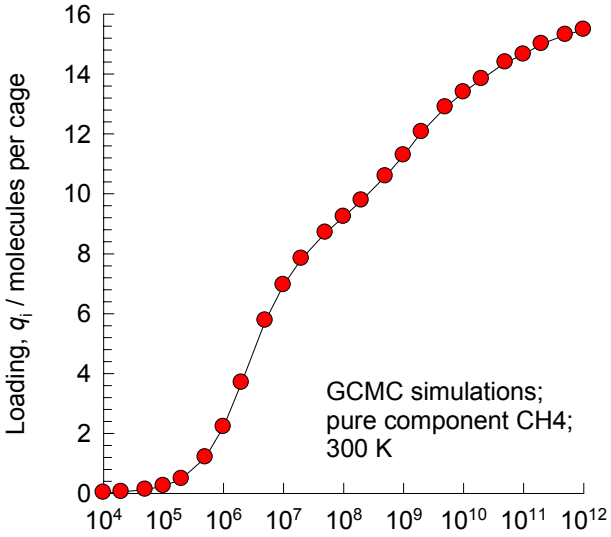

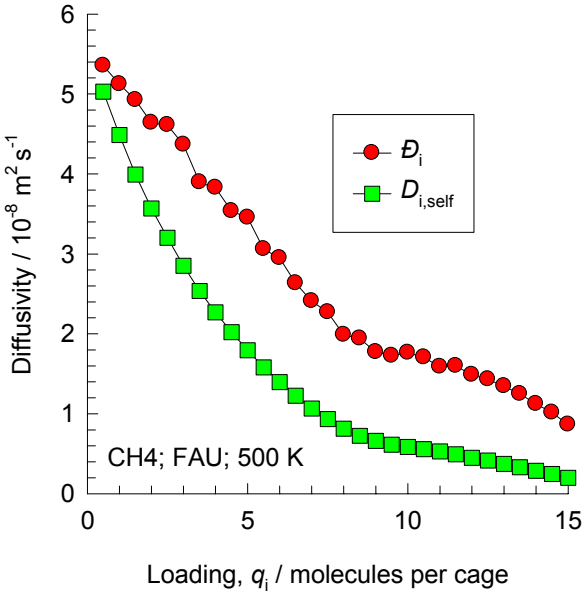

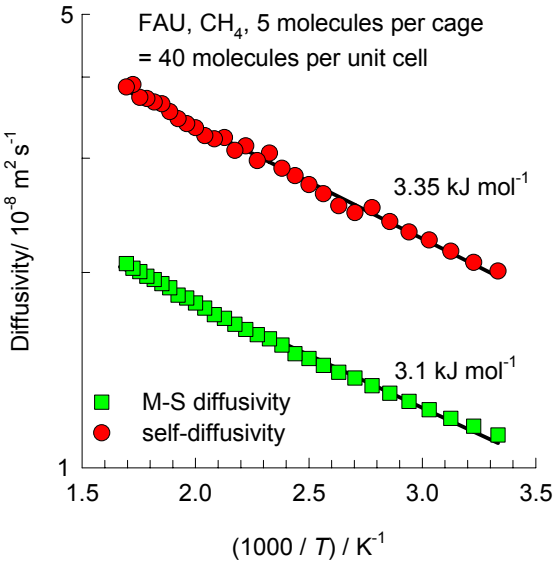

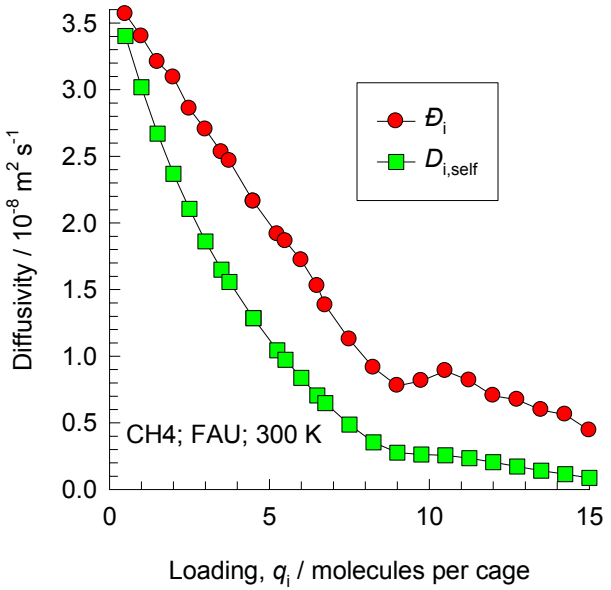

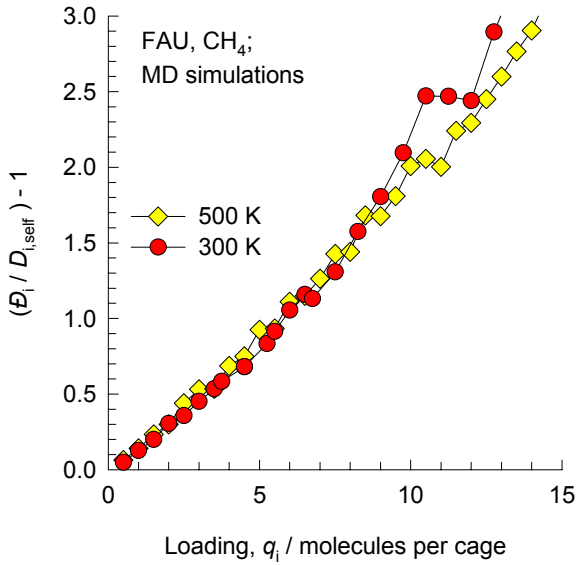

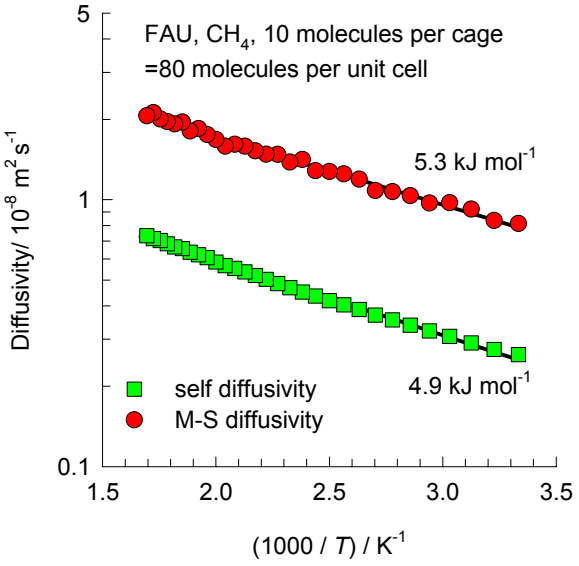

MFI (all silica)

Figure 11

10 ring channel
of MFI viewed along [100]

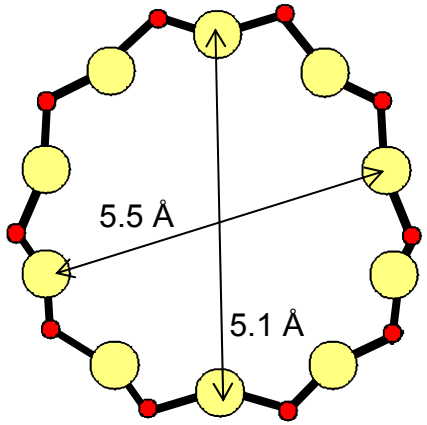

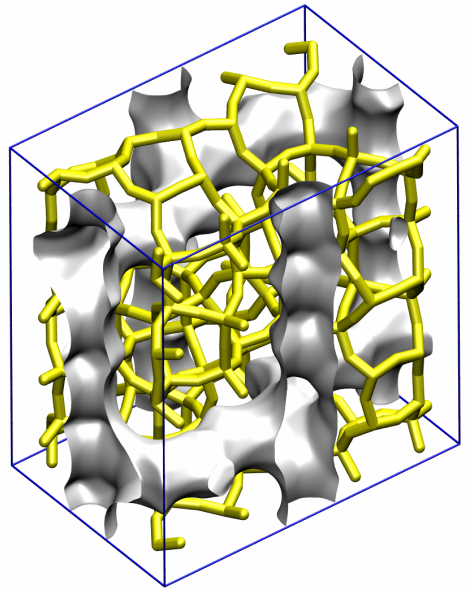

10 ring channel
of MFI viewed along [010]

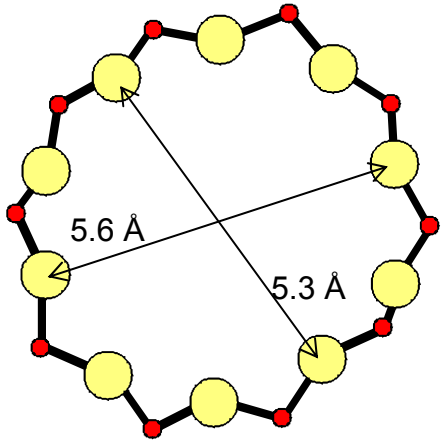

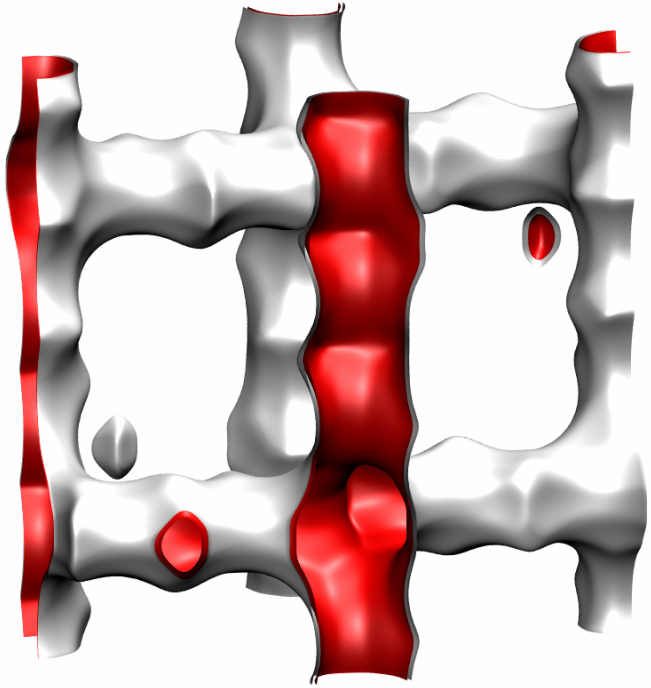

Figure 12

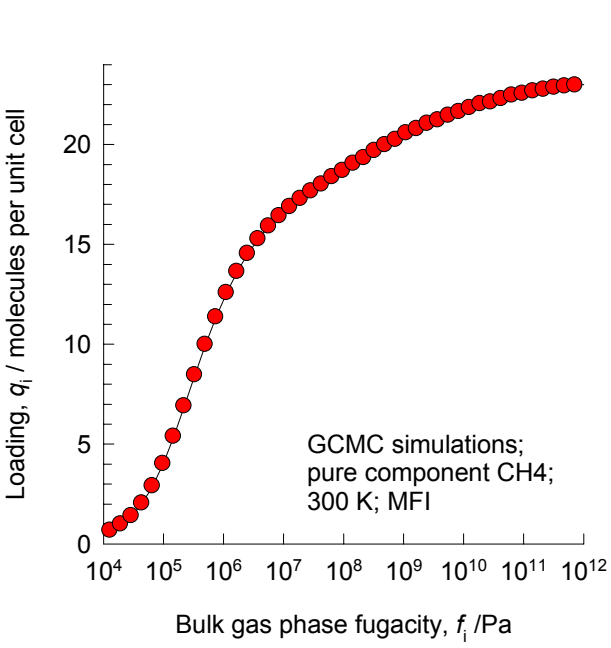

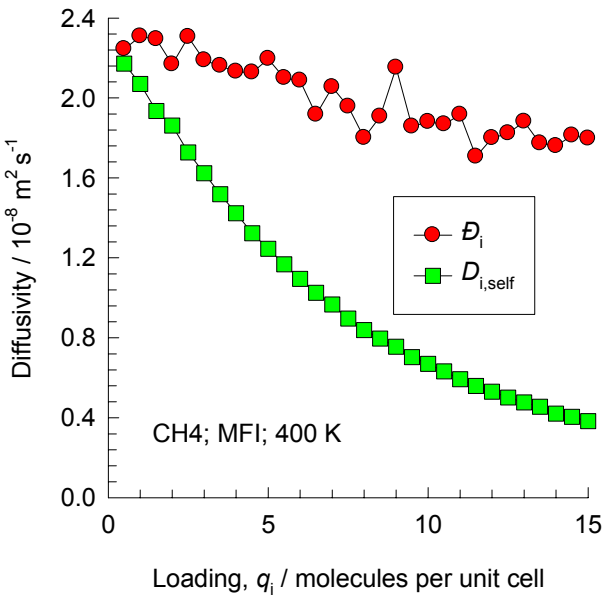

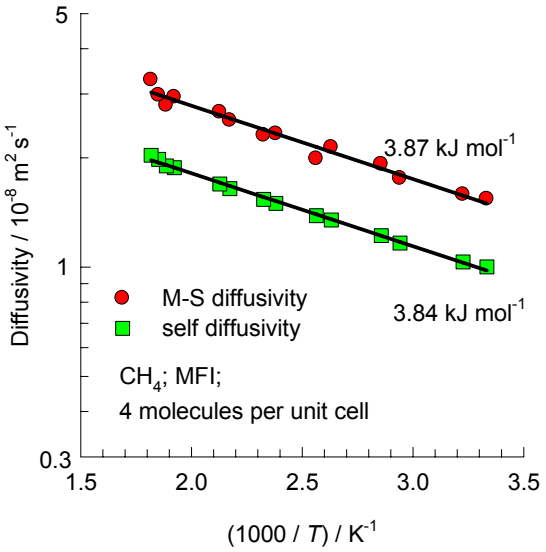

MFI, 300 K, CH4

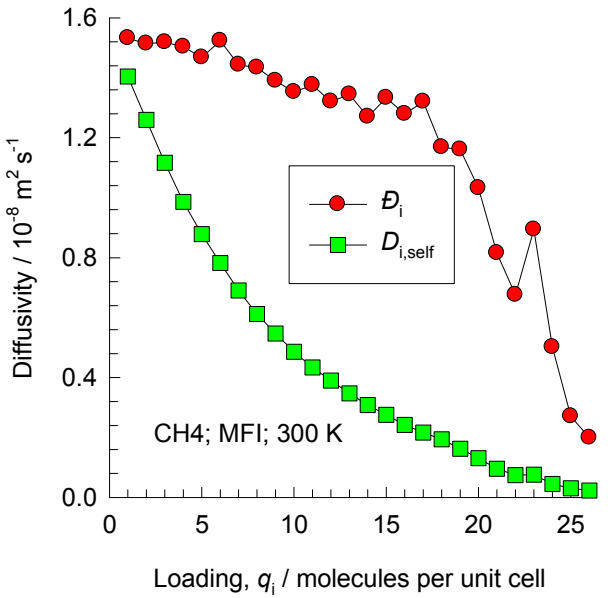

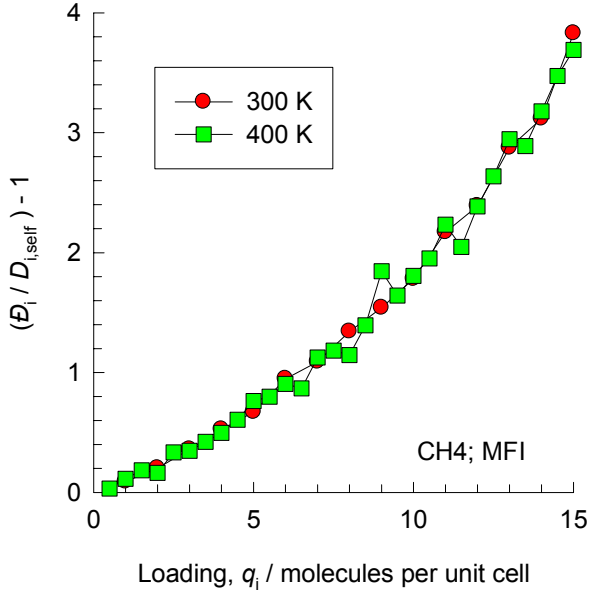

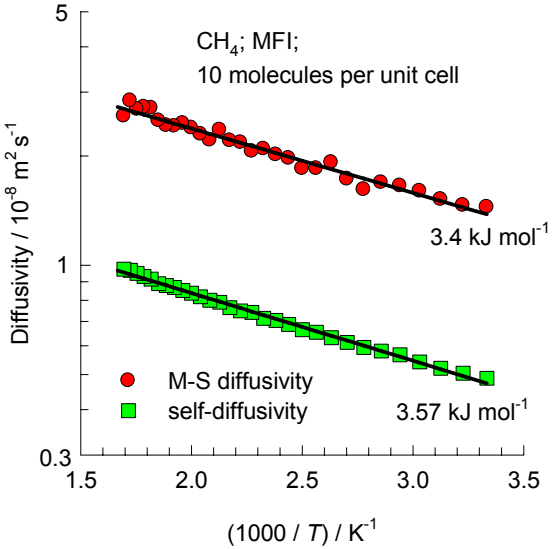

Ethene in MFI, 300 K, isotherm

Figure 13

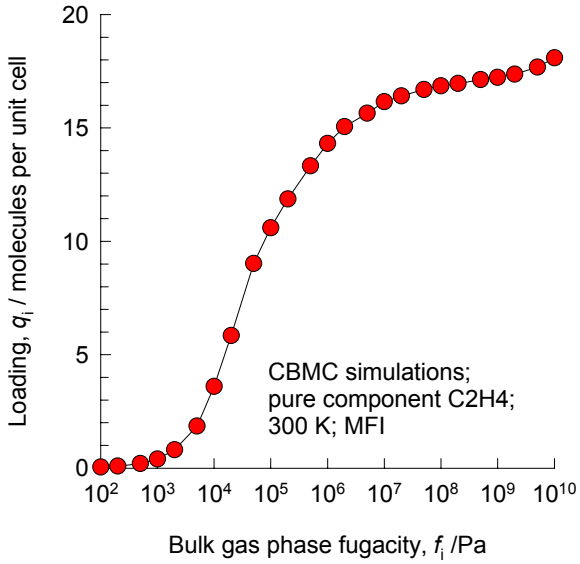

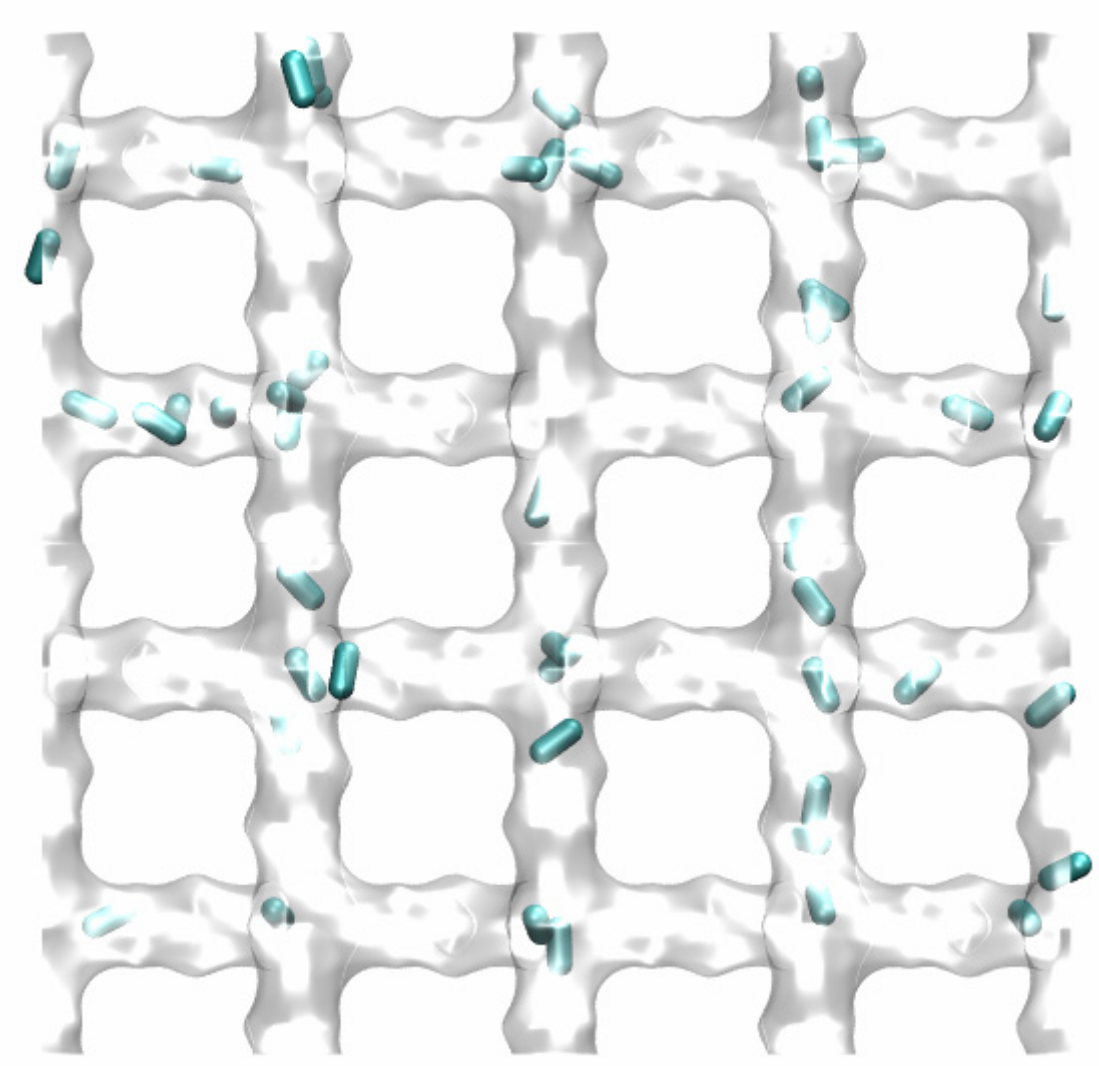

Figure 14

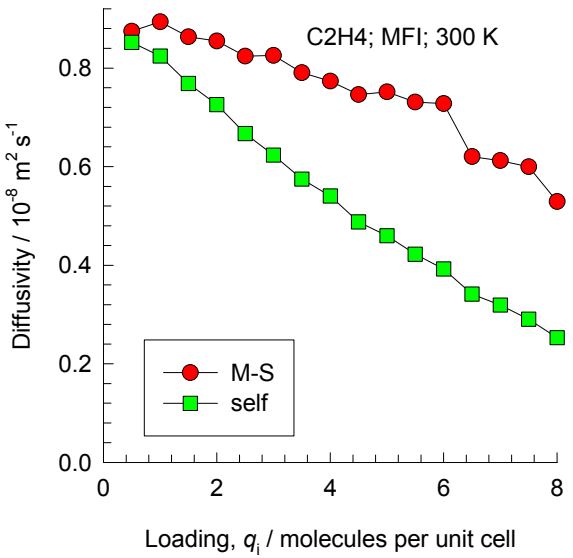

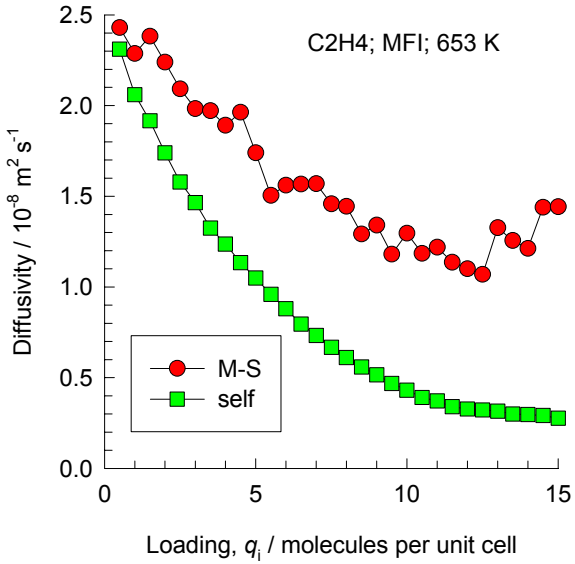

MFI, C_2H_4, diffusivities

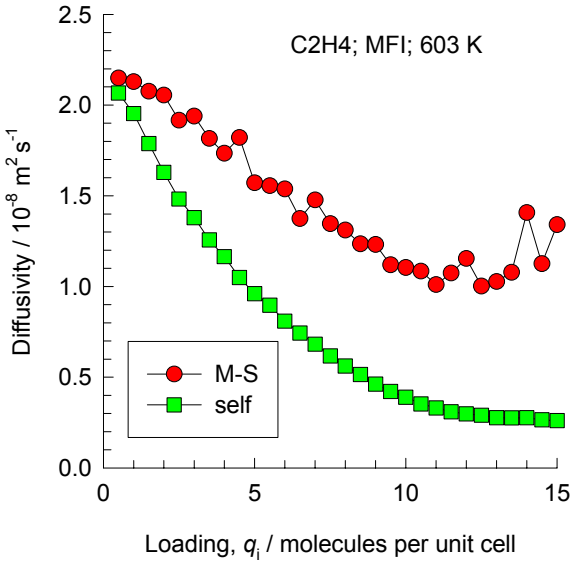

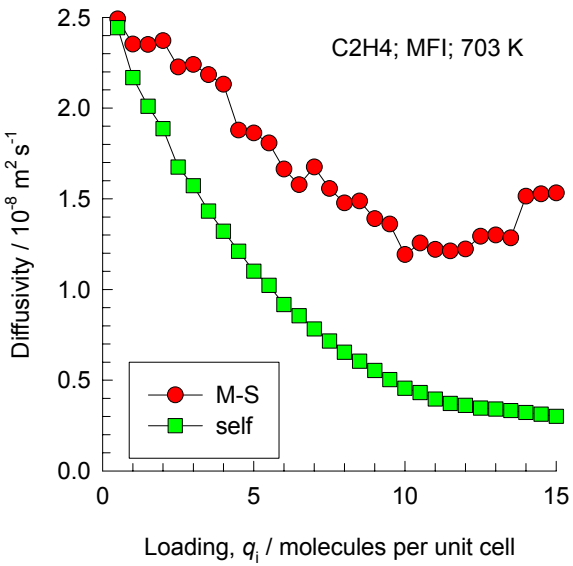

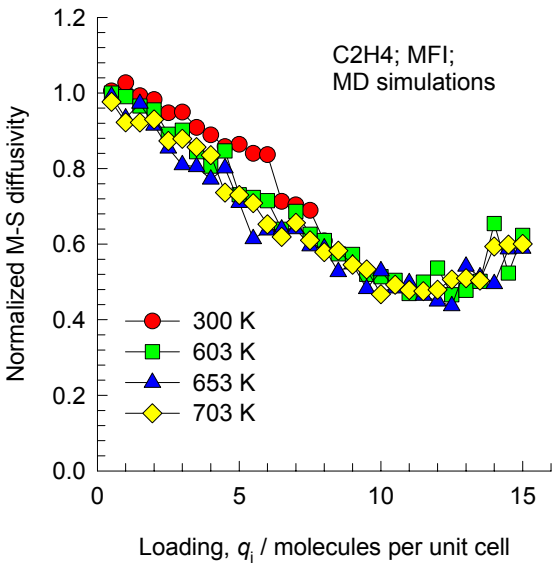

Figure 15

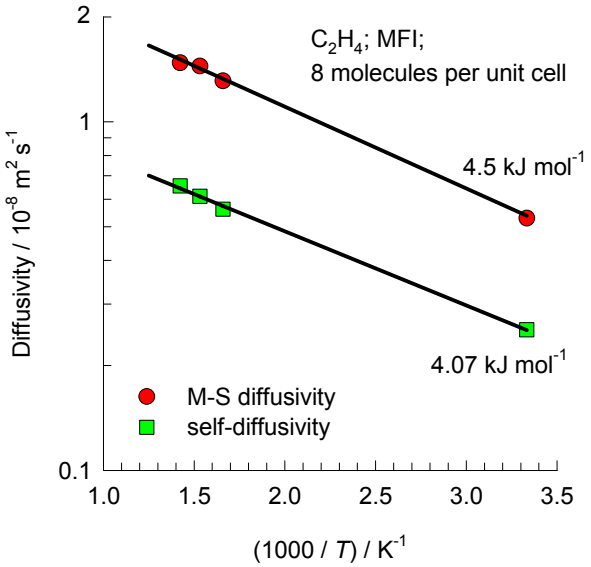

MFI, C_2H_4, activation energy correlations

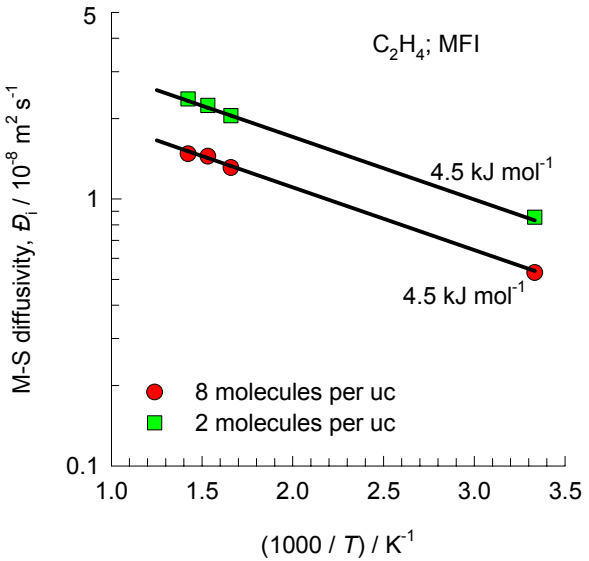

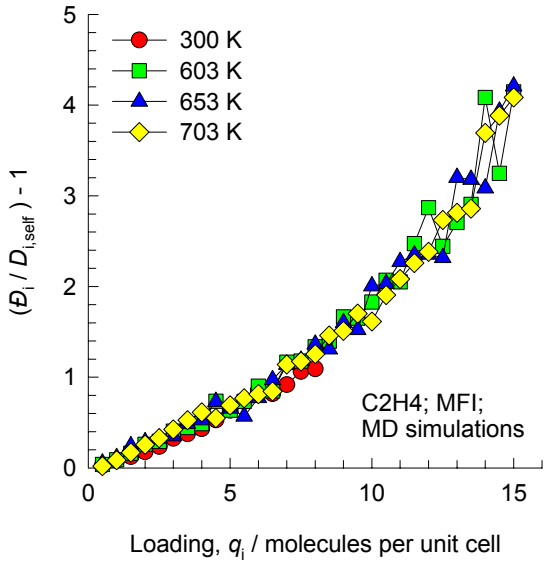

DDR (all silica)

Figure 16

8-ring window of DDR

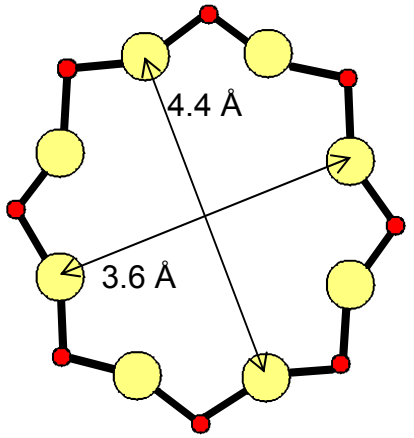

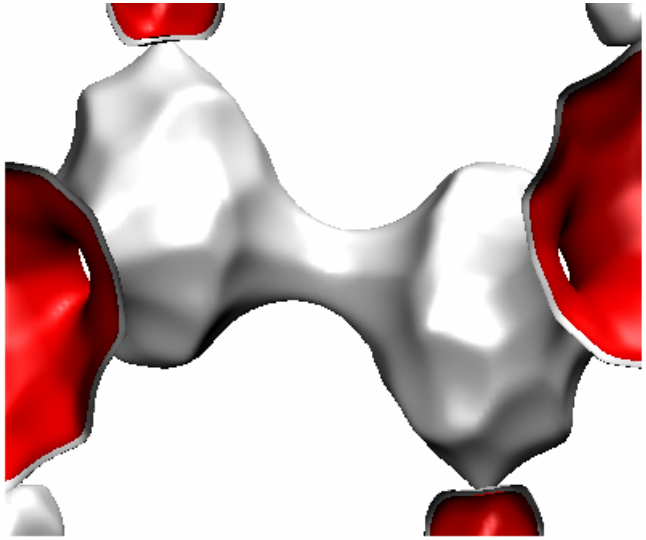

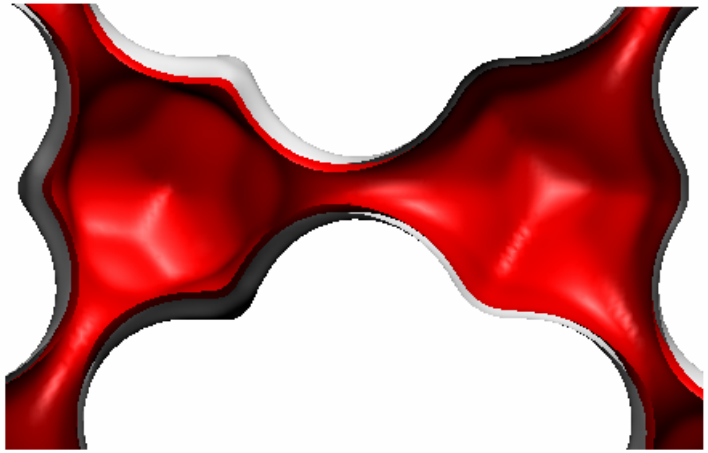

DDR, CH4, isotherms

Figure 17

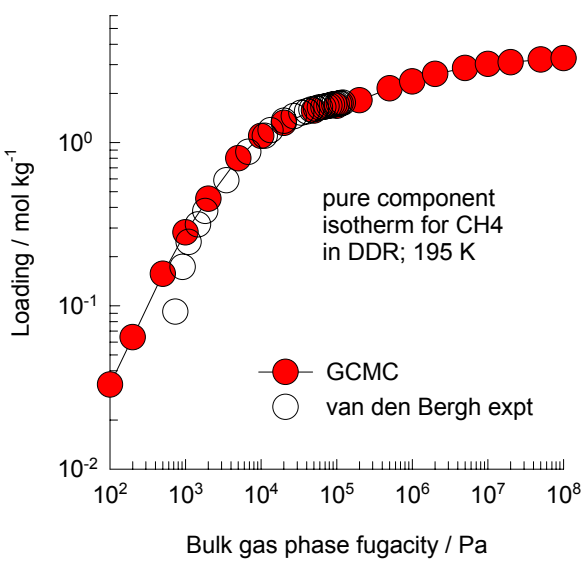

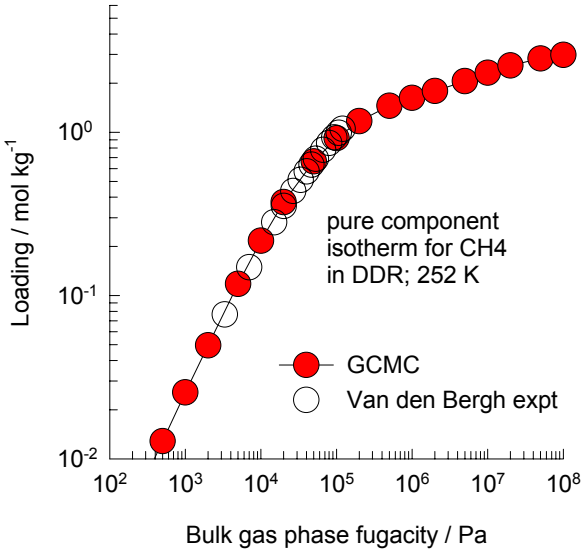

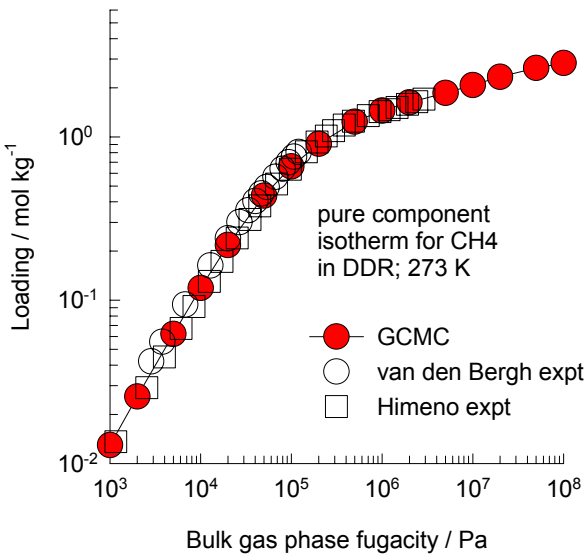

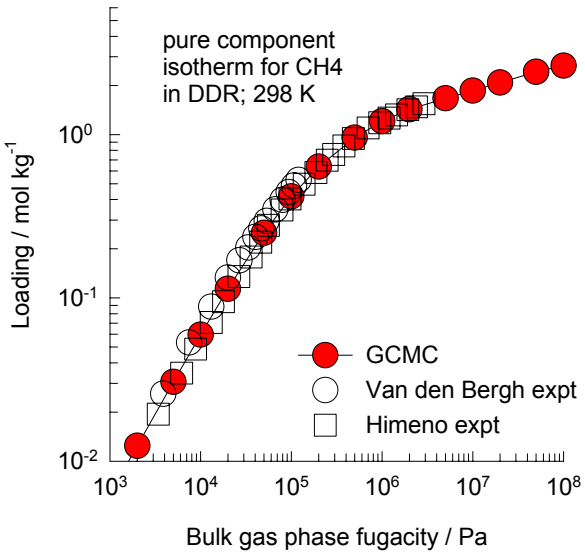

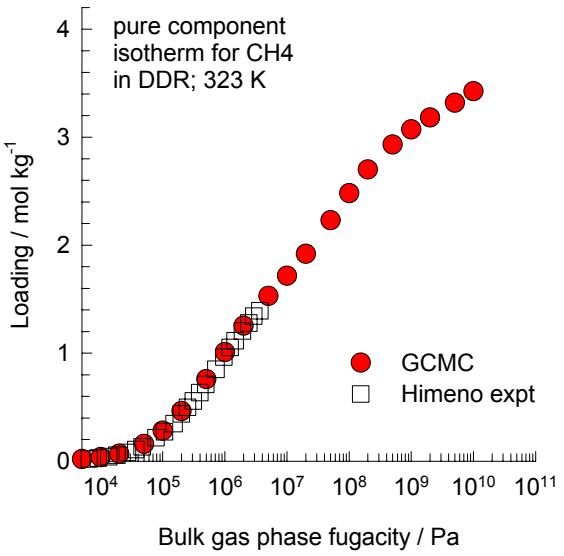

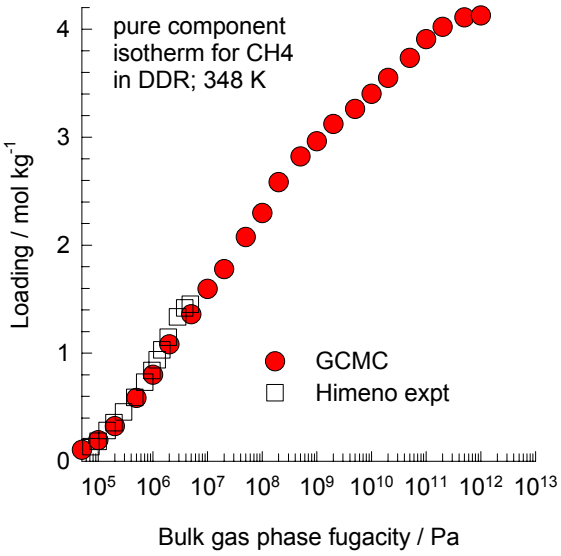

DDR, CO2, isotherms

Figure 18

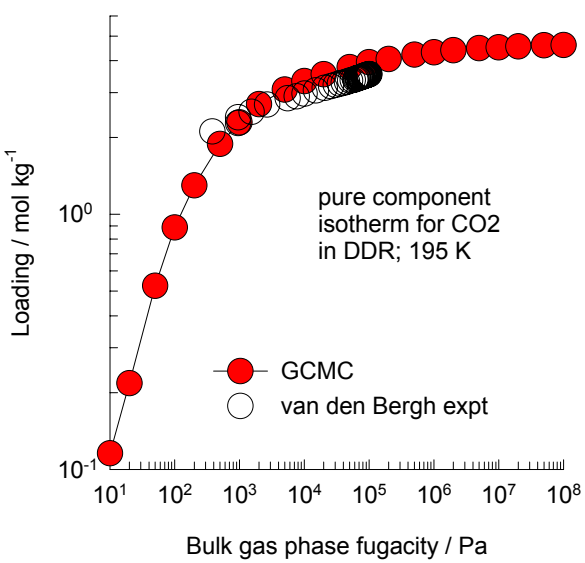

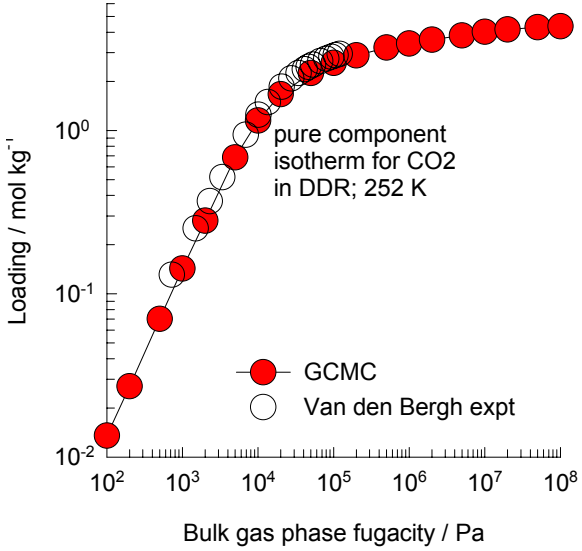

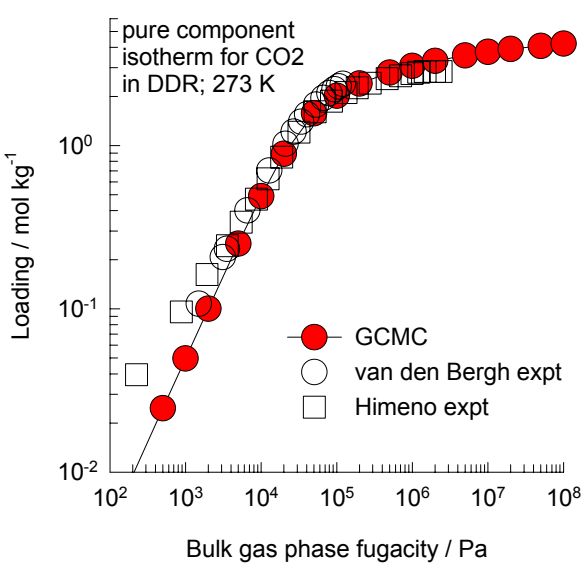

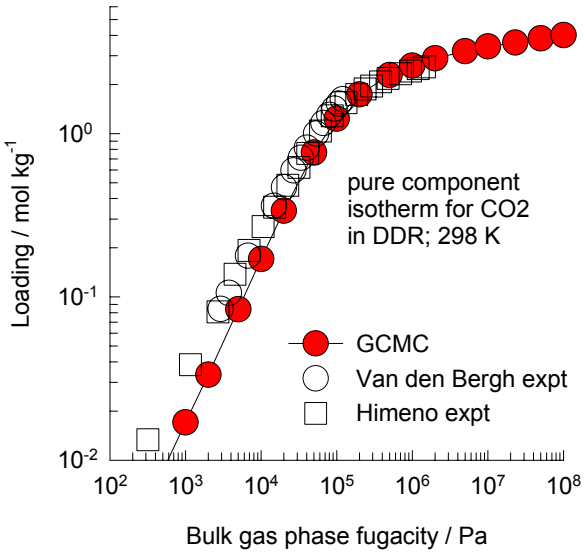

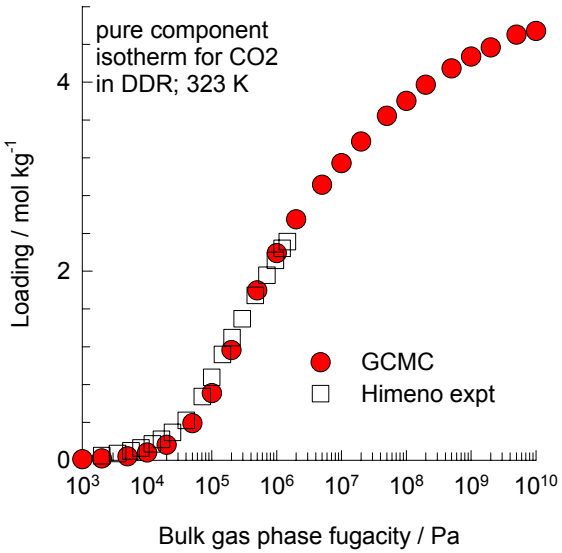

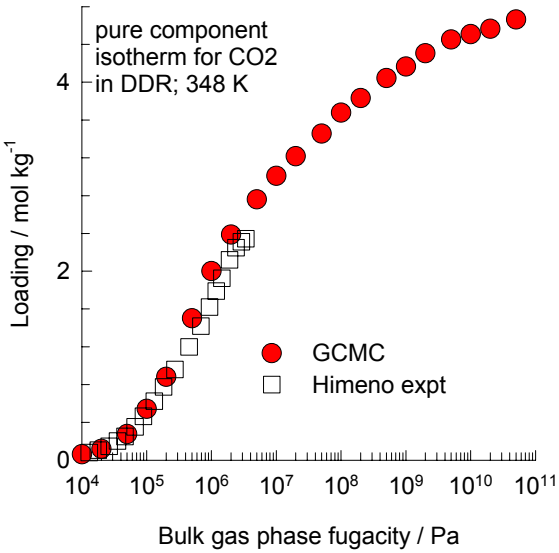

DDR, N2, isotherms

Figure 19

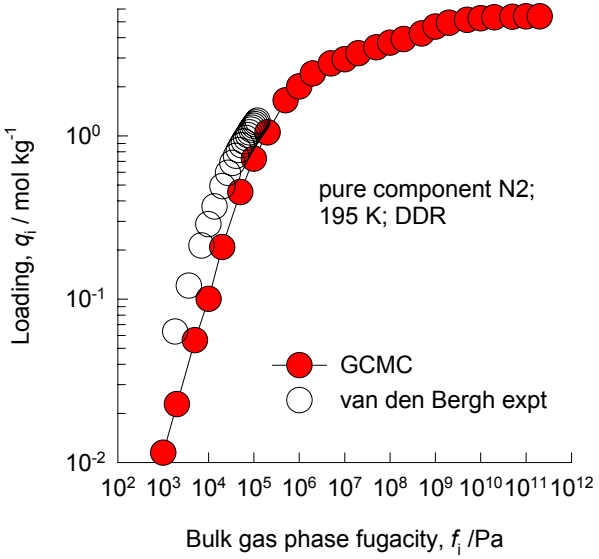

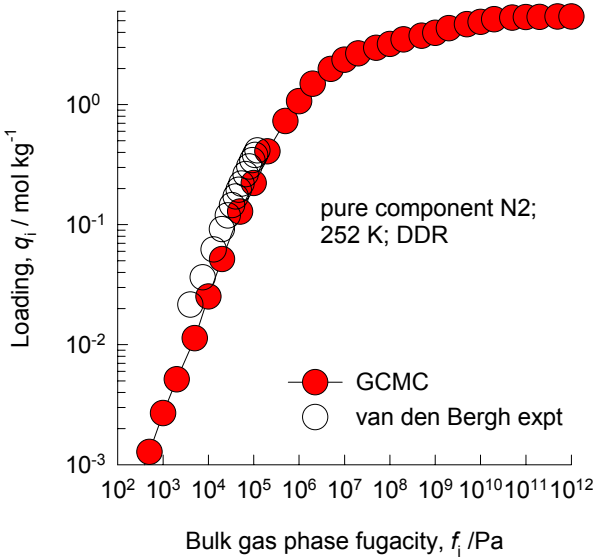

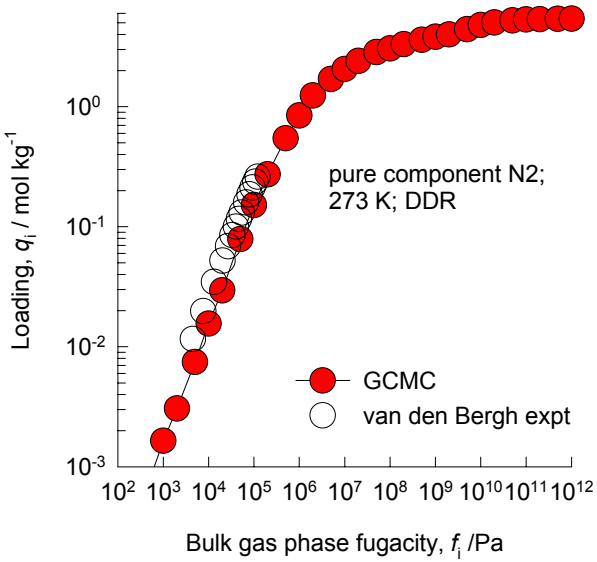

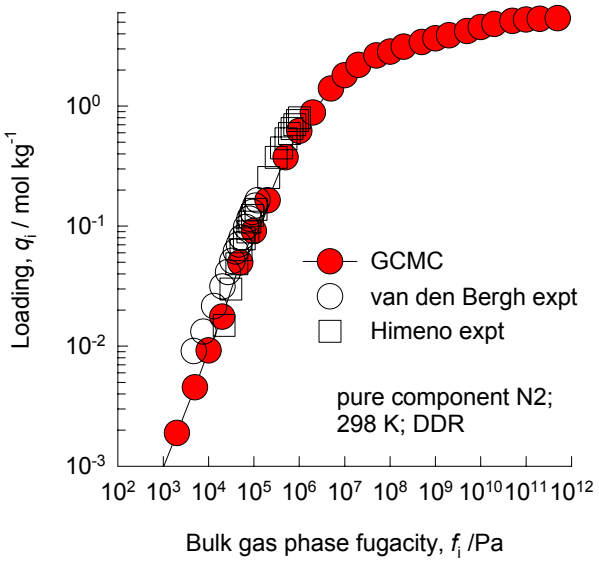

For Reed & Ehrlich fits we take
$q_{i,sat}$ = 16 molecules per cage for all T.

DDR, O2, isotherms

Figure 20

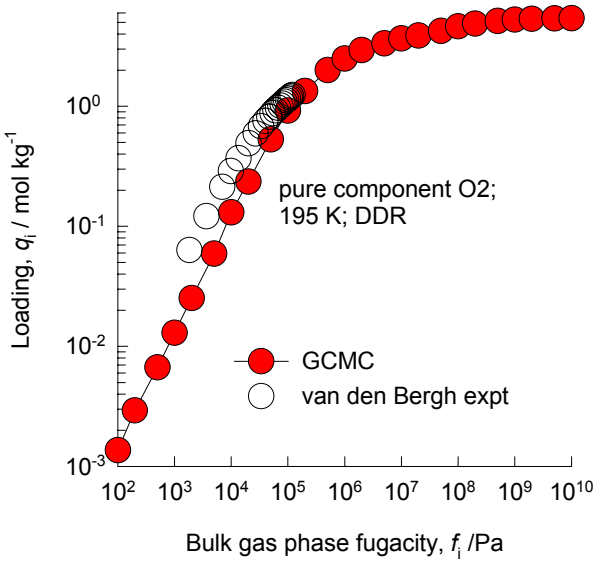

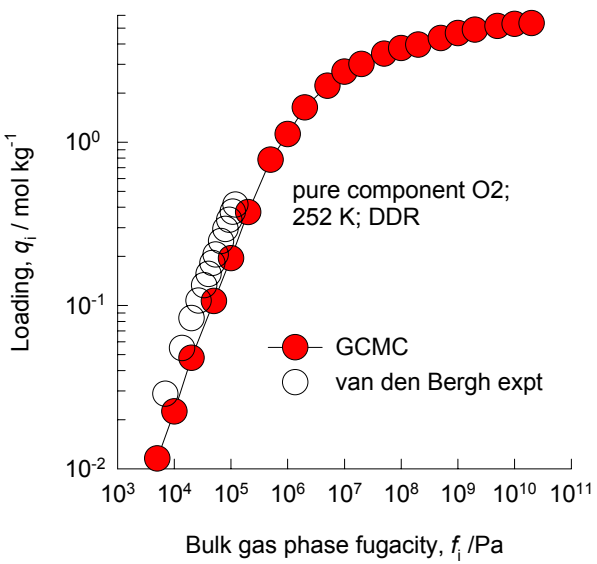

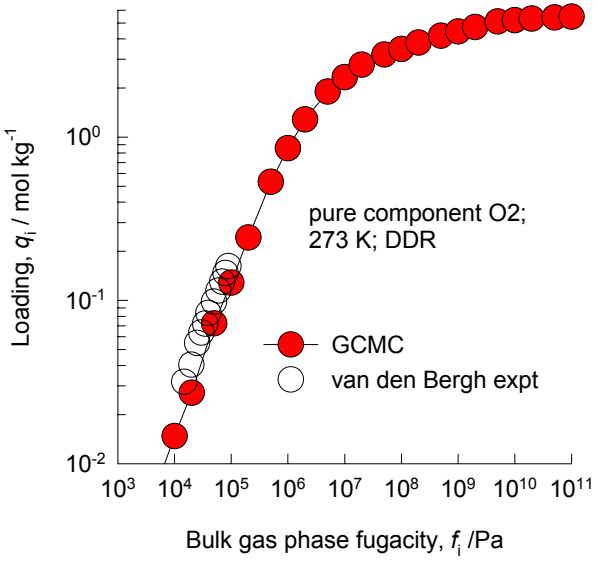

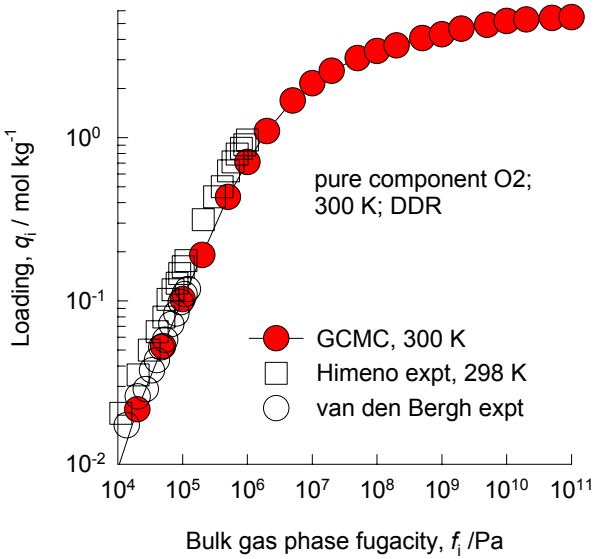

DDR, Ar, isotherms

Figure 21

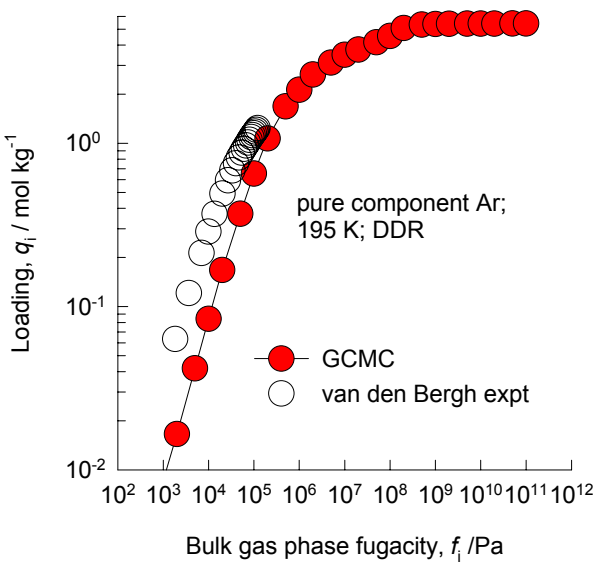

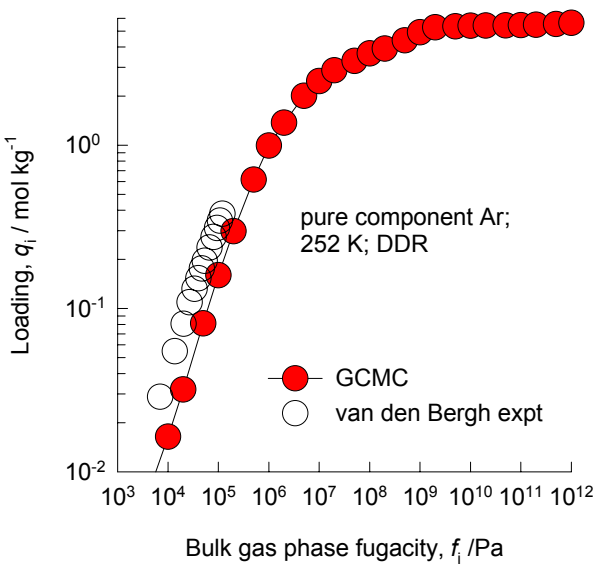

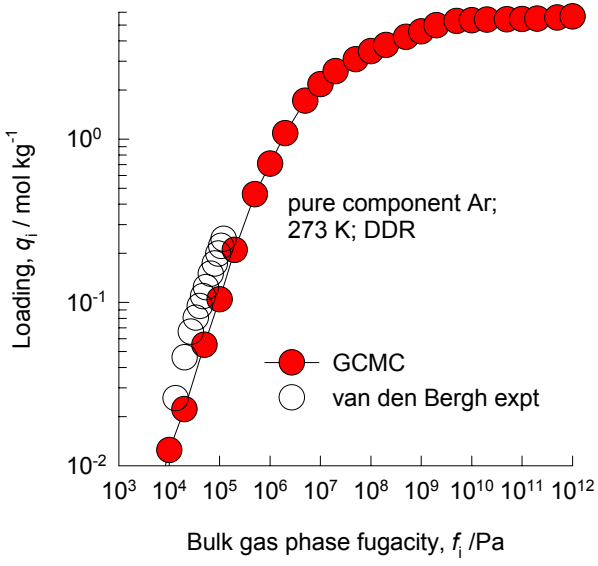

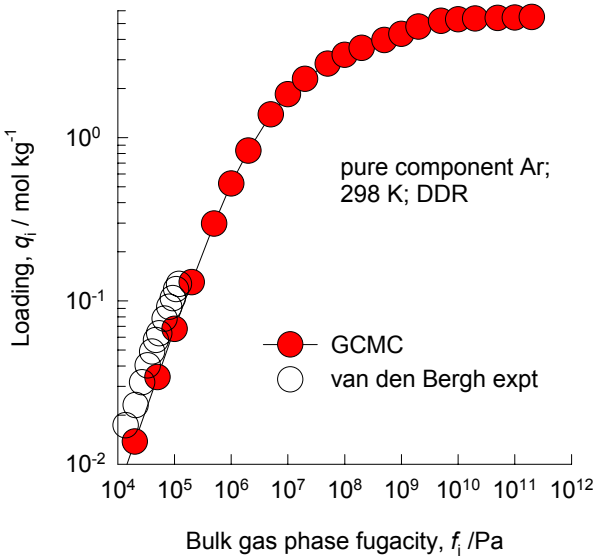

DDR, Kr, isotherms

Figure 22

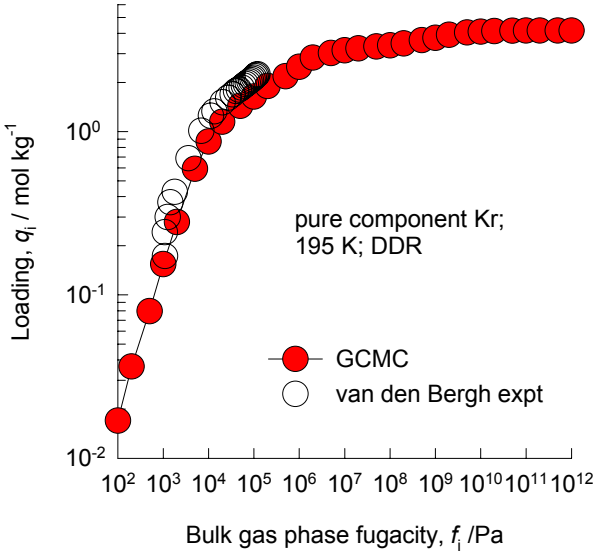

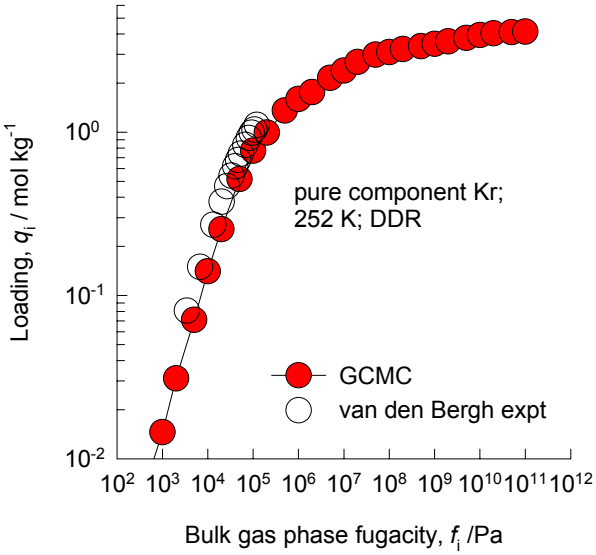

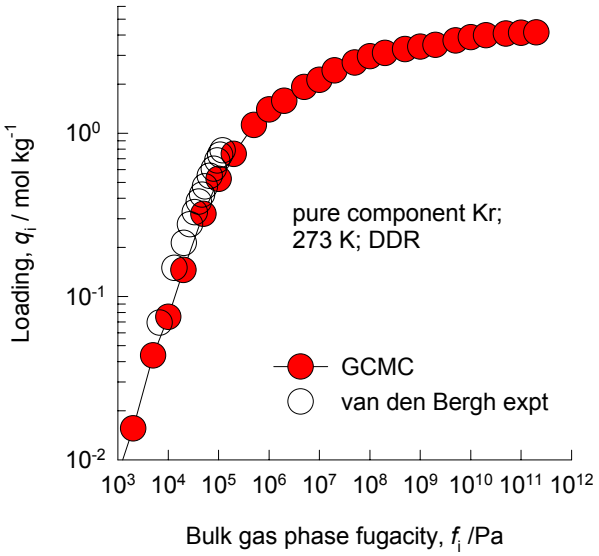

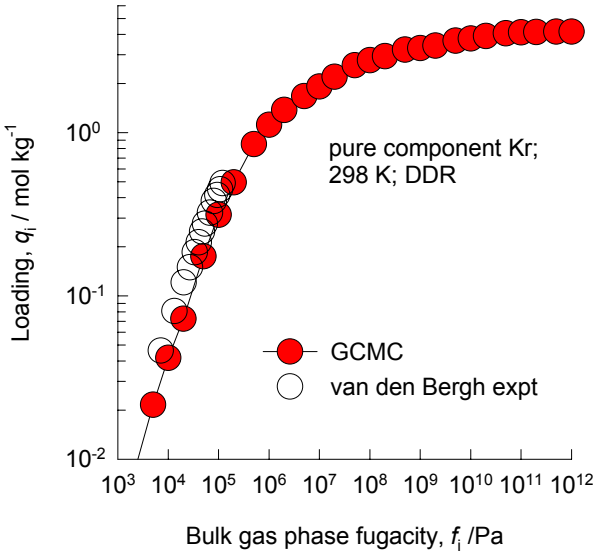

Figure 23

DDR, CO_2, diffusivities

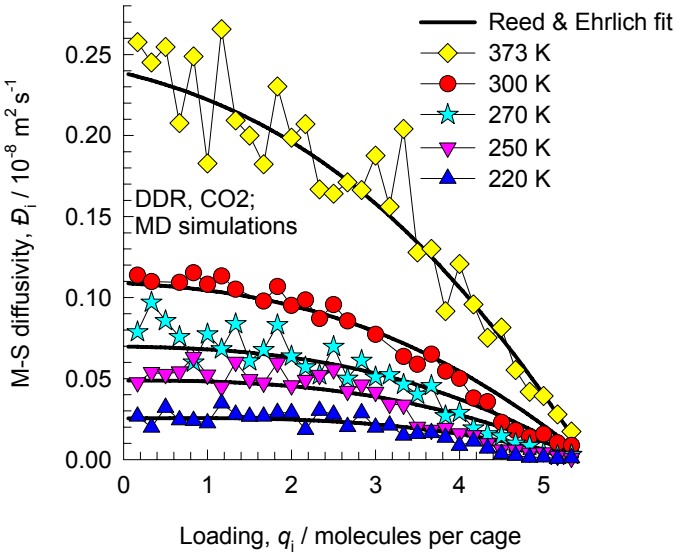

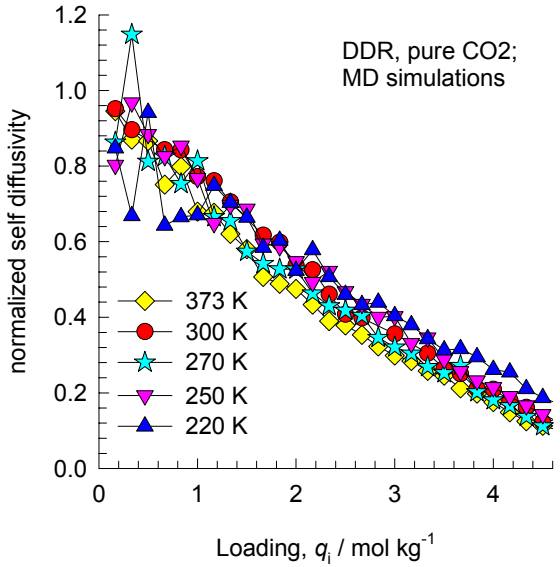

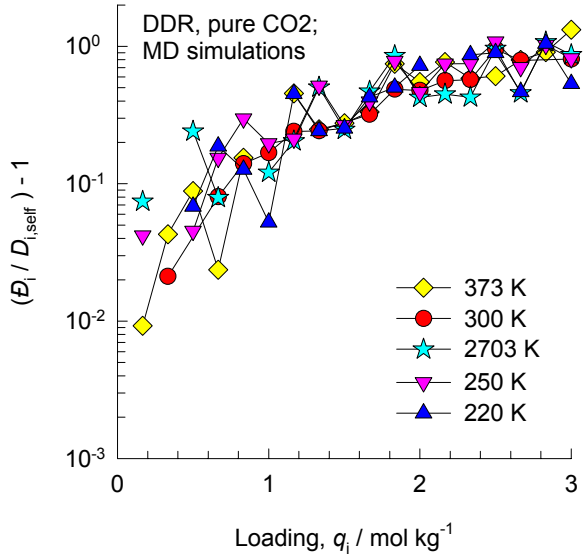

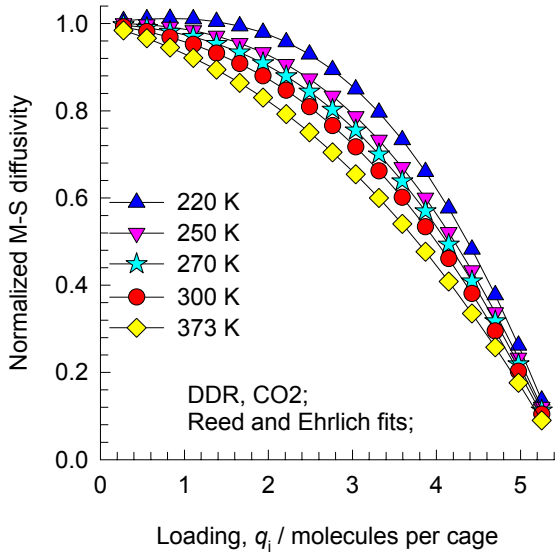

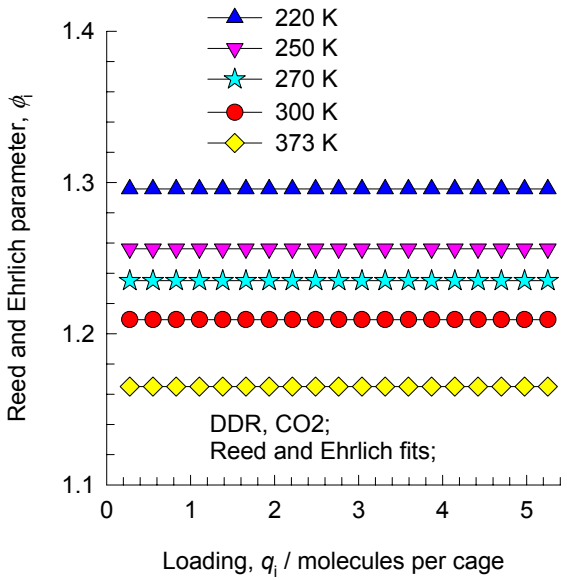

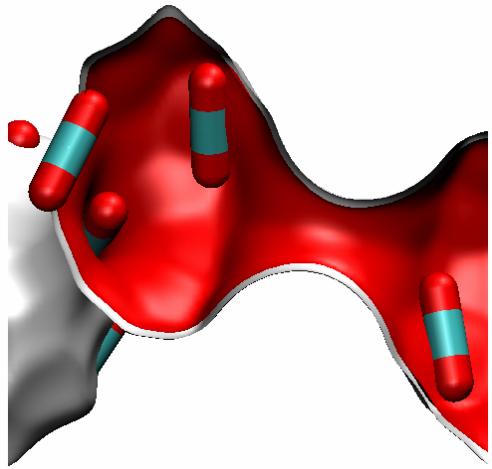

Figure 24

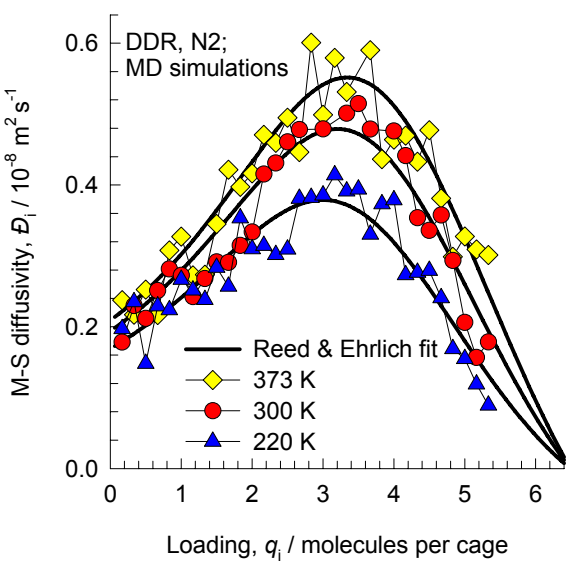

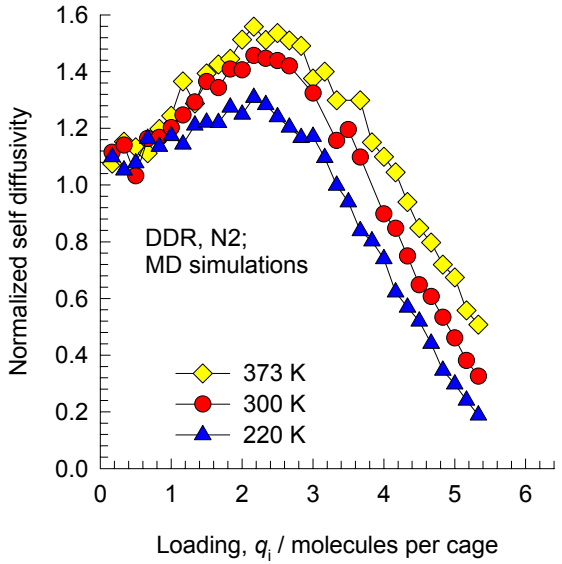

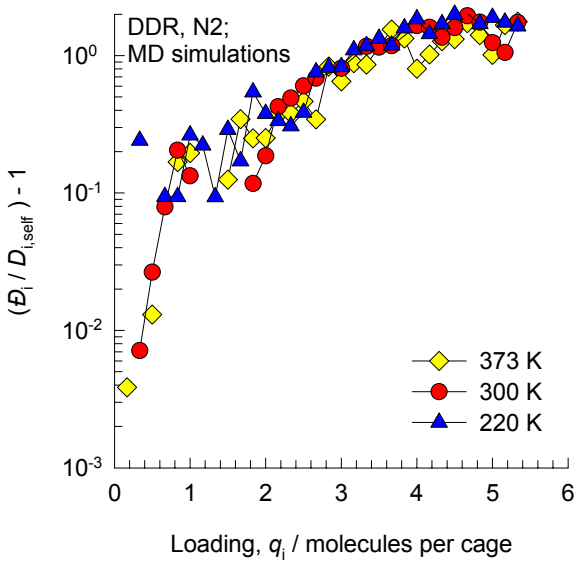

DDR, N_2, diffusivities

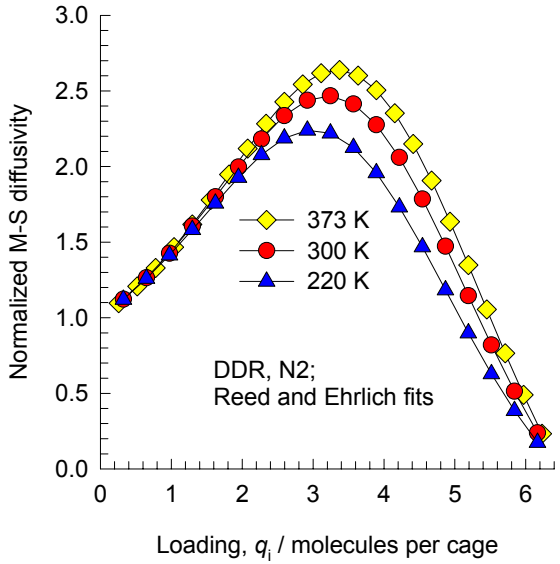

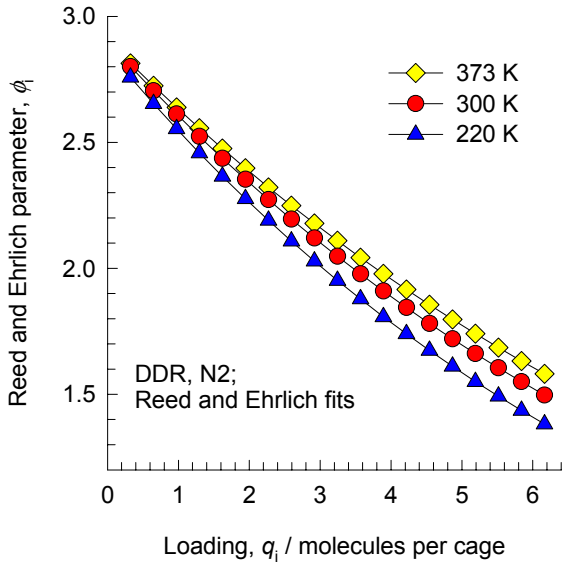

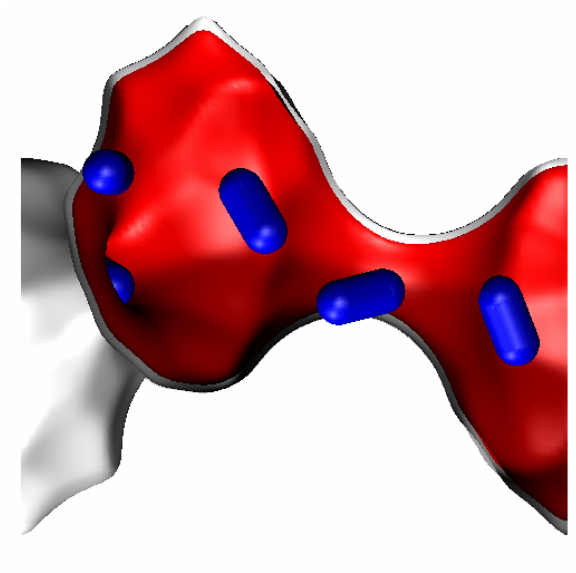

Figure 25

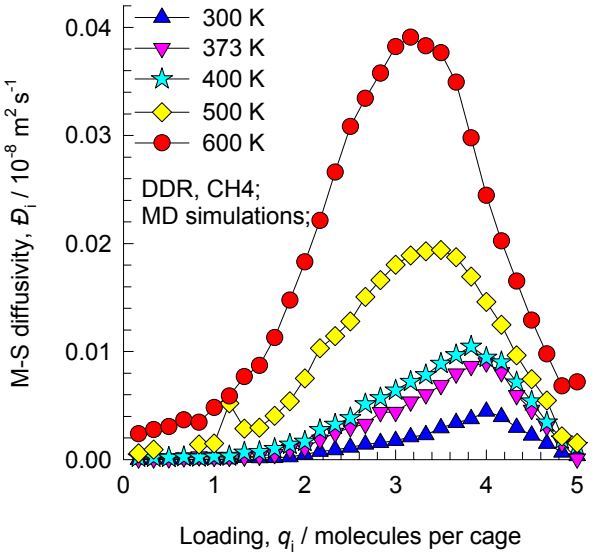

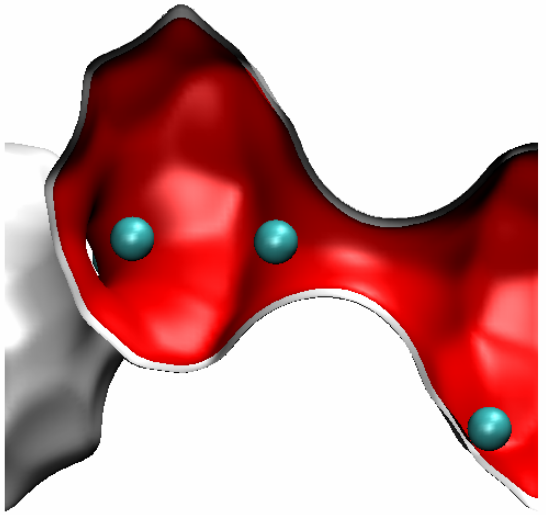

DDR, CH_4, diffusivities

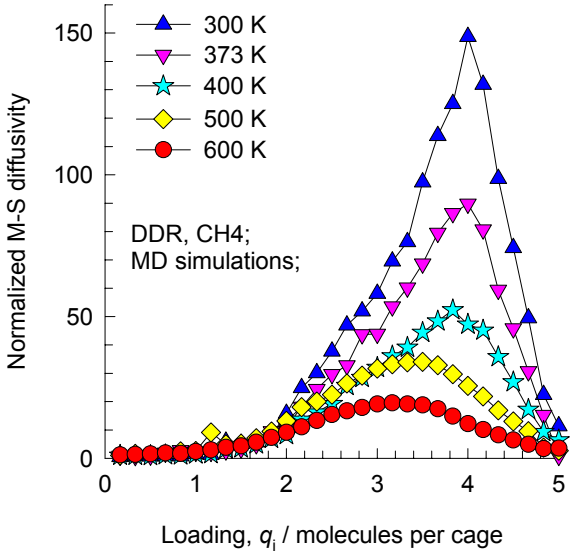

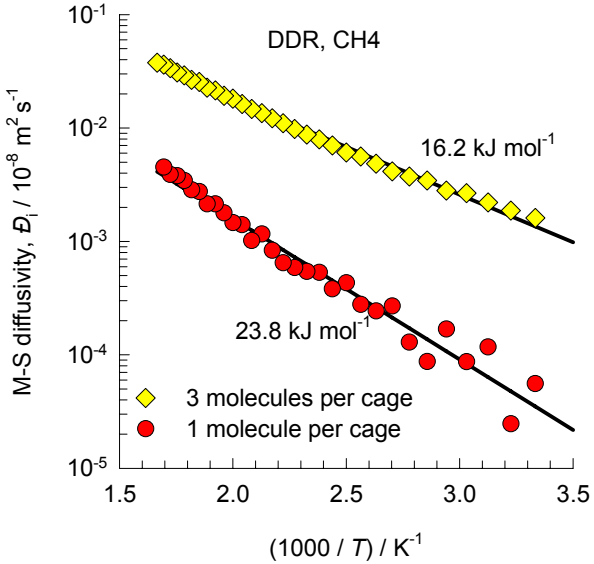

Figure 26

DDR, Ar, diffusivities

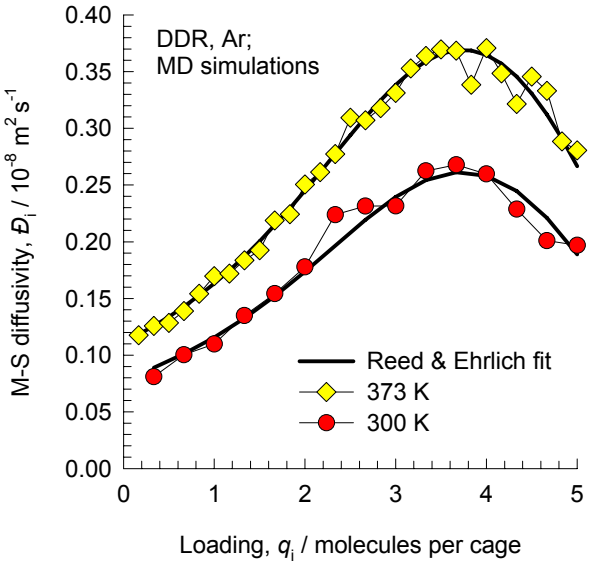

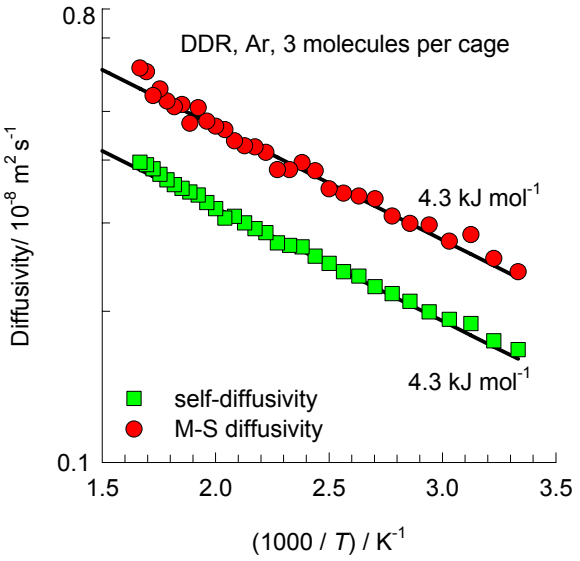

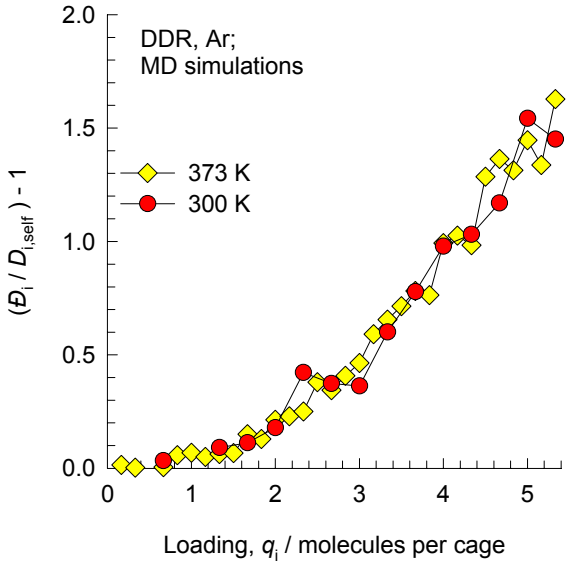

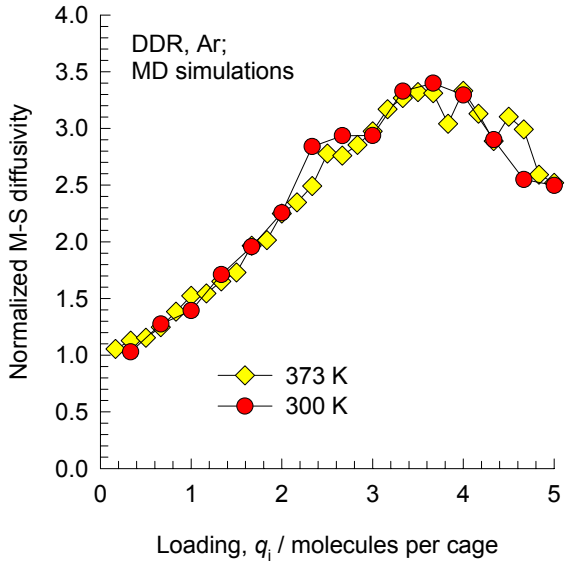

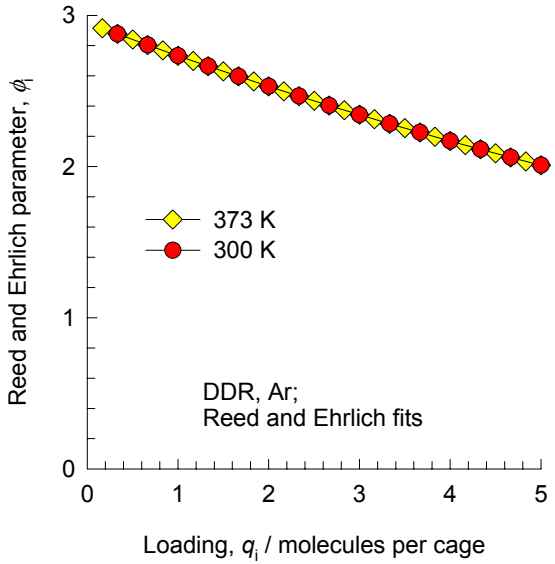

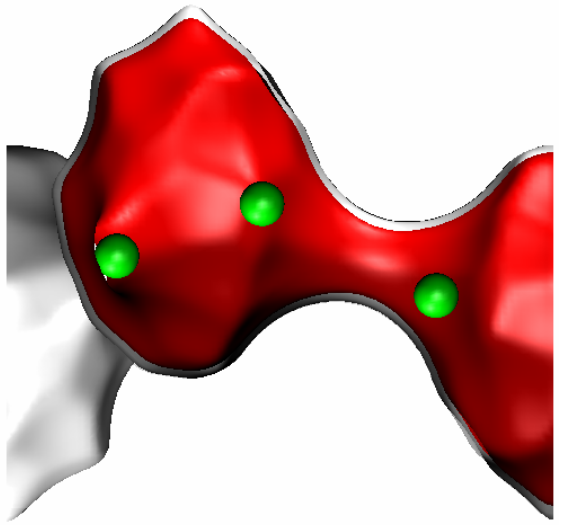

Figure 27

DDR, O_2, diffusivities

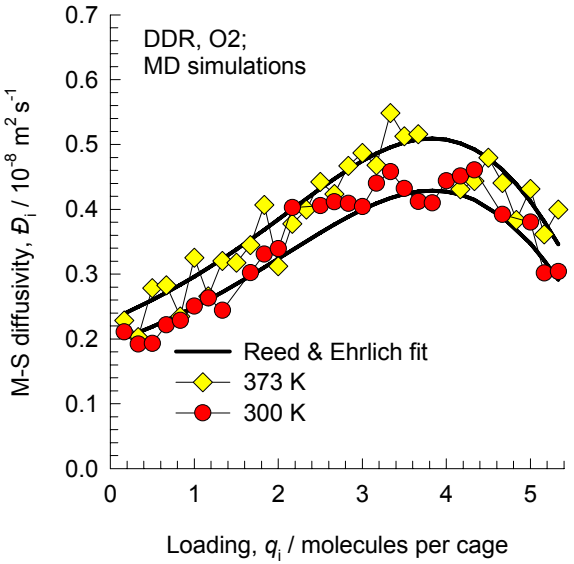

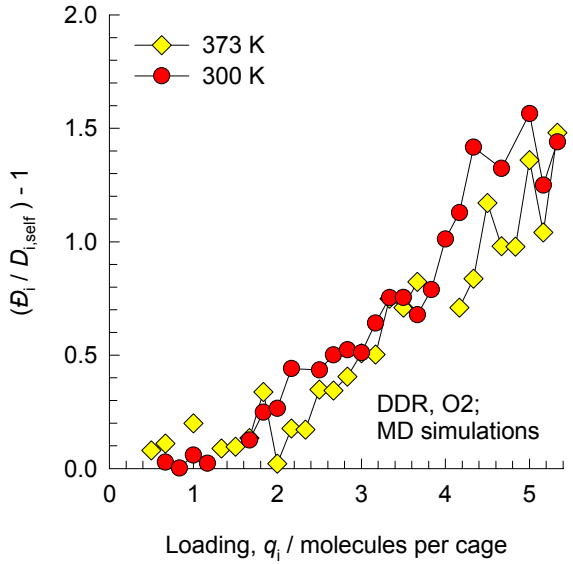

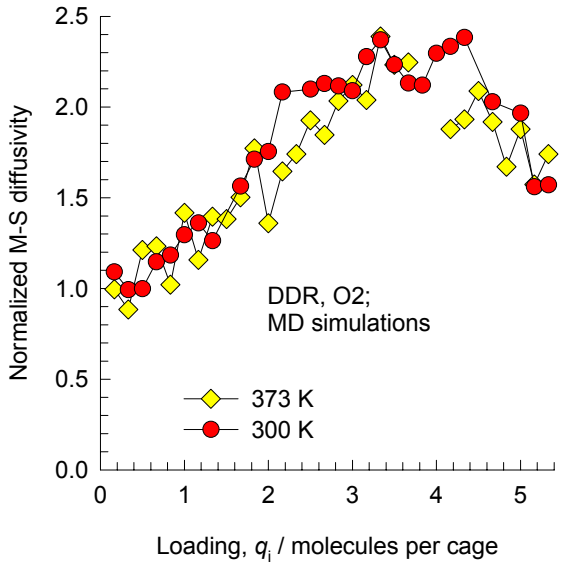

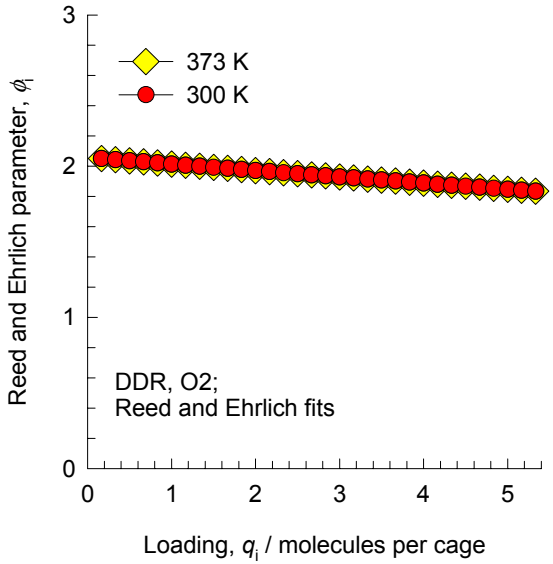

Figure 28

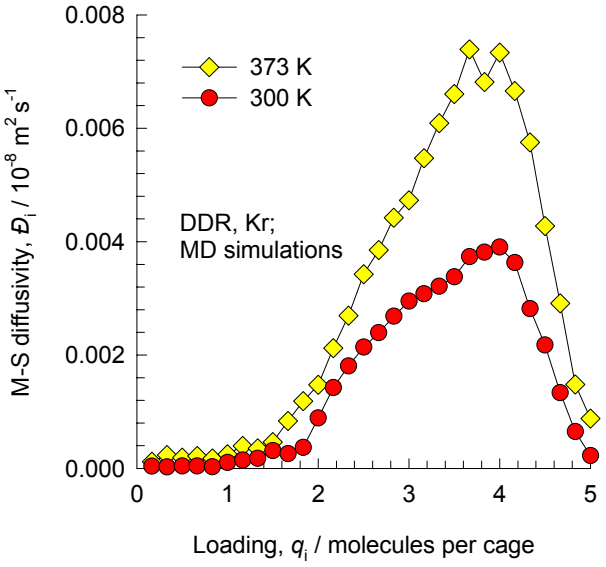

DDR, Kr, diffusivities

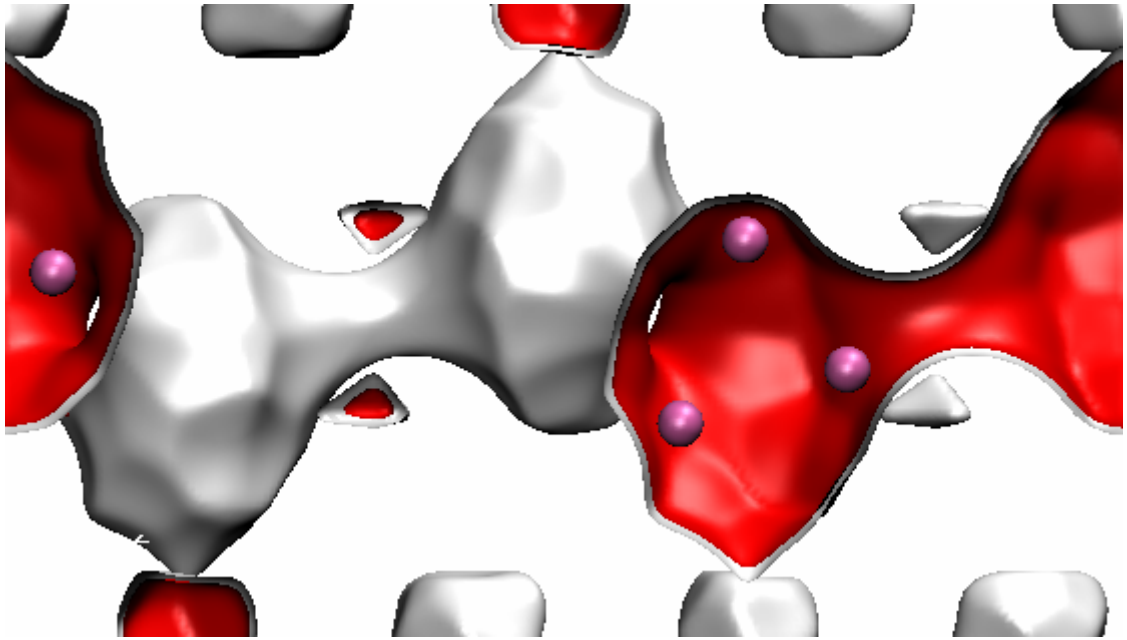

Figure 29

DDR, Ne, diffusivities

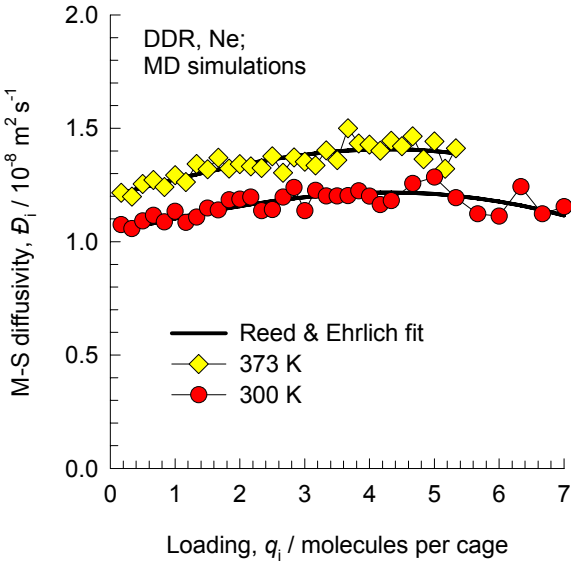

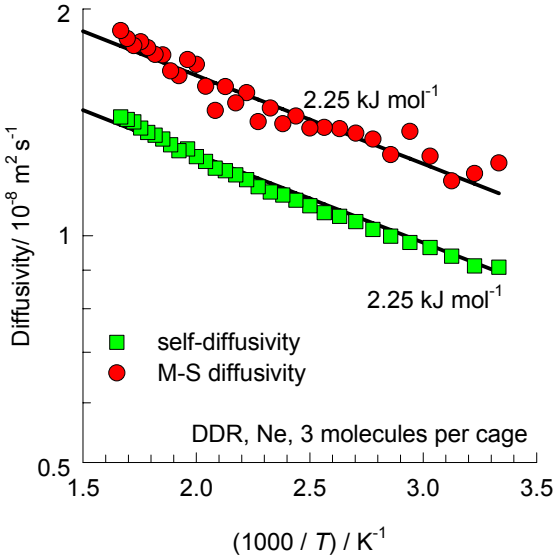

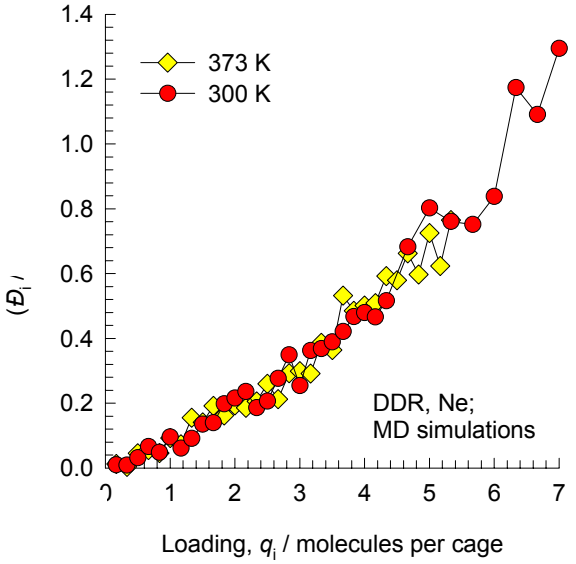

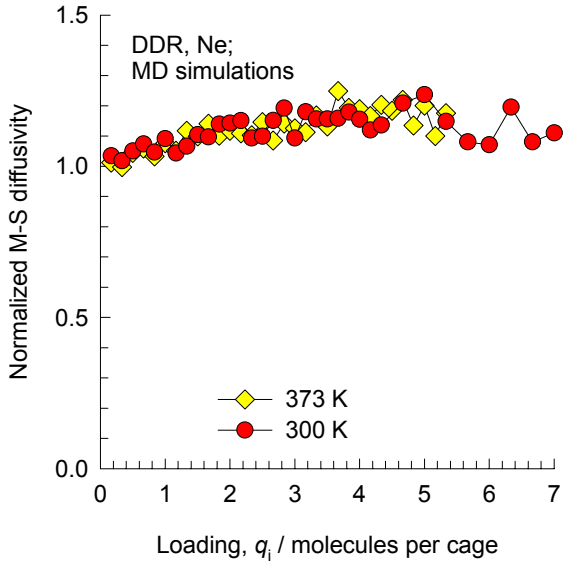

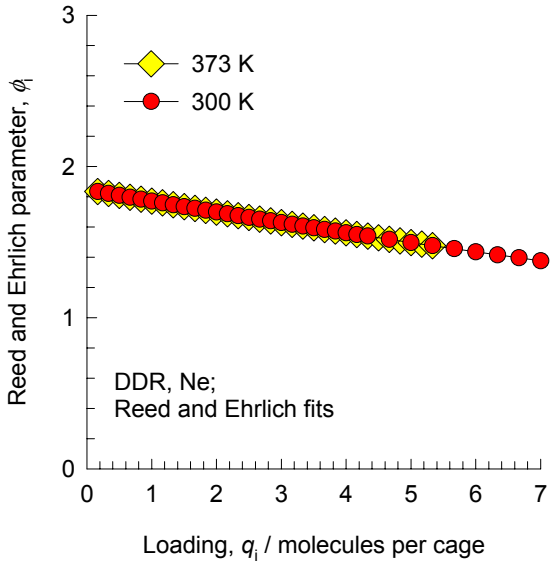

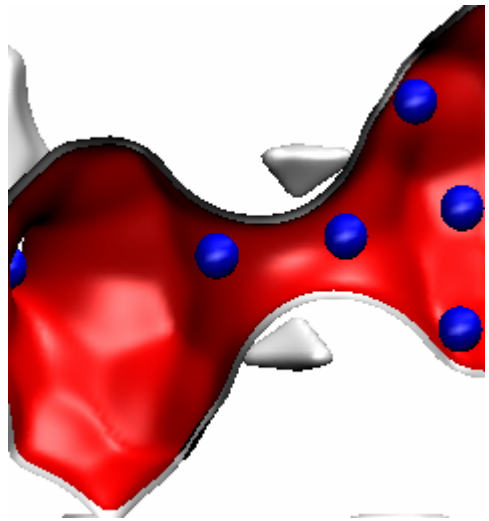

Figure 30

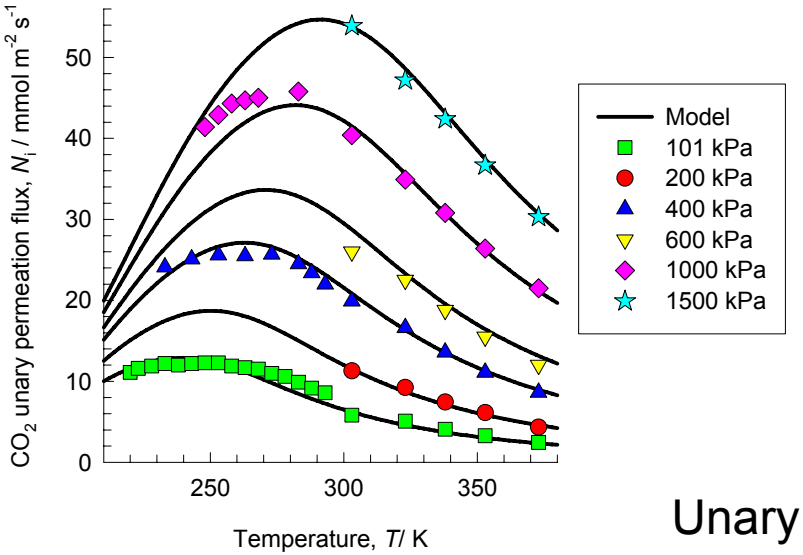

Unary permeation data of van den Bergh (2007, 2008) compared to Reed & Ehrlich model calculations

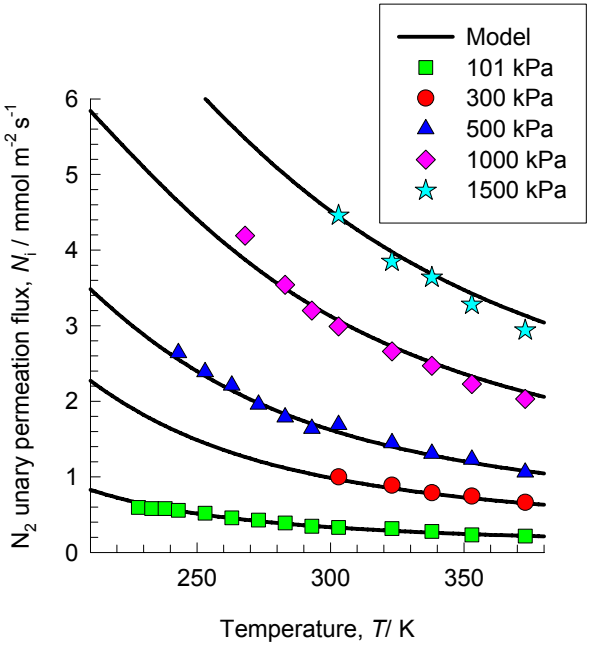

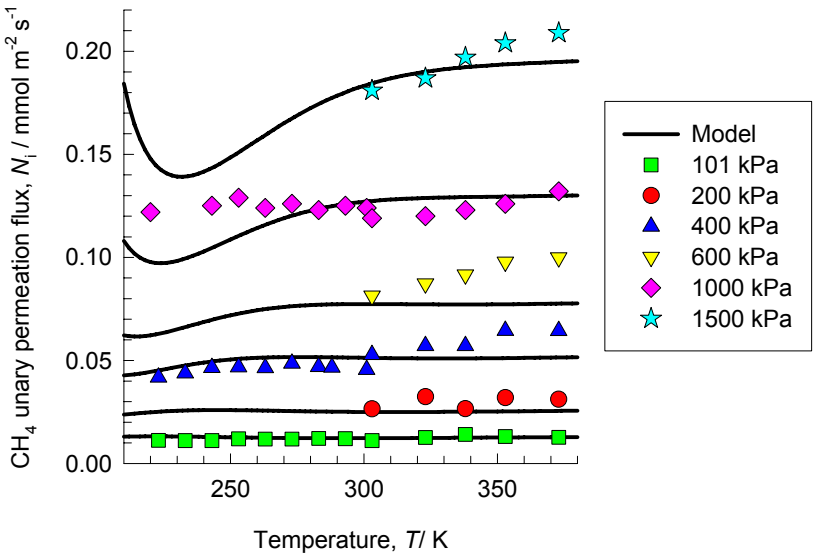

Figure 31

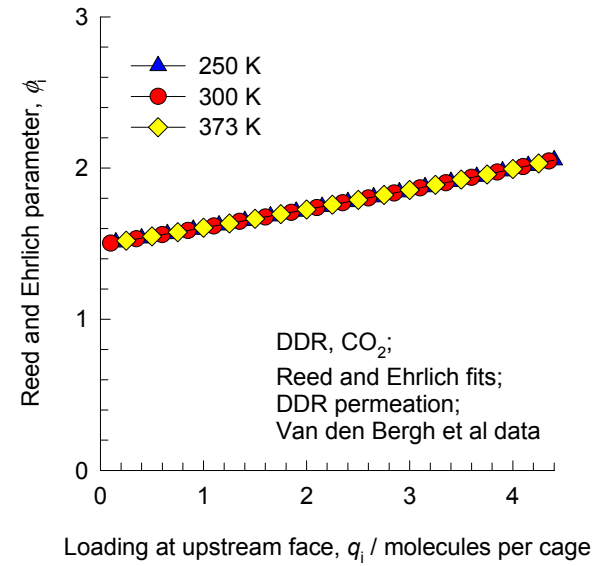

Reed & Ehrlich fitted ϕ_i

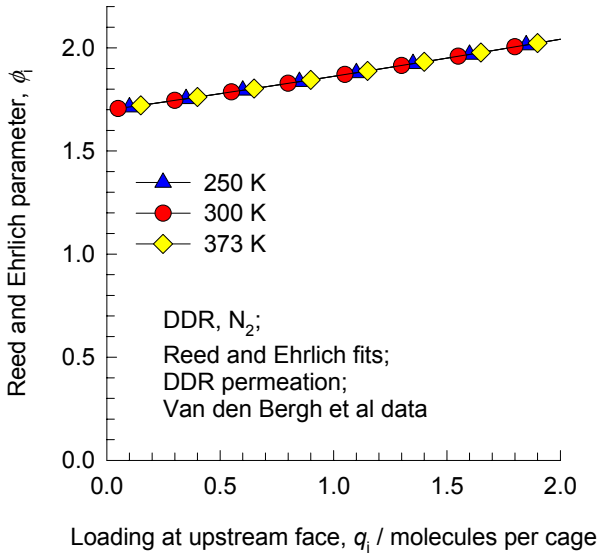

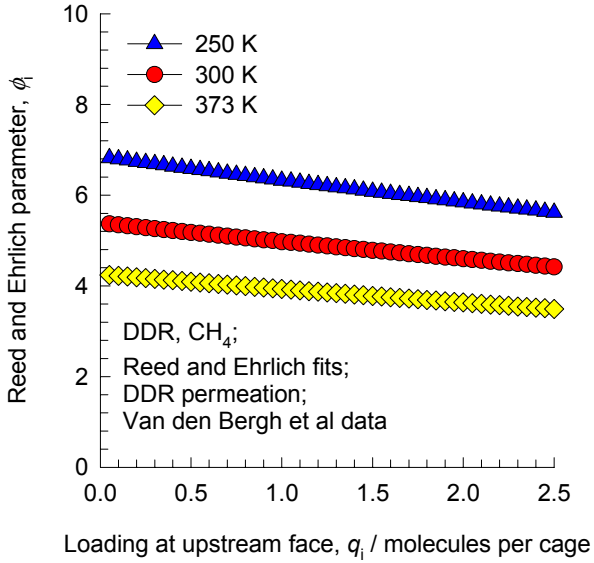

Figure 32

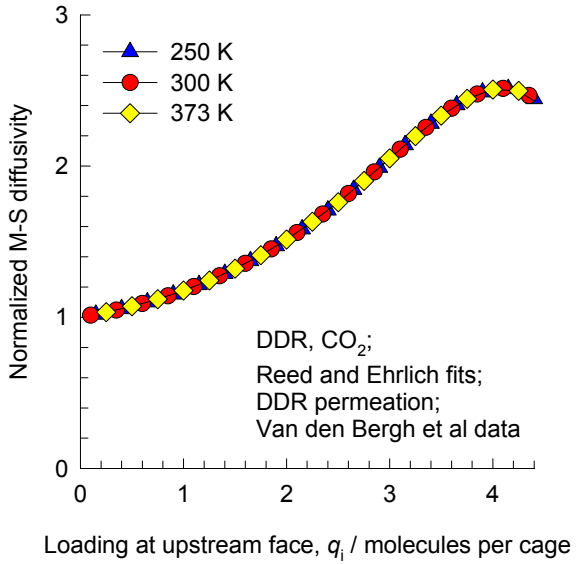

Reed & Ehrlich model calculations of normalized M-S diffusivities